

FOR REFERENCE ONLY

[Faint, illegible text]

DIGITISED

5702049014

ProQuest Number: 10290192

All rights reserved

INFORMATION TO ALL USERS

The quality of this reproduction is dependent upon the quality of the copy submitted.

In the unlikely event that the author did not send a complete manuscript and there are missing pages, these will be noted. Also, if material had to be removed, a note will indicate the deletion.



ProQuest 10290192

Published by ProQuest LLC (2017). Copyright of the Dissertation is held by the Author.

All rights reserved.

This work is protected against unauthorized copying under Title 17, United States Code
Microform Edition © ProQuest LLC.

ProQuest LLC.
789 East Eisenhower Parkway
P.O. Box 1346
Ann Arbor, MI 48106 – 1346

326637

THE NOTTINGHAM TRENT
UNIVERSITY LLR

SHORT LOAN

PHD/BNS/OS

Rey

BEL

THE INFLUENCE OF SMALL
MOLECULES ON THE
PRECIPITATION OF SILICA

DAVID J BELTON

A thesis submitted in partial fulfilment of the requirements of the
Nottingham Trent University
for the degree of Doctor of Philosophy.

July 2005

Dedication.

To Debbie for providing the love, support, shelter and sustenance for me to be able to carry out this work, and being more pleased than anyone else to see it completed.

Acknowledgements.

First and foremost my thanks go to Professor Carole Perry for offering me the opportunity to carry out this research and her patience in the compilation of it.

Thanks also go to those in the inorganic research department some of whom I have spent the last few years working with, especially, Paul Roach, Neil Shirtcliffe, Simon Thompson, Graham Tilbury, Heather Currie, David Eglin, Olivier Deschaume, Kirill Shafran, Agathe Fournier and Geetangali Patwardhan. Extra special thanks go to Siddharth Patwardhan for the generous gift of his time and humour, both of which I hope I didn't drain too much (thanks Sid).

Thanks also to those who helped in collecting data associated with this thesis including, (but in no particular order), Anthony Franklin, Fran Karpowitz, Arthur Richards, Simon Mazengarb, Mick Woods, Simon Stebbings and generally everybody in the chemistry department who made the time spent at Nottingham Trent University not only rewarding but also very entertaining. Also anyone reading this who feels they should have had a mention please accept my apologies, you're absolutely right, you should have.

Finally funding for this research was gratefully received from Ineos silicas, AFOSR and the European union.

Contents.

Abstract	i
Chapter 1.	
Introduction.	
1.1 Silica in the natural world	1
1.2 In vitro Condensation of Orthosilicic acid	4
1.2.1 The Condensation Process	4
1.3 Industrial Silica Production and Usage	6
1.4 Biomineralisation	9
1.4.1 Biosilicification in Diatoms	11
1.4.2 Isolates from silica in plant species	13
1.5 Bioinspired and biomimetic approaches to silica formation.	14
References	17
Chapter 2.	
Experimental Methods	
2.1 The molybdenum blue method.	21
2.2 Photon Correlation Spectroscopy	25
2.3 Nitrogen gas adsorption/desorption analysis	27
2.4 Nuclear magnetic resonance spectroscopy	37
2.5 Thermogravimetric analysis	40
2.6 Mass spectrometry	41
2.7 Fourier transform infrared spectroscopy	45
2.8 Scanning electron microscopy	46
2.9 Experimental details	
2.9.1 Experimental details for Chapter 3	49

2.9.2 Experimental details for Chapter 4	49
2.9.2 (i) Reagents	49
2.9.2 (ii) Silica synthesis and kinetic studies	49
2.9.2 (iii) Photon correlation spectroscopy	51
2.9.2 (iv) Scanning electron microscopy	51
2.9.2 (v) Surface area analysis	52
2.9.2 (vi) Thermogravimetric analysis	52
2.9.2 (vii) Fourier transform infrared spectroscopy	52
2.9.3 Experimental details for Chapter 5	
2.9.3 (i) Reagents	53
2.9.3 (ii) Deviations from 2.9.2	53
2.9.4 Chapter 6	53
2.9.4 (i) Reagents	53
2.9.4 (ii) Deviations from 2.9.2	53
References	55

Chapter 3.

Experiments with the model system

3.1 The model system	57
3.2 Inherent difficulties with the model	58
3.2.1 Attempts to eliminate the conversion factor	58
3.2.2 experimental details of the model system	61
3.2.3 Statistical analysis of the standard model system	62
3.3 Solution species	63
3.3.1 Stabilised silica solution	64
3.3.2 ²⁹ Si magnetic resonance investigation	64
3.3.3 Mass spectrometric investigation	65
3.3.4 Mass spectrometry of the model system	66
3.4 The rate of dissociation of dipotassium tris (1,2-benzenediolato- OO'),2H ₂ O complex upon pH adjustment	70
3.5 The affects of changing controllable parameters on the kinetics of the model system	72
3.5.1 Temperature dependence	72
3.5.2 Concentration dependence	77
3.5.3 pH dependence	79

Summary	83
References	84

Chapter 4.

The effects of amino acids on the condensation and aggregation of silica in the model system

4.1 Introduction	85
4.2 experimental	86
4.3 Results	
4.3.1 Solution Chemistry	86
4.3.2 Photon correlation spectroscopy	89
4.3.3 Residual organic material in sedimented silica	92
4.3.4 Gas adsorption analysis	94
4.3.5 Scanning electron microscopy	97
4.4 discussion	102
4.5 Conclusions	106
References	107

Chapter 5.

The importance of non covalent interactions of diamines on the condensation and aggregation process in silica.

5.1 Introduction	108
5.2 Experimental	108
5.3 Results and discussions	
5.3.1 Solution chemistry	108
5.3.2 The hydrophobic effect	109
5.3.3 Particle growth and aggregation	112
5.3.4 Electrostatic effects	114
5.3.5 Silica Maturation	116
5.3.5(I) Nitrogen gas adsorption	116
5.3.5.(II) Thermogravimetric analysis	118
5.3.5.(III) Scanning electron microscopy	119
References	121

Chapter 6.

The importance of interamine spacing in polyamines on the silica condensation process.

6.1 Introduction	122
6.2 Experimental	
6.2.1 reagents	124
6.2.2 Methods	124
6.3 Results	125
6.4 Discussion	134
6.4.1 Proposed mechanism for the production of glassy “spheres”	137
6.5 Conclusions	141
References	143
Conclusions	144
Further work	149
Appendix	
Error analyses	151
Publications	156

Abstract.

A study has been conducted into the mechanisms of interactions between silicic acid solutions and silica surfaces with a range of amino acids, homopeptides, diamines and short polyamines. The dissociation mechanism of the monosilicic acid precursor, (a 1,2-diolato benzene complex), was investigated and the dissociation confirmed to be rapid and stoichiometrically controllable at the desired pH. Investigations by mass spectrometry and monitoring the development profile of silicomolybdic acid from condensing monosilicic acid solutions did not indicate the presence of any kinetically interfering species and statistical analysis of the isolated kinetic domains showed good experimental control of the model system. Activation energies for the early condensation stages were determined and the process was shown to be controlled by the ease of anion formation of silicate species and the solubility limit for amorphous silica estimated by extrapolation of the kinetic data.

The addition of amino acids to the model system showed most pronounced effects when basic side chain functionalities were present and amine species were shown to influence the condensation and aggregation rates in line with the relative proportions of hydrophobic domains to amine functionality, chain length and electrostatic effects, allowing the formation of unusual non-porous material at circumneutral pH when partially protonated polyamine species were introduced. The mechanistic change in the condensation process was found to be a function of the number of repeat ethyleneamine units in the polyamine and the consequent amine charge density, and entrainment of the polyamine in the highly condensed silica resulted in microporous channels after removal.

Chapter 1.

Introduction

1.1 Silica in the natural world.

Silicon makes up 25.7% of the earth's crust by mass and is the second most abundant element. It does not occur free in nature but occurs chiefly as the oxide and as silicates. In its pure form (as the oxide), it occurs in three crystalline forms, quartz, tridymite and cristobalite and is found as quartz, rock crystal, amethyst, agate, flint, jasper and opal. As silicates it is found in combination with a number of other elements including potassium and aluminium in orthoclase feldspar, sodium or calcium and aluminium in plagioclase feldspar, iron and magnesium in olivine and pyroxenes and with calcium and magnesium in hornblende. All of these minerals contain silicon-oxygen tetrahedra arranged as isolated units (nesosilicates), single or double chains (inosilicates), sheets (phyllosilicates), or three-dimensional frameworks (tectosilicates). Silica is also found in sedimentary rocks such as sandstone which is a terrigenous sedimentary rock i.e. derived from the weathering of pre-existing rocks and cherts and diatomite which are biochemically formed and consist of amorphous silica.

In the process of weathering silica dissolves slowly to give solutions of monosilicic acid, $\text{Si}(\text{OH})_4$, at low concentrations usually between a few parts per million up to about 100 parts per million. The emergence of silicon- metabolizing biological systems began five hundred to six hundred million years ago¹ and resulted in a drastic alteration of the concentration of dissolved silica in the oceans especially through the effects of diatoms (unicellular algae), reducing monosilicic acid levels to a few ppm. In the case of diatoms the importance of silicon to survival is obvious with the highly ornate silica frustule which comprises of two valves, the thecae, consisting of almost pure amorphous silica. Silicon is essential for normal growth and development of species throughout the natural world even though it's metabolism is not clearly understood and silicon is only found bonded with oxygen in nature. The biological need for silicon begins at the embryonic level with development of connective tissues and subsequent maintenance of the them,¹ and it has been known for some time that silicon, calcium, phosphorus, and magnesium all accumulate in the mitochondria of

osteoblasts before any evidence of extracellular ossification occurs.¹ Silicon deficiency in animals causes reduced mineralization of bone, reduced collagen content of bone, reduced skeletal growth, bone deformities, thinner articular cartilage, smaller and less well- formed joints, and adverse effects on skin, hair, nails, and mucous membranes.¹ Under normal conditions silicon is found in highest concentration in the aorta, trachea, tendons, ligaments, bone, cartilage, skin, dental enamel, cornea, and sclera.

The active role of biological systems in the condensation and deposition of silica structures has been demonstrated by the ability of organisms to reduce concentrations of dissolved silica from their environment to well below saturation levels whilst building up amorphous silica structures with both control of particulate and morphological features,^{2,3} and their subsequent stabilisation of the structures against redissolution of the silica. The role of silica is mainly structural (eg diatoms, radiolaria), defensive (eg sponge spicules) or as a defence against herbivory or fungal attack in plants.⁴ Structures include the highly ornate diatom frustule and radiolaria skeletal and surface motifs in *equisitaceae*. In plants silica is found in appreciable quantities in all dry matter, some no doubt arising by passive transfer and deposition through transpiration (many plants continue to accumulate silica throughout their lives by this mechanism),⁵ but those which contain more than 1% by weight in dry leaf matter are considered silicon accumulators.⁴ In species of *equisetaceae* the levels of silica can exceed 10% (some up to 25%) dry weight. It is found in the needles of white spruce (largely confined to the hypodermis and mesophyll tissue)^{6,7} in the leaf blades (silica cells, bulliform cells, micro hairs and prickle hairs) of bamboo species⁸ and has been reported to occur as α quartz in some species of *cactaceae* where its occurrence is considered to be a separation of non assimilable material from the transpiration stream since the kinetic barrier to the crystallization of amorphous silica is around 800kJmol^{-1} ⁹ although there is some debate over this. In species of *Equisetaceae* silica is found as pillulae on stomata and rosettes in the groove flank region of branch material, many of the structures remaining intact on removal of supporting or covering tissues.¹⁰ On closer inspection these structures were found to be built from silica particles which displayed fibrillar, globular and sheet like nanostructural motifs. It is generally accepted that macromolecules such as proteins, polysaccharides and glycoproteins all play a role in this process.¹¹⁻¹⁹ In most biogenic

silica structure primary aggregates are apparent under electron microscopy, but some species of diatoms and in the case of sponge spicules a continuous structure is observed with particles only being observed during intermediate stages of formation. These are then apparently in-filled during the morphogenesis of the final structure.

Early work on cell wall composition during silica deposition¹⁹ and the nature of the amino acid and sugar composition of diatom cell walls¹¹ which found them relatively enriched with threonine and serine (16-34 mol%) and a further 23 mol% of aspartic/glutamic species plus 11-21 mol% of glycine led to the hypothesis that silicification was protein mediated with silica deposition occurring at hydroxyl rich locations supplied by enrichment of serine residues, and that polysaccharides played a structural role. Proteinaceous extracts known as silicateins derived from the biogenic silica of the sponge, *Tethya aurantia*, have been shown to be highly homologous to the cathepsin L family, with active site conservation, but with distinct hydrophobic domains¹⁸ which suggests that those molecules may not operate as a monomer but may control macroscopic structure by surface contact through the hydrophobic domains. Silicateins have been shown to catalyse the condensation of silica from tetraethoxysilane at room temperature and neutral pH via the mechanism shown (Figure 1.1), results not previously observed *in vitro*. More recently an enzyme has been isolated from the demosponge *Suberites domuncula* which has been shown to degrade biogenous amorphous silica²⁰ and therefore either aid uptake of silicic acid by providing locally raised concentrations or may be involved in relocating particulate silica to other sites in the active monosilicic acid form.

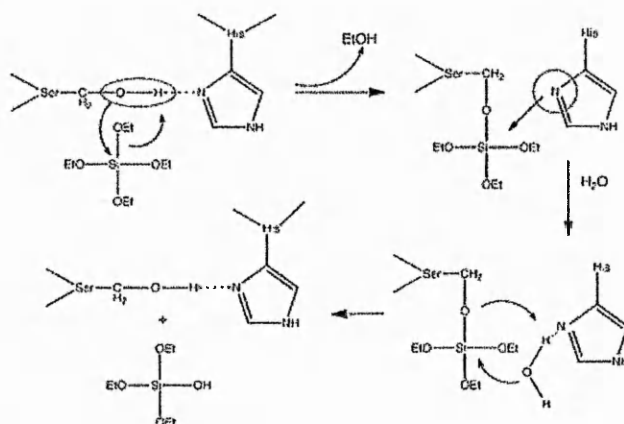


Figure 1.1. Proposed mechanism for the active site of silicatein mediated catalysis of tetraethoxysilane hydrolysis.

Intra siliceous material isolated from the horsetail fern, *Equisetum telmateia* has also been shown to affect the kinetics and morphologies of silica deposition when added *in vitro* to a condensing silica system.¹⁶ Levels of orthosilicic acid found in the silica deposition vesicle (SDV, the organelle of silica condensation in diatoms), have been found to be far in excess of stable levels (above 100-200ppm orthosilicic acid autocondenses to hydrated silica) and in the transpiration stream of plants levels ranging from 300ppm in *Equisetum hyemale*,²¹ to as high as 650ppm in rice sap²² have been observed. The mode of transport to these regions avoiding premature condensation is therefore of interest. There is considerable evidence of silicon complexing with polyphenolic acids such as humic and fulvic acids which occur in relatively large quantities in the humic material of soils.²¹ This would be the most obvious source of soil borne soluble silicon for uptake by plants. Destabilisation of the complex at the site of deposition may then be accomplished by enzymatic means, pH change (cf contents of the silica deposition vesicle in diatoms is thought to be acidic²³) or ligand exchange. Organic complexes found in the fir *Thuja plicata* have been identified as a tropolone derivative, β thujaplicin (4-isopropyl tropolone),²⁴ although it is not clear if these were a product of the isolation process or a component of the plants cellular material as investigations of silicon species in plant sap has so far failed to show anything other than mono and disilicic acid.^{25,26,27} Studies into the use of silicon complexes (such as the silicon tris catecholate complex) have shown them to be a potential source of supersaturated orthosilicic acid for a model system, being readily soluble in aqueous media and rapidly dissociating on lowering of the pH to around 7.^{28,29}

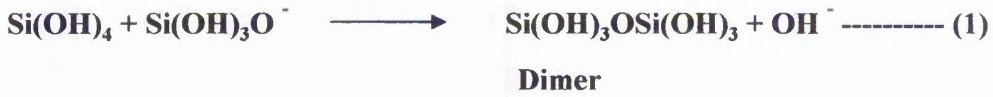
1.2 In vitro condensation of orthosilicic acid.

1.2.1 The condensation process.

The condensation of orthosilicic acid to silica *in vitro* occurs spontaneously (autopolycondensation) at concentrations in excess of the solubility of solid phase amorphous silica (100-200ppm) and is thought to involve an ionic mechanism since above pH 2 the rate is proportional to $[\text{OH}]^-$ and below to $[\text{H}]^+$. The process of condensation and aggregation²⁹⁻³⁴ has been divided in to 3 distinct stages:-

- i) Polymerisation of monomer to form stable nuclei of a critical size,
- ii) Growth of the nuclei to form spherical particles
- iii) Aggregation of particles to form branched chains or structural motifs.

The early stages of the process then can be summed up by:-



Polymerization proceeds in such a way as to minimize the uncondensed SiOH groups and maximize the Si-O-Si bonds, thus cyclic oligomers such as the cyclic trimer and tetramer are favoured at early stages. These are then linked together by free monomer and condense internally to form highly compact spherical units which become the nuclei for further growth to larger particles (Figure 1.2).

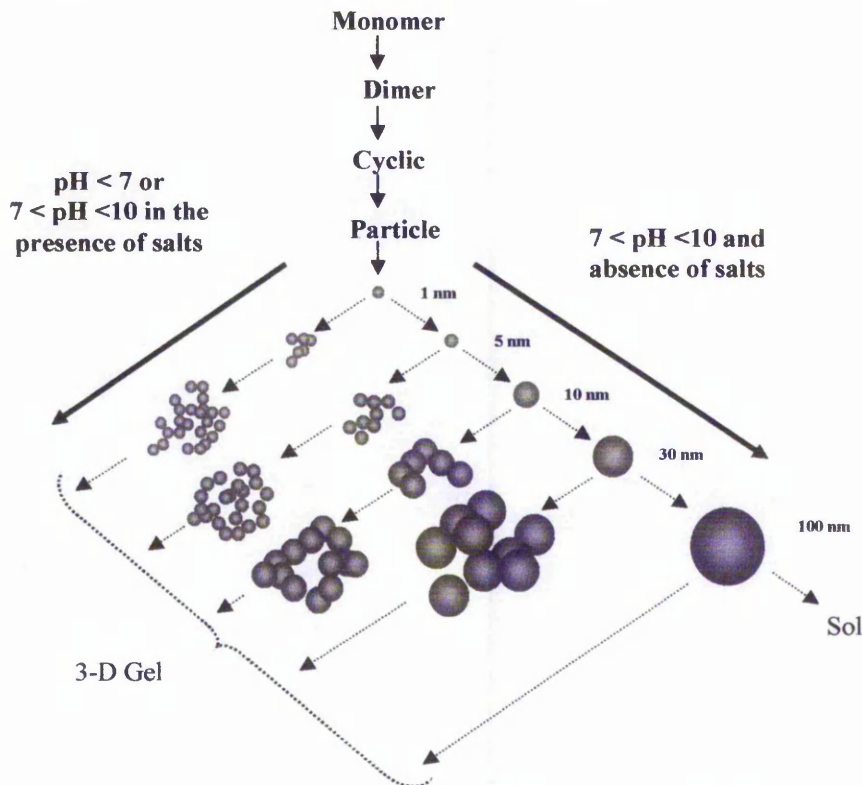
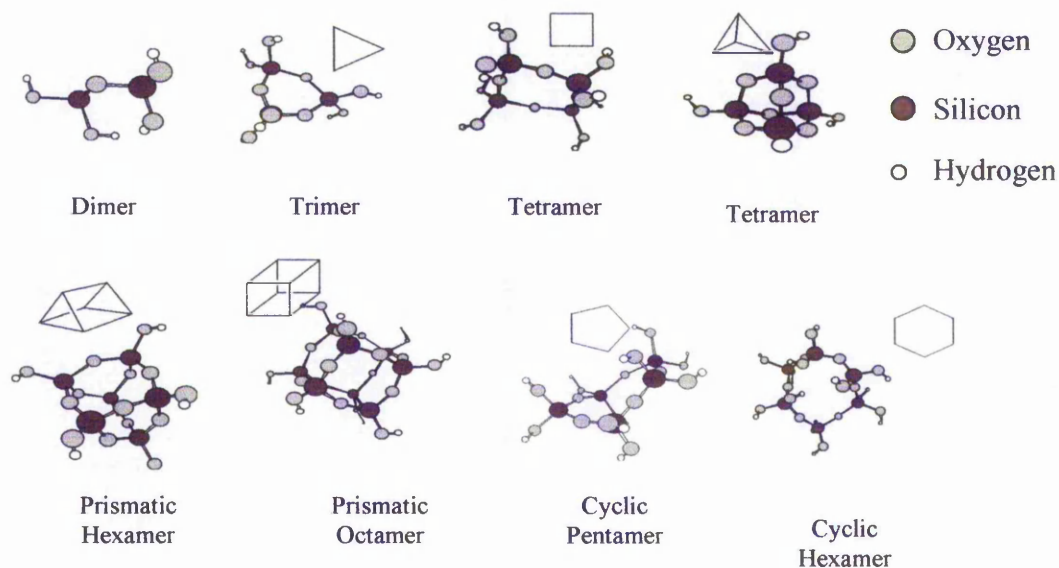


Figure 1.2 Scheme for the growth and aggregation of silica particles under contrasting conditions of pH and ionic strength. Redrawn from Iler²⁹.

Continued growth and size domain sharpening then occurs through Ostwald ripening as smaller particles redissolve and condensation occurs on the larger ones. Under conditions of low salt concentrations and high pH (>7.0), high rates of dissolution and deposition of silica and the tendency for the silica surface to become negatively charged results in mutual repulsion and prevention of aggregation and condensation becomes faster culminating in the continued growth of particles to sizes in excess of 100nm. Addition of salts removes the surface charge and result in aggregation and gelling. At sub neutral pH the silica surfaces bear very little charge and the solubility of silica is low, resulting in rapid aggregation of the already formed particles into chains and then gel networks. As a consequence at low pH and or high electrolyte concentrations the particles making up an aggregate are small (>20nm) whilst at high pH in low electrolyte concentration large (>500nm) isolated particles may be grown. Under various conditions of pH, ionic strengths and the additional presence of structure stabilising agents a whole host of oligomeric silicate species have been shown to exist in solution.



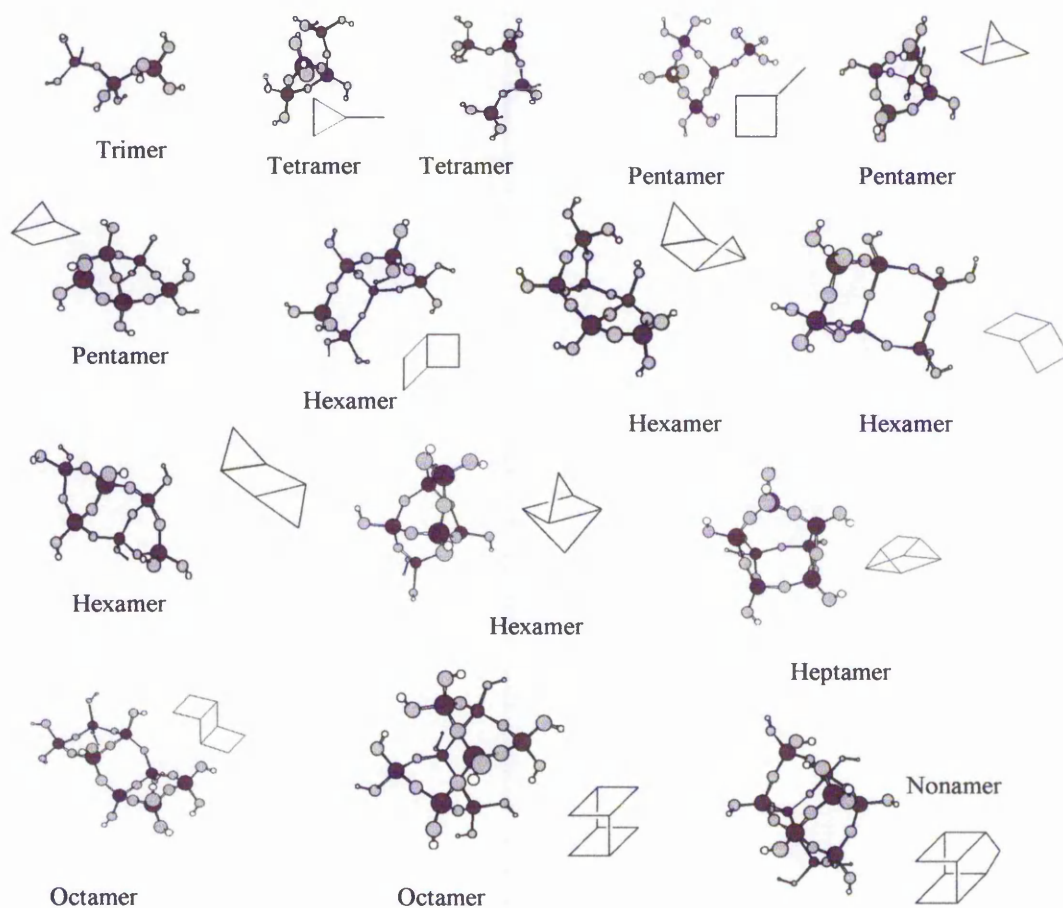


Figure 1.4 Oligomeric silicate species with multiple condensation states.

All of the above species, (Figures 1.3 and 1.4), have been detected and characterised by ^{29}Si nuclear magnetic spectroscopy in various aqueous media³⁵. Many of the structures are central to the formation of natural and synthetic zeolites especially the four five and six membered ring structures which make up the basis of zeolite structures. *Ab initio* calculations³⁶ have suggested that linear silicate species are favoured, but this would result always in the formation of amorphous silica. But recent work³⁷ taking into account aqueous solvation, the possibility of multiply charged species and entropic effects has shown that linear tetramers form from linear trimers in favour of trimer cyclization through the generation of multiply charged anionic species at high pH. However at circumneutral pH the condensation of linear trimers to cyclic ones is still favoured.

Under neutral pH conditions then the stages of condensation would follow:-

monomer > dimer > trimer (cyclization) > oligomers > particles > aggregates/gel

All of these stages can be monitored by the molybdenum blue assay method (a sensitive method for the determination of monosilicic acid in solution) and photon correlation spectroscopy (a method for measuring small ($\sim 2-3 - 3000\text{nm}$), so the effect of condition changes or the introduction of additives can be easily investigated. Further more permanent structural effects “frozen” in to the silica structure during maturation can also be studied by observing differences in porosity by nitrogen gas adsorption analyses and by imaging with electron microscopy.

1.3 Industrial silica production and usage.

Four main types of silica are manufactured globally³⁸, they are fumed silica, silica gel and sols, precipitated silica and microsilica (sometimes known as silica fume). Their uses and methods of production are quite different to each other.

Fumed silica is produced by the continuous high temperature hydrolysis of silicon tetrachloride in a hydrogen/oxygen flame. Submicron particles are produced and the size can be controlled by the process parameters. Uses of fumed silica are many, including additives to paints, sealants, adhesives and in the manufacture of silicone rubbers. Many of its application require its surface to be functionalised to improve mixing and adhesive properties with organic matrices.

Silica gel and silica sols are manufactured by the acid treatment (usually hydrochloric acid) of sodium silicate solutions. Sodium silicate solutions are very basic being effectively mixtures of silica and sodium hydroxide and quite stable. However when their pH is lowered to $< \text{pH } 7$ they spontaneously condense in to silica gel or a silica sol depending on the conditions of pH, concentration and ionic strength of the mixture. The gel or sol then has to be washed repeatedly to remove any entrained sodium ions. Silica gels are famously used as desiccants but they are also used as binding agents in mortar adhesives especially in refractory cements. It is also commonly used as a catalyst or catalytic support when it is co precipitated with alumina to produce synthetic zeolites.

Precipitated silica is produced by the addition of sulphuric acid to sodium silicate. Control of the process through pH, temperature, reaction time, acid concentration and agitation can all be used to manipulate the surface chemistry and physical structure of

the final product. Again considerable effort has to be made to remove sodium and sulphate ions from the silica. The washed silica is usually dried and milled to the required particle dimensions. The main uses of precipitated silica are as additives and fillers in the rubber industry. It is used as a replacement for carbon black to improve resilience in tyres where it shows distinct advantages. One is it reduces rolling friction to such an extent that fuel savings of between 5 and 10% can be made. It also grips the road surface better in wet weather. It is also widely used in improving the resilience of rubber products for other uses. The nature of these uses require its surface to be functionalised with organosilane coupling agents to improve its bonding with other organic materials.

Microsilica is a by product of the silicon and ferrosilicon industry. The waste gases from the furnace used in silicon production generate this material which typically has particle sizes of between 100 and 150nm. It is commonly used as a pozzolan in cements where due to its small particle size produces well ordered cements of high strength. Its use in cement reduces the water requirement and also adds additional binding calcium silicate hydrates as it is able to react with unreacted calcium hydroxide.

1.4 Biomineralisation.

Biomineralisation is the synthesis of minerals from simple compounds by organisms.

This can be for a variety of purposes, including:

- To improve mechanical strength (calcium phosphates in bone or silica in diatoms and radiolaria).
- to orient magnetotactic bacteria (magnetite particles- Fe_3O_4) and pigeons (magnetic particles in beak)³⁹
- for storage of iron (ferritin)

Biominerals also include shells, teeth and skeleta.

Table 1.1 (overleaf) outlines some commonly found Biominerals and their functions:-

CHEMICAL COMPOSITION	MINERAL FORM	FUNCTION/EXAMPLES
Calcium carbonate CaCO ₃	Calcite Aragonite Vaterite Amorphous	Exoskeletons in corals, egg shells, mollusc shells Gravity sensor
Calcium phosphates Ca ₁₀ (OH) ₂ (PO ₄) ₆	Hydroxyapatite	Endoskeletons (human and other vertebrates bones and teeth)
Calcium oxalate CaC ₂ O ₄ .nH ₂ O	Whewellite Weddelite	Calcium storage and defence of plants
Amorphous silica SiO ₂ .nH ₂ O	Amorphous	Valves of diatoms and defence mechanisms in plants
Iron oxides Fe ₃ O ₄ α,γ-Fe(O)OH.5Fe ₂ O ₃ .9H ₂ O	Magnetite Goethite, Lepidocrocite, Ferrihydrite	Magnetic sensors Teeth of chitons Iron storage

Table 1.1 Common biominerals.

The shells of molluscs are made of a material known as nacre, a composite material made of layers of aragonite (calcium carbonate) separated with layers of chitin. The resulting material is 3000 times more resistant to fracture than aragonite alone.⁴⁰

In the bones of vertebrates the inorganic part consists of calcium hydroxyapatite and the organic matrix is a mixture of collagen, glycoproteins and polysaccharides. The inorganic component confers rigidity to structures whilst the organic matrix adds elasticity and tensile strength.

TEM studies reveal that bacterial magnetites are almost perfect crystals,⁴¹ which often violate the cubic crystal symmetry of magnetite. They are usually elongate⁴² in the [111] direction^{43,44} are chemically quite pure Fe₃O₄, and are restricted in size and shape so as to be uniformly magnetized (single-magnetic-domains).

Biominerals have to be formed and dissolved on much shorter timescales than geological minerals so some control has to be exerted on the chemical formation process. For example Calcium carbonate deposition is in general controlled by an equilibrium shift due to the consumption of CO₂.



1.4.1 Biosilicification in diatoms.

Apart from silicification involving sponges, the routes and underlying principles of biosilicification have been studied most intensely in diatoms.

Diatoms have developed a specific organelle for the production of silica called the silica deposition vesicle or SDV for short. And since the thecae fully form inside the SDV the species specific variations in frustule structure must therefore be a consequence of the structure or contents of it. Studies showing that the membrane of the SDV, the silicalemma, has an electrochemical potential across it and that the contents of the lumen must therefore be acidic^{45,46} and resemble the vacuoles and lysosomes of plant and animal cells respectively. A gene family encoding 7 different silicon transporter proteins has been characterised (named SIT1-SIT7) from the diatom *Cylindrotheca fusiformis*⁴⁷ and one member of this family (SIT1) has been shown to mediate sodium ion dependant silicic acid uptake. The amount of silica present in the cell walls of diatom species *Thalassiosira weissflogii* and *Ethmodiscus castri* have been estimated^{48,49} and indicate that prior to formation of the diatom thecae the silicic acid must be at concentrations in the region of 10-100mMdm⁻³, and it has been suggested that soluble and stable silicon complexes may be involved in the storage and transport, although to date apart from one reported transient hypervalent intermediate⁵⁰ this has not been reproducibly verified. Closer inspection of the thecae (epitheca and hypotheca) has shown the presence of a 200kda protein called HEP200 tightly localised at the overlap region. That these are not involved in the deposition of silica around the girdle bands was demonstrated by the inability of HEP200 antibodies to label for girdle band SDV's at any stage of their development. The hypothesis was therefore made that to ensure mechanical integrity of the girdle band following cell division the HEP200 associates with it to maintain structural rigidity.⁵¹ The most significant organic components isolable from the silica frustule after HF treatment were three relatively low mass polypeptides named silaffin 1A, silaffin 1B and silaffin 2 with m/z of 4k, 8k and 17k respectively.⁵²

The C terminal domain of these was found to be dominated by the basic amino acids lysine and arginine and consisted of 7 repeat sequence elements (R1 – R7). Amino acid analysis showed that all of the lysine residues had been post translationally modified. These modifications were found to be ϵ N dimethyl and ϵ N methyl N (propylamine)_n where n = 5 – 10. *In vitro* studies of silica formation using

prehydrolysed tetramethoxysilane solutions showed rapid precipitation of silica on addition of silaffin 1A and an unfractionated mixture of the silaffins. In the presence of silaffin 1A spherical particles of 500 – 700nm were produced whilst with the mixed silaffins smaller particles of ~50nm were produced. Levels of silica precipitated were in proportion to the amount of peptide added and the peptides fully co precipitated with the silica provided that the silicic acid levels were in excess. When less harsh treatments were applied to isolate the silaffins from the silica matrix using ammonium fluoride adjusted to pH 5 with hydrofluoric acid the observed molecular masses of all of the silaffins increased by an amount equivalent to 8 phosphate groups per mole of peptide.⁵³ Analysis by ¹H NMR spectroscopy showed that all of the serine Nat sil 1A residues were phosphorylated. Previous in vitro studies had been conducted using phosphate buffers and when these were repeated with sodium acetate buffers the silaffin Nat sil 1A maintained its effect of precipitating silica particles of 400 – 700nm diameter. Under the same conditions silaffin 1A failed to precipitate but when the presence of phosphate buffer was restored both the Nat sil 1A and silaffin1A

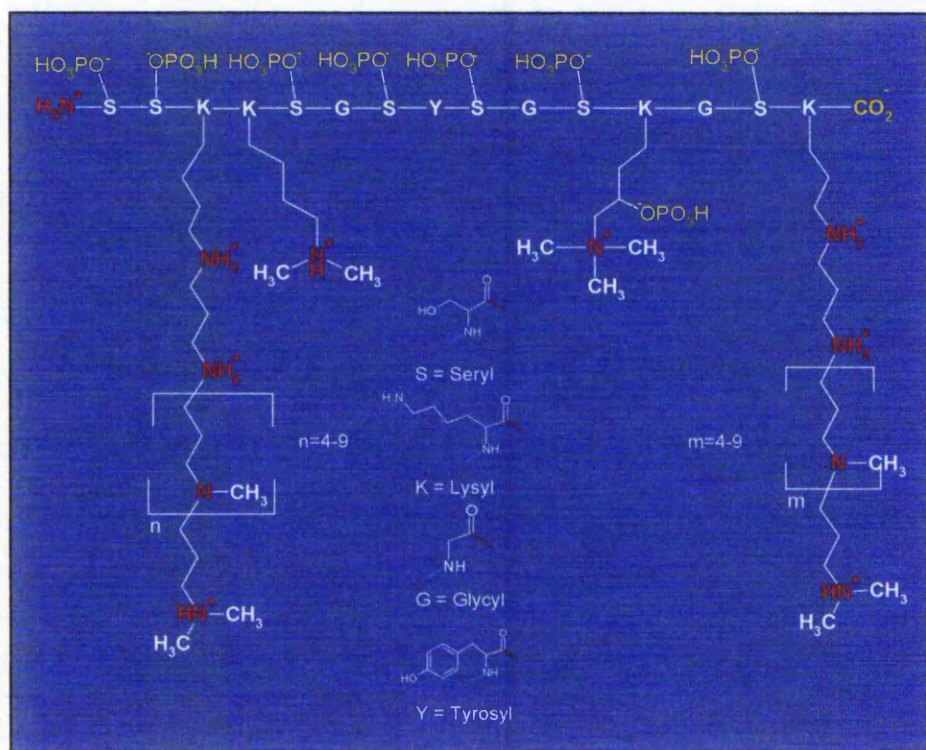


Figure 1.5 Peptide Nat sil 1A isolated from the diatom *Cylindrotheca Fusiformis*.

precipitated equal amounts and morphologically similar material. ³¹P NMR spectroscopy showed that Nat sil 1A formed aggregate structures consisting of no less than 700 molecules in solution. No such assemblages were envisaged for the unphosphorylated silaffin 1A due to its lack of zwitterionic character. It is believed therefore that the formation of self assembled structure is a requirement for silicic acid condensation by a templating mechanism.

A model was proposed where the structure of diatom silica could be mimicked using the amphiphilic nature of methylated polypropylamines resulting in microemulsion formations in aqueous solution. Hexagonal close packed arrangements of the droplets were envisaged to encourage condensation and precipitation of silica at the droplet/water interface. As the silica precipitates, the droplets reduce in size due to their co-precipitation with the silica. Due to this reduction the droplets spontaneously segregate in to smaller droplets and the silica condensation/precipitation continues at the newly formed interface. This process repeats again resulting in three levels of ordered structure of 2µm, 300nm and finally 50nm.⁵⁴

1.4.2 Isolates from silica in plant species

In silicifying plants organic matrices intimately associated with biogenic silica^{55,56} have been isolated. In the horsetail fern, *Equisetum telmateia*, three fractions were identified showing different levels of attachment to the silica. The most easily removed was found to be relatively enriched in the hydroxyl amino acids, serine and threonine, glycine and acidic residues (glutamic and aspartic acids) which together accounted for 70% of the amino acid residues. The 2nd most easily removed fraction showed a partial replacement of the glycine and the hydroxyl amino acids with proline and lysine. The third insoluble fraction contained high levels of lysine, proline and aliphatic amino acids, again lysine is implicated as an active amino acid and proline along with the aliphatic amino acids could play some structural role with proline forming rigid protein structures which may then self assemble under the influence of the more hydrophobic aliphatic residues. These extracts were shown to influence silica condensation both kinetically and morphologically.^{14,57}

Cucurbitae species are also observed to deposit silica as a response to fungal attack.⁵⁸ Again similarly to the C terminal amino acids observed in the diatom these were found to contain 6 repetitive cationic sequences with high levels of lysine in

conjunction with high levels of proline. The suggestion here is that the lysine aids condensation of silica and the proline may provide some rigid structure. Conversely fungal species have been shown to produce silica and titania particles when challenged with solution containing anionic complexes of silicon hexafluoride.⁵⁹

A number of biomimetic or bioinspired approaches have been made in an attempt produce silicas of unusual form and are briefly reviewed here:

1.5 Bioinspired and biomimetic approaches to silica formation.

A distinction has to be made between biomimetic and bioinspired strategies of silica formation. Biomimetic strategies aim to produce silica which resembles biogenic silica, often only at a superficial level, from the whole gamut of chemical species available. The reactions involved therefore have little to do with the biological environment. Bioinspired strategies on the other hand seek to invoke the underlying principles of biosilicification *in vitro* to produce material which quite often doesn't remotely resemble biogenic silica but which has been produced under as much as possible the same benign conditions as occur in nature.

Biomimetic approaches are currently dominant in the search for methods of synthesis of industrially applicable materials but as our knowledge of natural deposition mechanisms improves so will our ability to produce tailored materials for a range of functions. The driving force for this is the desire to move towards green chemistry due to environmental and fiscal cost of industrial synthesis. To this end a large amount of research has been focussed at identifying the subtle mechanisms behind self assembly and catalysis. Results of investigations into bioinspired silica production have resulted in the formation of a number of novel silica structures. The use of extracts from diatomaceous silica has resulted in the controlled formation of variously sized silica spheres^{13,60,61,62} using pre hydrolysed TMOS as the precursor. Polylysine has been shown to produce spherical particles of 100-200nm diameter with solutions of sodium silicate⁶³ and hexagonal platelets with shaken pre hydrolysed TMOS.⁶⁴ Polyallylamine hydrochloride produces large spherical particles with prehydrolysed TMOS when shaken⁶⁵ and chains of smaller particles when stirred,⁶⁶ and the unmodified R5 peptide has produced 400-700 nm spheres under the influence of an electric field and 100-300nm diameter fibres under shear⁶⁷ with pre hydrolysed TMOS. Other studies of polypeptides have shown that at acidic pH polyserine,

polylysine and polyaspartic acid all increase the level of molybdenum active species over time in solutions of sodium silicate.⁶⁸ These solutions are known to contain small silicate oligomers so it appears that the polypeptides here are destabilising them. At higher pH the opposite was found but no specific structures were developed. Continuation of this work⁶⁹ showed that polylysine and polyarginine accelerated the condensation of silicic acid produced from sodium silicate and that the increased rate was dependent on polymer chain length. When colloidal silica was treated with the peptides the sol remained stable until the ratio of polypeptide to silica reached a critical level which was dependent on chain length, the longer chain polypeptides precipitated the silica at lower amine functionality concentrations. Analysis of the supernatant showed that all traces of the polypeptide were removed from solution with the silica. Studies of polypeptides with TEOS⁷⁰ at neutral pH showed that polycysteine, polyserine and polylysine all hydrolyse the TEOS with polylysine being the most effective. This effect was also enhanced with chain length increase. An analysis of the effect of polypeptide secondary structure was conducted using polylysine in both the α helix and β sheet conformations.⁷¹ The results showed that silica produced from TEOS in the presence of α helical poly lysine had a smaller pore size than that condensed in the presence of β sheet, and that the pore diameter mirrored the cross-sectional diameter of the polymer chain. When polyarginine was used with prehydrolysed TMOS⁷² rapid precipitation of silica spheres resulted with incorporation of the macromolecule.

A number of studies with polyallylamine have been conducted. One which used pre hydrolysed TMOS showed the formation of increasingly large spheres the size of which depended on the phosphate buffer concentration.⁷³ Sumper looked at polyallylamine in phosphate buffer systems⁷⁴. It was found that the sol produced with pre hydrolysed TMOS in tris buffer was stabilised with particles as measured by dynamic light scattering measuring 40 to 60nm depending on the pH (smaller particles at lower pH). However it wasn't clear how much polyallylamine was contributing to this value (polyallylamine weight average molecular weight was 15000gmol⁻¹). When the stabilised sol was introduced to phosphate buffer immediate precipitation of silica with a honeycomb structure was produced. This was explained as phase separation of the polyallylamine/phosphate buffer to produce micro-sized droplets. These are viewed as having a net positive charge matching the negative charge on the stabilised sol particles. The consequence of this is that the stabilised sol

is concentrated at the aqueous interface where the excess phosphate ions act as a flocculating agent leaving silica deposition in the gaps between the micro droplets which act as the template. The pore diameters in the honeycomb were about 1 μ m which is around the size of the largest ordered domains observed in diatoms.

In a study to mimic the formation of sponge like silica spicules⁷⁵ polyethyleneimines were used with different side chain functionalities to confer specific linear conformations on the polymer. Precipitation of pre hydrolysed TMOS produced fibrous siliceous structures of about 20-30nm diameter with an axial filament of polyallylamine reminiscent of sponge spicules. Recently the group of Knecht et al⁷⁶ have been investigating the use of amine dendrimers as templates for precipitation from pre hydrolysed TMOS. Dendrimers from G0 to G6 were used in the study and silica spheres with the dendrimer entrapped in the centre were produced. There was some dependence of dendrimer size on the particle size but this dependency decreased with the larger (G3 and above) species suggesting that the flexibility of the dendrimer chains limits the particle diameter.

The state of the current research suggests that there are many methods of producing spherical silica particles (all based on the use of some form of amine) of controlled size, but little success in the control of ordered deposition. The mechanism is also still under debate as the vast majority of data has been collected using pre hydrolysed TMOS which will be made up of a disperse variety of species including partially hydrolysed and partially condensed species. Whether the amines act on monosilicic acid or merely aggregate primary particles is not clear as yet. However the observation that polyamines are involved in a number of biosilicifying systems indicates that research is going to follow this path at least for a while.

References.

- 1) J.L. Kirschvink , J.W. Hagadorn, *in.*, The Biomineralisation of Nano- and Micro-Structures, ed., E. Bäuerlein, Wiley-VCH Verlag GmbH, Weinheim, Germany, 2000, 139-150,
- 2). Frondel C., 1962, - *The system of mineralogy of DANA*, 7th edition, volume 3, Wiley, New York
- 3). P.W Lucas, I.M Turner, N.J Dominy, N Yamashita. *Annals of botany* 2000, 86, 913-920.
- 4). E Epstein. *Proc. Natl. Acad. Sci. USA*. 1994, 19, 11-17.
- 5). H. Motomura, N. Mita, M. Suzuki. *Annals of botany*, 2002, 90, 149-152.
- 6). M. J Hodson, A.G Sangster. *Annals of botany*. 1998, 82, 375-385.
- 7) A. L Carnelli, M. Madella, J. P Theurillat,. *Annals of botany*. 2001, 87, 425-434.
- 8). H. Motomura, T. Fujii, M. Suzuki. *Annals of botany*. 2000, 85, 751-757.
- 9). P.V Monje, E.J Baran. *J. Plant. Physiol.* 2000, 157, 457-460.
- 10). C.C Perry, M.A Fraser. *Phil. Trans. R. Soc. Lond. B*. 1991, 334, 149-157.
- 11). R.E. Hecky, K. Mopper, P. Kilham, E.T. Degens. *Marine biology*. 1973, 19, 323-331.
- 12). D.M Swift, A.P Wheeler, *J. Phycol.* 1992, 28, 202-209.
- 13). N. Kroger, G. Lehmann, R. Rachel, M. Sumper. *Eur. J. Biochem.*, 1997, 250, 99-105.
- 14). N. Kroger, R. Deutzmann, M. Sumper, *Science.*, 1999, 282, 1129-1132.
- 15). J. Kyte., R.F. Doolittle, *J. Mol. Biol.*, 1985, 82, 105-132.
- 16). C.C. Perry, T. Keeling-Tucker. *Journal of Biological Inorganic Chemistry* 2000, 5, (5), 537-550
- 17). "Biomineralization" Baeuerlein E., (Editor) 2000, Wiley VCH 208-214,.
- 18). Y. Zhou, K. Shimizu, J.N. Cha, G.D. Stucky, D.E. Morse., *Angew Chem Int* 1999, 38, 780
- 19). J.N. Cha, K. Shimizu, Y. Zhou, S.C. Christiansen, B.F. Chmelka, G.D. Stucky, D.E. Morse, *Proc Natl Acad Sci USA* 1999, 96, 361
- 20). H. C. Schröder, , A. Krasko, , G. Le Penneec, , T. Adell, , H. Hassanein, I. M. Müller, and W. E. G. Müller, *Prog. Mol. Subcell. Biol.* 2003, 33, 249-268
- 21). T.S Lovering, C.Engel. *Translocation of silica and other elements from rock into Equisetum and three grasses*. 1967, Contributions to general geology, Geological survey

professional paper 594-B U.S Government Printing Office, Washington.

- 22). A.G. Sangster, M.J Hudson,. *In Silicon Biochemistry*. 1986 Ciba foundation symposium 121, J.Wiley & sons, Chichester 90-107.
- 23). E.G Vrieling, W.W.C Giesskes, T.P.M Beelen. *J.Phycol.*, 1999, 35, 548-559.
- 24). "Biochemistry of Silicon and Related Problems" G. Bendz, I. Lindqvist (Editors). Nobel symposium, 40th, Lidinge, Sweden, Plenum press, New York, 1978.
- 25). A. Peggs, H. Bowen., *Phytochemistry.*, 1984, 23, 8, 1788-1789.
- 26). R.D. Hartley, L.H.P. Jones, *Journal of experimental botany.*, 1972, 23, 76, 637-640
- 27). W.H. Casey, E. Epstein, S.D. Kinrade, C.T.G. Knight. D.W. Rains, R.J. Zasoski., 5th Keele meeting on aluminium Feb 2003.
- 28). C.C. Perry, Y. Lu. *J.Chem.Soc.Faraday Trans.*, 1992, 88, 19, 2915-2921.
- 29). C.C. Harrison and N. Loton, *J. Chem. Soc.Faraday Trans.*, 1995, 91, 23, 4287-4297.
- 30). R.K. Iler, *The chemistry of silica*. J Wiley and sons 1979
- 31). S.A. Greenberg, D. Sinclair., *J Phys Chem.*, 1955, 59, 435-440.
- 32). R.K. Iler, *J Colloidal and Interface Sciences.*, 1980, 75, 1, 138-148.
- 33). G.J. Bratton, B.R. Currell, J.R. Parsonage, M.J.K. Thomas. *J Mater Chem.*, 1993, 3, 4, 343-346.
- 34). Mora C. V., Davison C. V., Wild J. M. & Walker M. M. *Nature.*, 2004, 432, 508 - 511.
- 35). C.T.G. Knight, S.D. Kinrade, *J Phys Chem. B.*, 2002, 106, 3329
- 36). J.C.G Pereira, C.R.A Catlow, G.D. Price, *J. Phys. Chem A* 1999, 103, 3268
- 37). M.J. Mora-Fonz, C.R.A. Catlow, D.W. Lewis. *Angew. Chem. Int. Ed.* 2005, 44, 3082-3086.
- 38). T. Kendall, "Industrial minerals", March 2000,49-59
- 39). M. Hanzlik, C. Heunemann E. Holtkamp-Rotzler M. Winklhofer, N. Petersen, G. Fleissner, *Biometals.*, 2000, 13, 4, 325-31.
- 40). C.M. Zaremba, A.M. Belcher, M. Fritz, Y. Lu, S. Mann, P.K. Hansma, D.E. Morse, J.S. Speck, G.D. Stucky. *Chemistry of materials.*, 1996, 8, 3, 679-690.
- 41). S. J. Gould, E. S. Vrba, *Paleobiology.*, 1982, 8, 4.
- 42). P. Westbroek, F. Marin, *Nature* 392 (1998) 861.
- 43). S. Mann, R. B. Frankel, R. P. Blakemore, *Nature* 310 (1984) 405.

- 44). S. Mann, T. T. Moench, R. J. P. Williams, *Proceedings of the Royal Society of London, series B 221* (1984) 385.
- 45). C-W. Li, S. Chu, M. Lee, *Protoplasma.*, 1989, 151, 158-163
- 46). E.G. Vrieling, W.W.C. Gieskes, and T.P.M. Beelen, *J.Phycol.*, 1999, 35, 3, 548-559
- 47). M. Hildebrand, B.E. Volcani, K. Dahlin, *Mol. Gen. Genet.*, 1998, 260, 480-486.
- 48). M.A. Brzezinski, D.J. Conley, *J. Phycol.*, 1994, 30, 45-55.
- 49). T.A. Villareal, L. Joseph, M.A. Brzezinski, R.F. Shipe, F. Lipshultz, M.A. Altabet, *J. Phycol.*, 1999, 35, 896-902.
- 50). S.D. Kinrade, A.M.E. Gillson, C.T.G. Knight, *J. Chem. Soc., Dalton Trans.*, 2002, 307-309.
- 51). N. Kroger, G. Lehmann, R. Rachel, M. Sumper, *Eur. J. Biochem.*, 1997, 250, 99-105.
- 52). N. Kroger, R. Deutzmann, M. Sumper, *J.Biol.Chem.*, 2001, 276, 28, 26066-26070
- 53). N. Poulsen M. Sumper N. Kroger, *Proc. Natl. Acad. Sci, U S A.*, 2003, 14, 100, 21, 12075-80.
- 54). M. Sumper, *Science.*, 2002, 295, 5564, 2430-2433.
- 55). C.C Harrison (now Perry), Y. Lu., *Bull, de l'Institut Oceanographique Monaco.*, 1994, 14, 151.
- 56). C.C Harrison (now Perry), *Phytochemistry.*, 1996, 41, 37-42.
- 57). C.C. Perry, T. Keeling-Tucker. *J. Biol, Inorg, Chem.*, 2000, 5, 5, 537-550.
- 58). H. Kauss, K. Seehaus, R. Franke, S. Gilbert, R.A. Dietrich, N. Kroger, *The plant journal.*, 2003, 33, 87-95.
- 59). V. Bansal, D. Rautaray, A. Bharde, K. Ahire, A. Sanyal, A. Ahmad, M. Sastry., *Journal of Materials Chemistry* 2005, 15, 26, 2583-2589.
- 60). N. Kroger, R. Deutzmann, C. Bergsdorf, M. Sumper, *Proc. Natl. Acad. Sci., USA.*, 2000, 97, 26, 14133-14138.
- 61). N. Kroger, S. Lorenz, E. Brunner, M. Sumper., *Science*, 2002, 298, 584-586.
- 62). N. Poulsen, M. Sumper, N. Kroger., *Proc. Natl. Acad. Sci. USA.*, 2003, 100, 12075.
- 63). T. Coradin, O. Durupthy, J. Livage., *Langmuir.*, 2002, 18, 2331-2336.
- 64). S.V. Patwardhan, N. Mukherjee, M. Steinitz-Kannan, S.J. Clarson., *Chem Commun.*, 2003, 1122-1123.

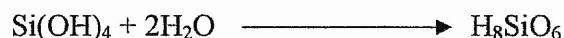
- 65). S.V. Patwardhan, N. Mukherjee, S.J. Clarson., *J. Inorg. Organomet. Polym.*, 2001,11,117-121.
- 66). S.V. Patwardhan, S.J. Clarson., *Mater. Sci. Engin. C*, 2003, 23, 495-499,
and F. Rodriguez, D.D. Glawe, R.R. Naik, K.P. Hallinan, M.O. Stone.,
Biomacromolecules, 2004, 5, 261
- 67). T. Coradin, J. Livage., *Colloids and Surface B: Biointerfaces*, 2001, 21, 329-336.
- 68). T. Coradin, O. Durupthy, J. Livage., *Langmuir*, 2002, 18,2331-2336.
- 69). L. Sudheendra, A.R. Raju., *Materials Research Bulletin*, 2002, 37, 151-159.
- 70). K.M. Hawkins, S.S.S. Wang, D.M. Ford, D.F. Shantz., *JACS*, 2004,
10.1021/ja049936O
- 71). S.V. Patwardhan, S.J. Clarson., *J. Inorg. Organomet. Polym*, 2003, 13,4,
193-203.
- 72). E. Brunner, K. Lutz, M. Sumper. *Phys. Chem. Chem. Phys.*, 2004, 6, 854-857.
- 73). M. Sumper., *Angew. Chem. Int. Ed.* 2004, 43, 2251-2254
- 74). Jian-Jun Yuan, Ren-Hua Jin, *Chem Comm*, 2005, (11), 1399 – 1401
- 75). M.R. Knecht, D.W. Wright., *Langmuir*, 2004, 20, 4728-4732
- 76). M.R. Knecht, S.L. Sewell, D.W. Wright., *Langmuir*, 2005, 21, 5, 2058-2061.

Chapter 2. Experimental methods.

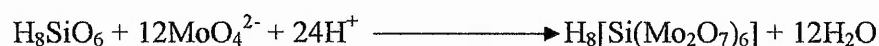
2.1 The molybdenum blue method.

The molybdenum blue method is ideal for the determination of low levels of monosilicic acid in aqueous solution. Being carried out at low pH ensures minimum solubility of any particulate silica present, thus minimizing any interference in the condensing system.

The formation of the complex requires that the monosilicic acid first coordinates with two water molecules:



The fully saturated silicic acid can now react with the acidified molybdate ions to form the yellow silicomolybdate complex which has an absorbance maximum of around 400nm:



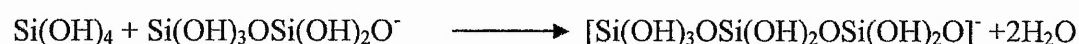
The silicomolybdic acid complex formed by the reaction of molybdic acid with monosilicic acid has a cage structure formed by twelve MoO_6 octahedra made up of four groups of three where each of the three octahedra share an oxygen atom which forms one corner of a central tetrahedron to which the central silicon atom coordinates. The geometry is such that only one silicon atom can reside in the cavity so the method is sensitive only to monomer, or, oligomers which dissociate rapidly to the monomer. Studies of the formation of the complex with silicic acid have shown the reaction to be complete within 75 seconds at 293K when the monomer complexes and 1st order kinetics to be observed with polysilicic acids with slower rates suggesting that the polymer must dissociate to monomer before reaction. Disilicic acid was found to require approximately 10 minutes to fully dissociate and react with the molybdic acid at 293K.

Reduction of silicomolybdic acid produces the blue silicomolybdous acid complex which has an absorbance maximum at 810nm with a much greater extinction coefficient than the silicomolybdic species, making it more sensitive and able to give

reliable quantitative data at concentrations of monosilicic acid as low as 0.1 ppm. The reducing agent used for this purpose has to be strong enough to reduce the silicomolybdic acid complex fast enough to prevent any interference from silicate oligomer dissociation but gentle enough to prevent reduction of any uncomplexed molybdenum reagent. A method developed for the analysis of silicate species in sea and natural waters uses an acidic mixture of 4-methylaminophenol (METOL), oxalic acid and sodium sulphite to perform the reduction within 90 minutes to give a solution of silicomolybdous acid which is stable for at least 48 hours at room temperature. The additional benefit of this method is that silicate oligomer dissociation is minimised by the acidic pH (~1.5) of the Molybdic acid reagent.

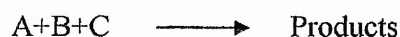
Kinetic analysis.

The observed changes in the absorbance of the molybdenum blue assay are a result of the loss of both monomer and dimer from the condensing system and during the early stages of condensation this is due solely to the formation of the trimer:



So the apparent net loss of monomer is equivalent to 3 Si(OH)₄

Accordingly the reaction appears termolecular i.e.:



With A,B and C being monosilicic acid the normal rate expression reduces to:

$$\frac{dx}{dt} = k(a-x)^3 \quad (1)$$

Where a = concentration of reagent at time t = 0

x = concentration of product at time t

Rearranging and integrating gives:

$$\frac{1}{2(a-x)^2} = kt + \text{constant} \quad (2)$$

When t = 0, x = 0 the constant reduces to 1/2a² and therefore:

$$kt = \left(\frac{1}{2(a-x)^2} \right) - \left(\frac{1}{2a^2} \right) \quad (3)$$

Rearranging gives:

$$\frac{1}{2(a-x)^2} = kt + \frac{1}{2a^2} \quad (4)$$

(a-x) here represents the measured $[\text{Si}(\text{OH})_4]$ at a time, t,

So a plot of $1/[\text{Si}(\text{OH})_4]^2$ against time should give a straight line of gradient 2k where 3rd order kinetics are observed.

After this stage further reduction in the observed absorbance is the result of condensation of monomer on to increasingly large oligomers, a process which is reversible as some of the oligomers redissolve. This stage can be represented as:



k_+ and k_- are the rate constants for the forward and reverse processes, respectively, which are both assumed to be first order. The rate expression is:

$$\text{Rate} = -d[A]/dt = k_+[A] - k_-[B] \quad (5)$$

The rate of change in the concentration of A is the difference between its rate of consumption via the forward process and its rate of production via the reverse process. If the initial concentration of B is 0, then at any point during the process, $[B] = [A]_0 - [A]$. So the equation becomes:

$$-d[A]/dt = (k_+ + k_-)[A] - k_- [A]_0 \quad (6)$$

This can be integrated, but the resulting expression will not be linear. To eliminate the $k_- [A]_0$ term, let $[A]_\infty$ represent the equilibrium concentration of A,

$$-d[A]_\infty/dt = (k_+ + k_-)[A]_\infty - k_- [A]_0 \quad (7)$$

Subtracting (7) from (6) eliminates the $k_+ [A]_0$ term, giving

$$-d([A] - [A]_{\infty})/dt = (k_+ + k_-)([A] - [A]_{\infty}) = K([A] - [A]_{\infty}) \quad (8)$$

Where

$$k = (k_+ + k_-)$$

Integration gives:

$$\ln([A] - [A]_{\infty}) = -kt \quad (9)$$

This equation is integrated in the variable $[A] - [A]_{\infty}$, which is the *deviation* of the concentration of A from the equilibrium value. Thus (9) shows that in a reversible first-order process, the approach to equilibrium is governed by first-order kinetics. A plot of $\ln([A] - [A]_{\infty})$ against t will be linear, with slope $-k$, the sum of the forward and reverse rate constants.

Isolation of the forward and reverse rate constants:

The equilibrium constant:

$$k = \frac{k_+}{k_-} = \frac{p_{\infty}}{a_{\infty}} \quad (10)$$

here p_{∞} is the concentration of silica and a_{∞} is $[\text{Si}(\text{OH})_4]$, both at equilibrium.

Rearranging gives:

$$k_+ = \frac{p_{\infty} k_-}{a_{\infty}}$$

Substituting in to slope = $-k$ gives:

$$\text{Slope} = \left(\frac{p_{\infty}}{a_{\infty}} + 1 \right) k_-$$

2.2 Photon correlation spectroscopy (PCS).

Colloidal submicron particles are subject to diffusion through Brownian motion through collisions with molecules of the suspension medium. The diffusion coefficient of this process is a measure of the rate of diffusion of the particles through the medium, and this is a function of particle size, medium viscosity and temperature. The particle movement can be detected by the way that a beam of light is scattered and modulated as the particles move through it. The particles move randomly in 3 dimensions under Brownian motion and consequently the distance, x , of a particle from its origin at time 0 to its position at a later time, t , will be \sqrt{Dt} where D is the diffusion coefficient.

The movement of the particle through a fluid is subject to the particles size and viscous drag, F_d , of the fluid and is related by the Stokes' law:

$$F_d = \frac{6\pi\eta r \bar{x}}{t}$$

where, η = fluid viscosity
 r = hydrodynamic radius of the particle.
 \bar{x} = the mean distance of the particle from the origin

The viscous drag is also dependent on the kinetic energy, E , of the system:

$$E = F_d \bar{x}$$

and,

$$E = kT$$

where k = Boltzmann's constant
 T = temperature Kelvin

and since,

$$D = \frac{x^2}{t}, \quad \text{and } r = \frac{d}{2}$$

then,

$$KT = \frac{6\pi\eta dD}{2}$$

so

$$D = \frac{KT}{3\pi\eta d} \quad \text{The Stokes-Einstein equation}$$

Measurement of D:

D is determined by comparing consecutive measurements of the light signal received by the detector (photomultiplier) in a process termed autocorrelation. The autocorrelation function which depends on the fluctuations observed between these measurements is defined as:

$$G(\tau) = \langle I(t) \cdot I(t + \tau) \rangle$$

where $I(t)$ = intensity at time t

$I(t + \tau)$ = intensity at time t + tau

τ = delay time

$\langle \rangle$ = average time

G = auto-correlation function

In this way if G has a high value then consecutive measurements correlate closely meaning that the particle motion between measurements was small and therefore slow indicating a large particle. Similarly if G has a low value then there is little correlation between the measurements so the particle must be fast moving and therefore small. Measurement of G over a range of delay times allows fluctuation rates to be observed as a decaying exponential where the decay time is related to the particle size. For a

monodisperse colloid this will be a single decaying exponential but in the case of a polydisperse system the signal measured is a composite auto-correlation function of all the particles interacting with the light beam and these are mathematically separated to give individual diffusive measurements.

The decay constant, ($\gamma = \frac{1}{\text{decaytime}}$), can be related to the diffusion coefficient D by:

$$\gamma = DK^2$$

and

$$K = \frac{4\pi n \sin\left(\frac{\theta}{2}\right)}{\lambda}$$

where λ = wavelength of the light source

θ = angle of scattering measurements

γ = decay constant

n = refractive index of suspension medium

So with a fixed wavelength laser as the light source the radii of particles can be determined as long as the temperature, solvent viscosity, angle of scattering and particle density are known.

2.3 Nitrogen gas adsorption/desorption analysis.

Samples for nitrogen adsorption/desorption analyses are first degassed under suitable temperature and pressure to remove water and other adsorbed contaminants. Once degassed the samples are evacuated and held at the boiling point of the adsorbate gas, e.g. if the adsorbate is nitrogen then the samples are held in evacuated tubes immersed in liquid nitrogen, and the temperature allowed to equilibrate. After equilibration a small measured amount of adsorbate is then admitted into the sample holder and the pressure continually monitored. Further additions of adsorbate are made until a predetermined partial pressure, p/p_0 , value is attained and the total adsorbate admission required to reach this is determined. An adsorption isotherm is then constructed by repeating this process for increasing p/p_0 values up to unity i.e. for

p/p_0 values of 0- 1. A desorption isotherm is then constructed by stepwise reduction of p/p_0 by the application of a vacuum. The isotherms thus developed are a measure of the amount of adsorbate on a surface over a range of relative pressures. The nature of the surface and adsorbate in terms of surface area , porosity and energy of adsorption all affect the shape of the isotherms which can then be used to gain an insight in to the nature of the material under analysis.

Brunauer, Deming, Deming and Teller (BDDT) classified these isotherms in to 5 types (figure 2.3.1).

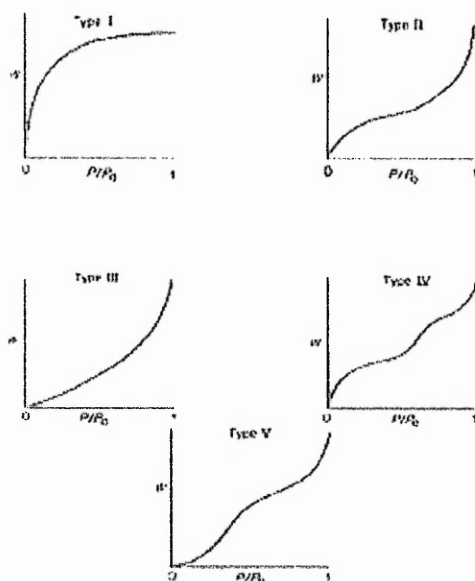


Figure 2.3.1. Type I – V isotherms according to BDDT. Reproduced from Quantasorb, NOVWin2 / 2-P Ver. 2.1 Operation Manual P/N 05079

Type I or Langmuir isotherms are concave to the P/P_0 axis and the amount of adsorbate approaches a limiting value as P/P_0 approaches 1. Type I physisorption isotherms are exhibited by microporous solids having relatively small external surfaces, for example, activated carbons and molecular sieve zeolites. The limiting uptake of adsorbate is governed by the accessible micropore volume rather than by the internal surface area.

Type II isotherms are the normal form of isotherm obtained with a nonporous or macroporous adsorbent. This type of isotherm represents unrestricted monolayer-

multilayer adsorption. The start of the linear central section of the isotherm, is usually taken to indicate the relative pressure at which monolayer coverage is complete.

Type III isotherms are convex to the P/P₀ axis over its entire range. Type III isotherms are rarely encountered. A well-known example is the adsorption of water vapour on nonporous carbons. The absence of a distinct point B on type III isotherms is caused by stronger adsorbate-adsorbate than adsorbate-adsorbent interactions.

Type IV isotherms are associated with capillary condensation in mesopores, indicated by the steep slope at higher relative pressures. The initial part of the type IV isotherm follows the same path as the type II.

Type V isotherms are uncommon, corresponding to the type III, except that pores in the mesopore range are present.

Surface area measurements.

Brunauer, Emmett, Teller (BET) method:

$$\frac{1}{W\left[\frac{p_0}{p} - 1\right]} = \frac{1}{WmC} + \frac{(C-1)p}{WmC p_0}$$

Where: W = The weight of nitrogen adsorbed at a partial pressure of p/p₀

Wm = The monolayer weight of nitrogen

C = The BET constant which is related to the magnitude of adsorbant/adsorbate interactions (heat of adsorption) = $e^{\frac{E_1 - E_l}{RT}}$ where:

E₁ is the heat of monolayer adsorption and E_l the heat of liquefaction of the adsorbate. For high adsorbant/adsorbate affinities C is large and for low affinities C is small but still positive.

Using the multipoint method typically a partial pressure range of 0.05-0.30 for monolayer coverage is employed and a plot of:

$$\frac{1}{W\left[\left(\frac{p_0}{p}\right) - 1\right]} \text{ against } \frac{p}{p_0}$$

has a slope of:

$$\frac{C-1}{WmC} \text{ and an intercept of } \frac{1}{WmC},$$

so C can be found as

$$\frac{\text{slope}}{\text{intercept}} + 1$$

and Wm as:

$$\frac{1}{\text{slope} + \text{intercept}}$$

The total surface area of the analysed sample can then be calculated from:

$$St = \frac{WmNA_{cs}}{M}$$

where:

N = Avogadro's number (6.023×10^{23} molecules/mole)

M = Molecular weight of adsorbate

A_{cs} = Cross sectional area of a single molecule which for nitrogen is taken to be 16.2 \AA^2 for a hexagonal close packed monolayer at 77K.

Specific surface areas are then usually reported as area in m^2 per gram.

Porosity measurements.

Terminology:

Micropores - $\leq 20 \text{ \AA}$ diameter

Mesopores - 20 - 500 \AA diameter

Macropores > 500 \AA

Type IV isotherms which are associated with mesoporous materials usually exhibit hysteresis where the adsorption and desorption branches take different paths. deBoer identified 5 distinct hysteresis types (figure 2.3.2)

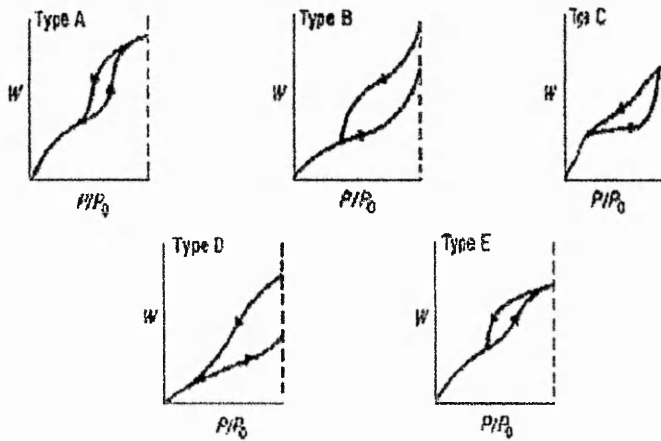


Figure 2.3.2 Hysteresis types according to deBoer. Reproduced from Quantasorb, NOVWin2 / 2-P Ver. 2.1 Operation Manual P/N 05079

Type A hysteresis is attributed to cylindrical pores; type B is associated with slit-shaped pores; type C hysteresis is produced by wedge-shaped pores with open ends; type D loops result from wedge-shaped pores with narrow necks at one or both open ends. The type E hysteresis loop has been attributed to "ink-bottle" pores. Characteristically, the hysteresis loops in all isotherms close before reaching a relative pressure of 0.3 in the desorption process except when microporosity is present.

Pore volume and average pore radii.

The total pore volume is determined by the amount of vapour adsorbed at $p/p_0 \sim 1$. Materials without macropores domains show a horizontal isotherm at higher p/p_0 values and the pore volume is therefore clearly defined. For macroporous materials the isotherms rapidly rise as p/p_0 values approach 1 and may become practically vertical. The adsorbed volume attained can however still be used for the determination of total pore volume provided careful control over temperature has been exercised.

Pore volume may be determined as the equivalent liquid volume of gas adsorbed using;

$$V_{liq} = \frac{P_a V_{ads} V_m}{RT} \dots\dots\dots(1)$$

where P_a and T are local pressure and temperature respectively V_{ads} is the volume adsorbed as vapour and V_m is the molar volume of liquid adsorbate which for liquid nitrogen is taken to be $34.7\text{cm}^3\text{mol}^{-1}$.

Average pore size.

The average pore size, r_p , can be estimated from the pore volume. In the case of type A hysteresis which assumes cylindrical pores $r_p = \frac{2V_{liq}}{S}$ where s = the surface area of the sample.

Pore size distributions.

Pore size distributions reflect the porosity of the material relative to the different pore size domains. The desorption branch is usually used for this measurement since isotherms usually show higher adsorption at lower p/p_0 values and hence a lower free energy state and is therefore closer to true thermodynamic stability. Using the Kelvin equation, (which assumes cylindrical pores), in the form:

$$r_k = \frac{-2\gamma V_m}{RT \ln\left(\frac{P}{P_0}\right)} \dots\dots\dots(2)$$

where:

γ = Surface tension of the adsorbate at its boilingpoint

V_m = Molar volume of adsorbate as liquid

R = Gas constant

T = Boiling point of adsorbate

p/p_0 = relative pressure

r_k = Kelvin radius of pore

For nitrogen this equation reduces to:

$$r_k = \frac{4.15}{\log \frac{P}{P_0}} \text{ in } \text{Å} \dots\dots\dots(3)$$

Here the Kelvin radius is the radius in which condensation occurs at p/p_0 . However since adsorption has already taken place on the walls of the pores, r_k is not actually

the pore radius and similarly on desorption a layer remains. The actual pore radius r_p is given by:

$$r_p = r_k + t,$$

where t is the thickness of the adsorbed layer which for nitrogen is taken to be:

$$t = 3.54 \frac{V_{ads}}{V_m} \dots\dots\dots(4)$$

Barrett, Joyner and Halenda (BJH) method.

Initially at $p/p_0 \sim 1$ the largest filled pore of radius r_{pi} is made up of a physically adsorbed layer of thickness t_1 and an evaporative inner (Kelvin) capillary of radius r_k :
The relationship between the pore volume V_{pi} and the inner capillary (Kelvin) volume V_K is given by:

$$V_{pi} = V_{ki} \frac{r_{pi}^2}{r_{ki}^2} \dots\dots\dots(5)$$

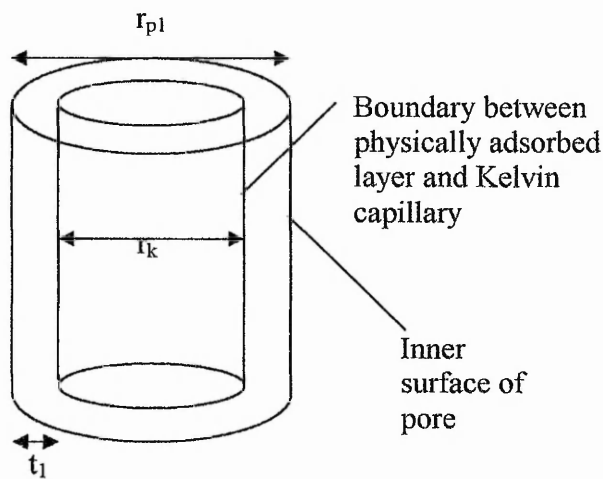


Figure 2.3.3 Cylindrical pore.

By lowering p/p_0 to $(p/p_0)_2$ a desorption of ΔV_1 of adsorbed gas occurs. This is a consequence of emptying of the largest pore and also a thinning of the physically adsorbed layer by an amount Δt_1 . As a consequence of the desorption (5) may now be rewritten:

$$\Delta V_1 = \frac{(r_{k1} + \Delta t_1)^2}{r_{p1}^2} V_{p1}$$

and if

$$\frac{r_{p1}^2}{(r_{k1} + \Delta t_1)^2} = R_1$$

then

$$V_{p1} = R_1 \Delta V_1 \dots\dots\dots(6)$$

When the pressure is reduced further from $(p/p_0)_2$ to $(p/p_0)_3$ the volume of liquid desorbed (V_2) comprises the loss of the Kelvin capillary from the 2nd largest pore, thinning of its physisorbed layer and a further thinning of the 1st pores adsorbed layer. The volume of liquid lost from the 2nd pore is therefore:

$$V_{p2} = R_2(\Delta V_2 - V\Delta t_2) \dots\dots\dots(7)$$

where,

$$R_2 = \left(\frac{r_{p2}}{r_{k2} + \frac{\Delta t_2}{2}} \right)^2$$

and

$$V\Delta t_2 = \pi L_2 (r_{k1} + \Delta t_1 + \Delta t_2)^2 - \pi L_1 (r_{k1} + \Delta t_1)^2$$

$V\Delta t_2$ is the volume desorbed by thinning of the 2nd pore and can also be expressed as:

$$V\Delta t_2 = \Delta t_2 A_{C_1} \dots\dots\dots(8)$$

where A_{c1} is the average area from which the physically adsorbed gas is desorbed. Equation (8) may be generalised to represent any one of the steps in a stepwise desorption process by writing in the form:

$$V\Delta t_n = \Delta t_n \sum_{j=1}^{n-1} A_{c_j} \dots\dots\dots(9)$$

This result is the sum of the average area of infilled pores down to but not including the pore that was emptied in the n^{th} desorption.

Substituting $V\Delta t_n$ for $V\Delta t_2$ in (7) gives

$$V_{pn} = \left(\frac{r_{pn}}{r_{kn} + \frac{\Delta t_n}{2}} \right)^2 (\Delta V_n - \Delta t_n \sum_{j=1}^{n-1} A_{c_j}) \dots\dots\dots(10)$$

This represents the exact expression for calculating the pore volumes at various relative pressures.

The quantity A_c is not a constant value as it varies with each decrease in p/p_0 . A_p (the area of each pore) however is constant and can be found from:

$$A_p = \frac{2V_p}{r_p} \dots\dots\dots(11) \text{ assuming cylindrical pores}$$

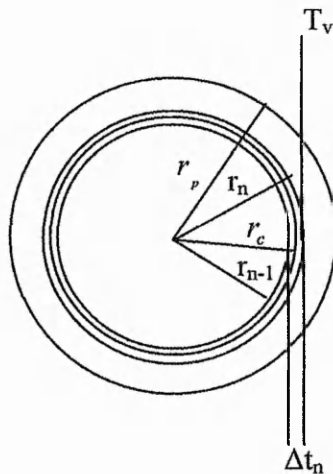


Figure 2.3.4 The change in thickness Δt_n of the physically adsorbed layer of a previously emptied pore of radius r_p during the n^{th} desorption step.

Assuming that all capillaries emptied during a relative pressure decrement have an average radius of r_p corresponding to the radii at the upper and lower pressure extremes. Figure 2.3.4 represents the change in thickness Δt_n of the physically adsorbed layer of a previously emptied pore of radius r_p during the n th desorption step. The capillary radius before desorption is r_{n-1} and after is r_n . The average radius is r_c . Since the capillary and pore are concentric the average area of the capillary during the desorption step which produces

$$\Delta t_n = A_p \frac{r_c}{r_p}$$

also $r_c = r_p - t_v$ where t_v is the thickness of the physically adsorbed layer at the corresponding value of p/p_0 .

So let

$$\frac{r_c}{r_p} = \frac{r_p - t_v}{r_p} = C \dots\dots\dots (12)$$

Then substituting C into (10) gives:

$$V_{pn} = \left(\frac{r_{pn}}{r_{kn} + \frac{\Delta t_n}{2}} \right)^2 \left(\Delta V_n - \Delta t_n \sum_{j=1}^{n-1} C_j A_{pj} \right) \dots\dots\dots (13)$$

Equation (13) provides a practical basis for the computation of pore volume distributions with respect to pore radii. It depends only on the two fundamental assumptions that: (1) the pores are cylindrical (in that pore volume and capillary volume are related to each other as the square of their cross sections), and (2) that the amount of adsorbate in equilibrium with the gas phase is retained by the adsorbent by two mechanisms: (a) physical adsorption *on* the pore walls, and (b) capillary condensation in the inner capillary volume.

2.4 Nuclear magnetic resonance spectroscopy (NMR).

Nuclei of elemental isotopes with odd numbers of protons, neutrons or both possess mechanical spin phenomenon characterised by a nuclear spin quantum number, I , where:

$$I = \frac{1}{2}n \quad (n = \text{integer } 1,2,3 \text{ etc})$$

The number of permissible energy levels = $2I + 1$, so for example nuclei such as hydrogen with a nuclear spin quantum number of $\frac{1}{2}$ there are $2 \times \frac{1}{2} + 1 = 2$ permissible energy levels. These are precessional energy levels where the frequency of precession = the Larmor frequency and the potential energy of the nucleus is given by:

$$E = -\mu B \cos \theta$$

Where θ = angle of precession = angle between the direction of the magnetic field and the axis of nuclear rotation. When energy is applied in the form of radio frequency irradiation the nucleus flips to the higher energy state such that its magnetic moment now opposes the direction of the applied field.

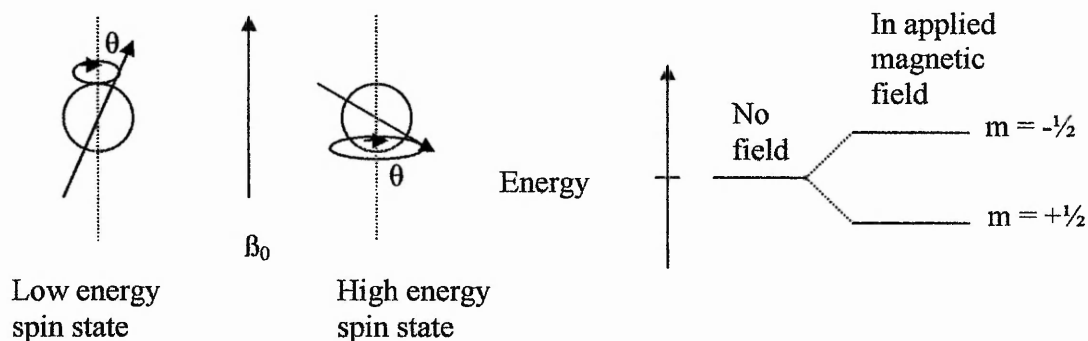


Figure 2.4.1 Alignment of nuclei with spin quantum number, $I, = \frac{1}{2}$ in a magnetic field.

The energy barrier between the two spin states.

Because the positively charged nucleus is spinning it generates a magnetic field and therefore possesses a magnetic moment, μ , which is proportional to the nuclear magnetic spin quantum number I such that:

$$\mu = \frac{\gamma h}{2\pi}$$

where γ = the magnetogyric ratio (a constant for a given nucleus)

and h = planks constant.

The energy of a particular energy level is:

$$E = \frac{\gamma h}{2T} MB$$

where B is the strength of the magnetic field at the nucleus.

The energy difference between levels (the transition energy) is given by:

$$\Delta E = \frac{\gamma h B}{2T}$$

So if the magnetic field, B is increased so too is the transition energy and hence the resolution of the spectrum is improved.

Once the population of the upper and lower energy states are equilibrated the system is said to be saturated. When the RF is removed the population of nuclei promoted to the higher energy states begin to lose energy by non radiative thermodynamic relaxation processes, resulting in a higher vibrational and rotational energy in the system and hence a small rise in temperature. The time required for this process is known as the relaxation time, t , and is defined as the average lifetime of a nucleus in the higher energy state. This value is dependent on the magnetogyric ratio and the mobility of the lattice. When collecting spectra it is desirable, especially where quantitative analysis is being attempted, to ensure that all populations of nuclei return to the pre-applied RF state since the size of the signal is dependent on the population

excess. When in the magnetic field the population of nuclei in the lower energy state is slightly more than that of the high energy state (for protons the excess is 6 in 10^6). To ensure that this is the state at the start of any pulse sequence a pulse delay is applied, following any nuclear perturbation, which exceeds the relaxation time required for the nucleus under investigation.

Chemical shift.

The magnetic field observed by the nucleus is modified by the presence of local electron densities. S orbitals orbiting in spherical shells produce a magnetic field which opposes the direction of the applied field. In order for the energy transfer required for the nuclear flip to occur, a higher field must be applied. This "upfield shift" is termed the diamagnetic shift. P orbital electrons by comparison produce relatively large magnetic fields at the nucleus and create a low field or paramagnetic shift. The position of proton signals is due entirely to S orbital electrons, the strength or, upfield shift being dependent largely on the electronegativities of adjoining species i.e. the more electronegative the neighbour the greater the electron withdrawal and the lower the field strength required.

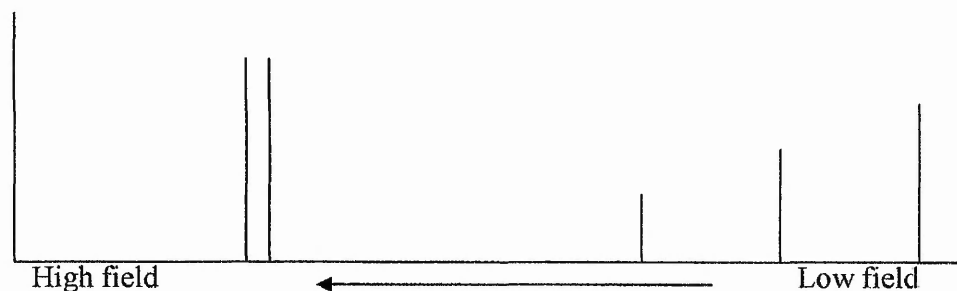


Figure 2.4.2 Direction of arrow - increasing electronegativity of neighbouring group and decreasing applied field strength.

Spin-spin coupling.

The local magnetic environment of a nucleus is affected by the magnetic spin state of neighbouring nuclei. For example a proton neighbouring a methene group

(e.g. $-\underline{\text{CH}}-\text{CH}_2-$) will have its magnetic environment modified by nuclei in high and low energy states. With 2 adjacent protons the chances of them being high or low energy can be depicted as:

$\uparrow\uparrow$ - both high

$\uparrow\downarrow$ or $\downarrow\uparrow$ - one high one low

$\downarrow\downarrow$ - both low

the signal is therefore split as a triplet with signal area ratios of 1:2:1. Similarly the methene group will couple with the methyne proton which can either be in the high or low energy state with equal possibility and hence the methylene group will be split as a 1:1 doublet. The magnitude of the separation of these peaks is known as the coupling constant (measured in hertz) and is observed to vary depending on proximity and steric constraints between neighbouring groups. This coupling is therefore often useful in assigning absolute chemical structures to the spectra of unknown compounds.

2.5 Thermogravimetric analysis (TGA)

Thermogravimetric analysis (TGA – sometimes thermal gravimetric analysis) is a simple technique which measures weight change in a sample against temperature change.

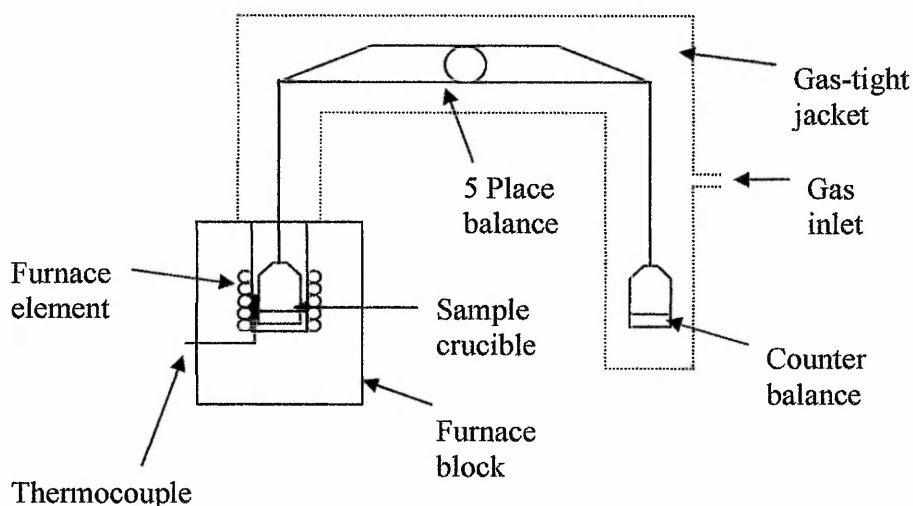


Figure 2.5.1 Schematic of Thermogravimetric balance.

Typically milligram samples in a platinum crucible are suspended from a sensitive balance into a furnace. The weight of the material in the crucible is then monitored as the temperature is increased at a known rate. The atmosphere in which the sample is held is selected depending on the type material and the thermal transformation expected. Typically with silica under nitrogen the loss of adsorbed water is observed over a wide range of temperature depending on the nature of adsorbance. Physisorbed water is removed from room temperature to about 150°C (the temperature range is due to relative ease of removal of surface water compared to that in narrow pores). At temperatures from 150° - 400°C hydrogen bonded water is removed and finally at higher temperatures silanol condensation occurs, a process which continues even at the highest temperatures employed due to the increasing difficulty of water removal as pore closure occurs due to the silanol dehydration. Non oxidative decomposition of organic components occurs typically from 300° - 600°C and results in sample darkening due to residual graphitic material which may be removed by heating in air to 800°C, however with some materials the formation of non volatile oxides may occur with accompanied weight gain.

2.6 Mass spectrometry (MS).

In a mass spectrometer ions generated from an analyte are separated according to their mass:charge m/z ratio. A number of methods for producing the ions and subsequent mass-charge separation are available, the method chosen being determined by the nature of the analyte. In addition a number of tandem techniques have been developed which use gas chromatography or high performance liquid chromatography interfaces to provide pre mass analysis separations.

2.6.1 Ion generation.

Electrospray ionisation(ESI).

This method of ion generation has advantages and disadvantages when compared with other ionisation techniques, but no other method combines the advantages with the ability to interface with aqueous solution samples so well. Advantages offered include: (i) ESI is a soft ionisation technique in that low energy transfer to the analyte ensures that minimal fragmentation of even labile compounds such as proteins takes

place enabling easy detection of molecular ions. (ii) Potential to generate positively, negatively and multiply charged ions extending the number and mass range of species which may be investigated. (iii) Analyte does not need to be volatile as ions are generated in aqueous solution. (iv) Ionisation is carried out at atmospheric pressure so the ions pass quickly under potential gradients into the evacuated region.

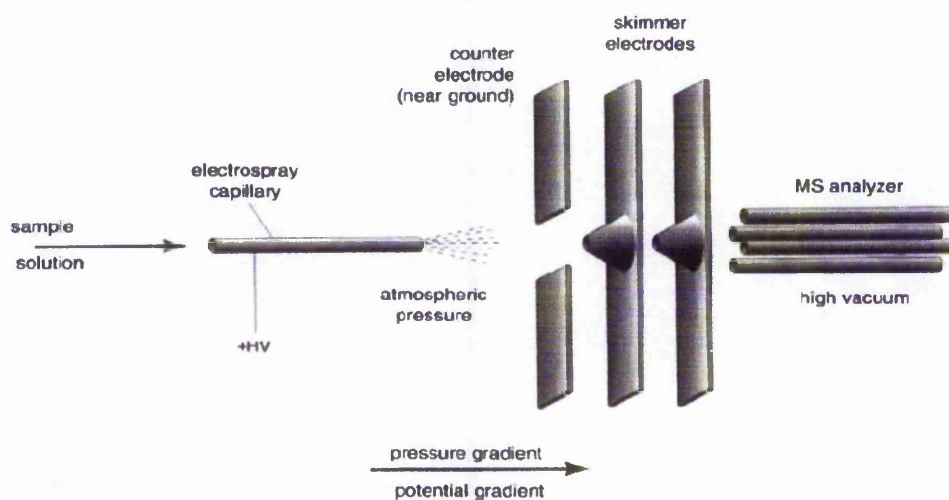


Figure 2.6.1 Electrospray ionisation mass spectrometer schematic – reproduced from *J. Mass Spectrom*, 32, 677-688 (1997)

The analyte solution is passed through a capillary held at high potential and ions in the solution circumlocate to the capillary/liquid interface. If the field applied is high enough the Taylor cone is drawn out as a filament which produces charged droplets as the surface tension of the solvent is exceeded by the applied electrostatic force.

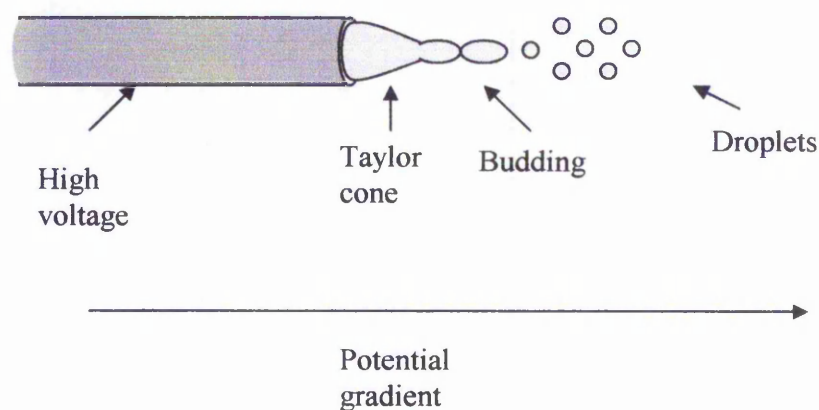


Figure 2.6.2 Charged droplet production in esi source.

The efficiency of the droplet formation, (number, size and dispersity of the droplets), is dependent on the applied field, solution flow rate and solvent properties.

As the droplets travel from the capillary tip towards the counter electrode solvent is lost through evaporation and the droplets begin to shrink. As the surface charge density increases due to this shrinkage the Rayleigh limit is reached and as this is the point at which charge density overcomes the surface tension holding the droplet together, coulombic explosion occurs. Upper charge estimates for stable spherical droplets is given by:

$$q^2 = 64\pi^2 \epsilon \sigma r^3$$

where q is the charge limit

ϵ is the permittivity of vacuum

σ is the surface tension

r is the radius of the droplet

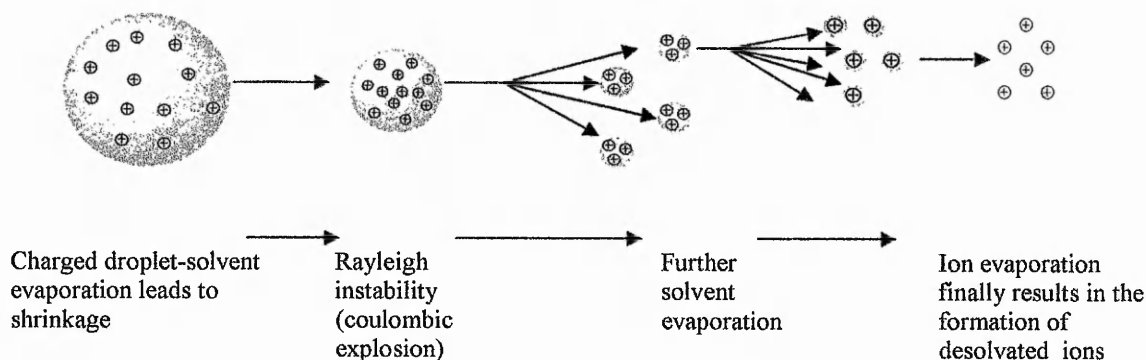


Figure 2.6.3 Ion formation at atmospheric pressure from charged droplets during evaporative processes.

Continued evaporation and fission result eventually in droplets containing single ions, a process thought to be aided by ion evaporation – the mechanism proposed to be driven by repulsive forces and resulting in the migration and eventual evaporation of ions from the droplet surface. The resulting solvent free ions which may hold a single or multiple charge then pass through the skimmer electrodes. A curtain gas of nitrogen applied perpendicularly to the ion beam sweeps any neutral or slow moving species away from the orifice.

The overall process of ion removal at the capillary tip and arrival at the counter electrode was recognised as an electrolytic cell process where oxidation processes at the capillary (in positive ion mode) are matched by reductive processes at the counter electrode. The flow of charge (the rate at which charge leaves the capillary as droplets) i.e. the current = i_{es} and can be expressed theoretically by the Hendrick equation:

$$i_{es} = H v_f^v \delta_s^n E_c^e$$

where H = a constant which depends on the dielectric constant and surface tension

v_f = flow rate

δ_s = specific conductivity

E_c = imposed electric field

The oxidation/reduction of species at the capillary can therefore be manipulated by altering solution conductivity with addition of electrolytes to increase the i_{es} and hence induce ionisation of less electroactive species.

2.6.2 Ion separation.

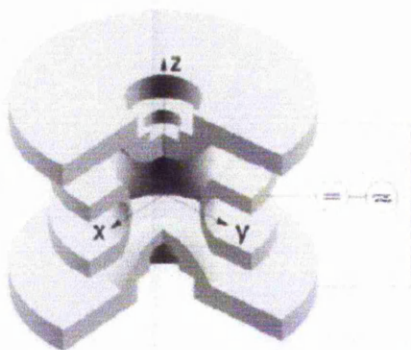


Figure 2.6.4 The ion trap – Ions held in a stable trajectory in the XY plane are destabilised and ejected through the Z axis. Image reproduced from *J. Mass Spectrom.* 34, 991–1006 (1999)

The ions, produced in the electrospray source, enter the trap through the inlet and are trapped through the action of the three hyperbolic electrodes: the ring electrode and the entrance and exit end cap electrodes. Voltages are applied to these electrodes which results in the formation of a cavity in which ions are trapped. The ring

electrode RF potential, an a.c. potential of constant frequency but variable amplitude, produces a 3D quadrupolar potential field within the trap. This traps the ions in a stable figure of eight oscillating trajectory. The motion of the ions is determined by the voltages applied and their individual mass-to-charge (m/z) ratios. For detection of the ions, the potentials are altered to destabilise the ion motions resulting in ejection of the ions through the exit end cap. The ions are usually ejected in order of increasing m/z by a gradual change in the potentials. This 'stream' of ions is focussed onto the detector of the instrument, usually an electron multiplier tube, to produce the mass spectrum

2.7 Fourier transform infrared spectroscopy (FTIR).

The energy of the radiation in the mid infrared region ($4000-200\text{cm}^{-1}$) induces vibrational and rotational transitions in covalently bonded molecules. Infrared spectroscopy uses this by measuring wavelength and intensity of the absorbances that occur during these transitions when a sample is irradiated at infrared wavelengths. The wavelength and frequency of the absorbance is dependent on the strength and the dipolar nature of the bond, so different functional groups for instance will have characteristic bands in the spectrum which allow inferences to be made about the structure. In general the stronger the bond the higher the frequency of the vibration, although this is complicated by the mass of the interacting atoms which are joined by the bond, and the greater the electronegativities of the atoms the greater the absorbance. Infrared spectroscopy is therefore an excellent tool for qualitative analysis although quantitatively it is somewhat limiting due to the varied broadness of the absorption bands, some being less than the spectral width result in deviation from Beer's law. The use of standard materials can however be used to lessen this problem. In this study infrared spectroscopy was used to confirm the siliceous nature of materials and to identify species which may be entrained in them. The type of additives used in the studies herein typically exhibit strong aliphatic nature so one region of interest lies at $3000-2900\text{cm}^{-1}$ which is the C-H stretching region for saturated hydrocarbons. None of the other species present in the model silicifying system should show a significant absorbance in this region. Other important absorbance frequencies of interest all relate to the transitions involved in the silica matrix. These are tabled below:

Wavenumber/cm ⁻¹	Transition
3745-3750	Isolated silanol group O-H stretch showing no hydrogen bonding
3650-3660	Isolated silanol group showing long range hydrogen bonding O-H stretch
3540-3550	Adjacent silanol pairs showing mutual hydrogen bonding O-H stretch
3400-3500	Adsorbed water molecule O-H stretch
1100-1250	Asymmetrical stretch of Si - O -Si in silica matrix
850-950	Si-OH vibration
800	Symmetrical stretch of Si-O-Si in silica matrix
460-520	Si-O-Si rocking and bending transitions

Table 2.7.1 Specific absorbance wavenumbers for silica species.

2.8 Scanning electron microscopy (SEM).

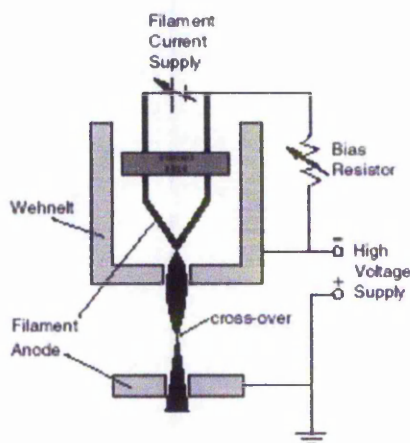


Figure 2.8.1 Electron Gun after Goldstein JI, Newbury DE, Echlin P, Joy DC, Fiori C & Lifshin E, 1981, Scanning Electron Microscopy and X-ray Microanalysis, Plenum Press, 673 pp.

The filament which is usually made of tungsten is heated until a stream of electrons is produced and functions as the cathode. A positive electrical potential is applied to the anode causing the electrons to accelerate due to the positive potential down the column. As the electrons move toward the anode any ones emitted from the filament's

side are repelled by the Whenelt Cap, which is held at ~ 500 V, toward the optic axis. A build up of electrons occurs in the space between the filament tip and Whenelt Cap. This collection is called a space charge Those electrons at the bottom of the space charge (nearest to the anode) can exit the gun area through the small (<1 mm) hole in the Whenelt Cap These electrons then move down the column to be later used in imaging. This process results in a parallel beam of electrons focussed as a point source all having similar energies.

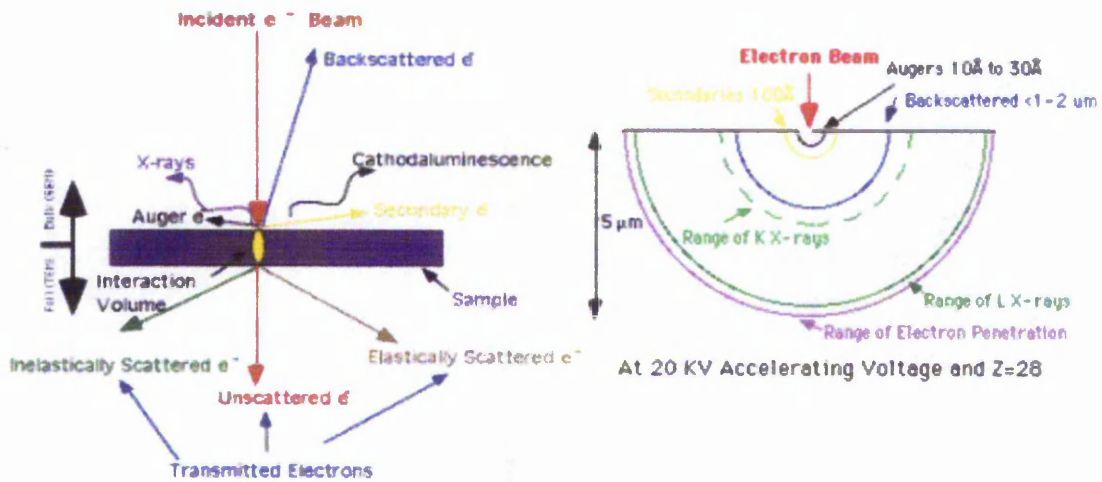


Figure 2.8.2 Sample stage and penetrative interactions in the sample.

The monochromatic electrons in the beam strike the sample and a series of interactions occur at different depths of penetration in the sample. The interactions of particular interest to us were the formation of lower energy which occurs from the first approximately 10nm of sample depth and the emission of x rays which occurs to a depth of about $2\mu\text{m}$.

Secondary electrons are caused by an incident electron an atom in the specimen, near enough to impart some of its energy to a lower energy electron (usually in the K-shell). This causes a slight energy loss and path change in the incident electron and the ionization of the electron in the specimen atom. This ionized electron then leaves the atom with a relatively reduced kinetic energy (5eV) and is termed a "secondary electron". Each incident electron can produce several secondary electrons.

Production of secondary electrons is very topographically related. Due to their low energy, 5eV, only secondary electrons that are very near the surface ($< 10\text{nm}$ depth)

can exit the sample and be examined. Any changes in topography in the sample that are larger than this sampling depth will change the yield of secondary electrons due to collection efficiencies. Collection of these electrons is aided by using a "collector" in conjunction with the secondary electron detector. The collector is a grid or mesh with a +100V potential applied to it which is placed in front of the detector, attracting the negatively charged secondary electrons to it which then pass through the grid-holes and into the detector to be counted. The beam is scanned in a raster fashion and an image is compiled from the collected secondary electrons.

X-rays are generated by the energy relaxations of the specimen atom after a secondary electron is produced. Since a lower (usually K-shell) electron was emitted from the atom during the secondary electron process an inner (lower energy) shell now has a vacancy. A higher energy electron can "fall" into the lower energy shell, filling the vacancy. As the electron "falls" it emits energy, usually X-rays to balance the total energy of the atom. X-rays emitted from the atom will have a characteristic energy which is unique to the element from which it originated. The X-rays generated are collected and plotted as a spectrum. Each peak on the spectrum represents a transition with a characteristic energy and so qualitative investigations on elemental compositions can also be undertaken.

2.9 Experimental details.

2.9.1 Experimental details for chapter 3.

As chapter 3 is a developmental chapter all experimental conditions are contained within it.

2.9.2 Experimental details for chapter 4.

2.9.2.(i) Reagents

Dipotassium tris(1,2-benzenediolato-*O,O'*)silicate ($K_2[Si(C_6H_4O_2)_3] \cdot 2H_2O$ (97%)), L-amino acids, L-lysine oligomers (99%), L-glycine oligomers (99%), poly L-lysine (97%, mw 15000–30000) and anhydrous sodium sulphite (97%) were purchased from Sigma Aldrich Chemicals; ammonium molybdate.4H₂O, hydrochloric acid (37%) and sulphuric acid (98%) were purchased from Fisher Scientific; oxalic acid.2H₂O (99%) and p-methylamino phenol sulphate (99%) were purchased from Acros Chemicals and standard stabilised silicate solution (1000 ppm as SiO₂) was purchased from BDH. All chemicals were used without further treatment. Distilled deionised water (ddH₂O) having a conductivity <1 $\mu S\ cm^{-1}$ was used. The purity of the dipotassium tris(1,2-benzenediolato-*O,O'*)silicate complex was checked by ¹H NMR (single peak at 6.63 ppm for complexed protons).

2.9.2.(ii) Silica synthesis and kinetic studies.

Experiments to study the oligomerisation reactions were carried out at room temperature (298 ± 2)K. Solutions (30 mMdm⁻³) were made up with doubly distilled water in plastic containers. The amino acid additives, when required were added immediately prior to acidification at a ratio of 2:1 to silicon and the pH of the resulting solutions was lowered to 6.8 ± 0.20 by addition of a known amount of 2M hydrochloric acid and the pH monitored for the duration of the experiment. Experiments using the lysine oligomers were performed as above except that the solution containing the lysine oligomers had its pH altered prior to mixing with the silicon complex to ensure that any interactions that occurred were with functional

groups in the form present at pH 7.0. The subsequent decomposition of the complex to orthosilicic acid and oligomerisation of the newly formed silicic acid was measured as a function of orthosilicic acid concentration by a modification of the molybdenum blue colorimetric method, as detailed in chapter 2 and refined in chapter 3. 10 μ l aliquots of solution were removed and added to solutions containing 15 ml of distilled water and 1.5 ml of an acidic solution containing ammonium molybdate and the resulting solution allowed to stand for 15 min, thereby allowing any dimers present to decompose to monomers which could be detected by the colorimetric method. 8 ml of a reducing solution containing Metol was then added and the absorbance of the blue silicomolybdate complex measured after 2 hours at 810 nm using a Unicam UV2 UV-VIS spectrometer. Calibration of this method using a standard silicate solution [BDH] showed a linear relationship between concentration and absorbance over the whole of the concentration range used (0–35 mMdm⁻³) and an experimental error in measurement of $\pm 1.0\%$. Orthosilicic acid concentrations were measured at intervals between 0.5 and 240 min after the initial pH reduction with 20–30 measurements being taken within the first hour. The equilibrium orthosilicic acid concentration (for an individual system) was reached within 2 hours reaction. Readings were continued for the first 24 hours of reaction with the precipitated silica being removed after 168 hours of reaction, washed three times with distilled water to remove traces of catechol and other solution species, centrifuged at 8000 rpm, rapidly frozen in liquid nitrogen and freeze-dried at 223 K using a Christ alpha 1–4 freeze-dryer.

Residual complex concentrations were determined by solution ¹H NMR spectroscopy at selected time points during reaction. Measurement of the peak area arising from the complex (a single peak at 6.63 ppm downfield from sodium-3-trimethylsilyl propionate-2,2,3,3-d₄ (TSP)) and comparison to the peak area for signals arising from the ligand alone in relation to known amounts of TSP enabled calculation of complex concentrations during the silicification reaction. After initiation of the reaction, solution complex concentrations immediately reduced to 0.1–0.7 mMdm⁻³ meaning that the majority of the silicon species were available for oligomerisation and for production of silica. Solution data were manipulated according to Harrison and Loton and time periods when the dominant molecular reaction followed third order kinetics (the formation of trimers from monomers and dimers), reversible first order kinetics (the addition or removal of orthosilicic acid to/from trimers or larger oligomers) or Ostwald ripening was the dominant reaction (with little measurable change in the

concentration of silicic acid being detected) were obtained. For the period where apparent third order kinetics were followed, a plot of $1/[\text{Si}(\text{OH})_4]^2$ vs. time gave a straight line with the rate constant being obtained from the gradient of the plot. For the period where reversible first order kinetics were followed a plot of $\ln(A - A_t)$ vs. time gave a straight line of slope $(k_+ + k_-)$ where A is the concentration at any time and A_t the concentration of orthosilicic acid at equilibrium (here taken as the value measured after 24 hours reaction). The separate rate constants for the forward and reverse reaction were obtained using the equilibrium constant K , which is the ratio of the forward and reverse rate constants and is also the ratio of the oligomerised silica and the equilibrium concentration of orthosilicic acid present in solution.

2.9.2.(iii) Photon correlation spectroscopy (PCS).

Samples were also prepared for Photon correlation spectroscopy. Samples were taken from the orthosilicic acid condensation experiments immediately on pH adjustment (amino acid study), or mixing (lysine oligomer study), and filtered through a 200 nm membrane into a 1 cm polymethylmethacrylate cell. Aggregation of silica particles was then monitored over a 40 hour period using a Coulter N4 plus photon correlation spectrometer with a He-Ne (632.8 nm) laser supply. All measurements were carried out at an angle of 90° and at 293 K. Measurements obtained were averages of the data collected over intervals of 2 to 60 minutes, the time selected depending on the rate of particle growth. Values of particle size are presented for comparative purposes and should not be taken as absolute values and are here referred to as 'apparent' particle size based on the hydrodynamic radii of aggregates.

2.9.2.(iv) Scanning electron microscopy (SEM).

For SEM studies, lyophilised samples were dispersed onto double-sided sticky tape and mounted on aluminium stubs with the edges of the sticky tape being painted with quick drying silver paint to prevent charging of the sample. All loose aggregates were removed by tapping the stub before the silica samples were gold coated with an argon plasma at 1.2 kV and 4 mbar pressure for 2 minutes using an Edwards S150B sputter coater. Images were acquired using a JEOL JSM-840A scanning electron microscope with an accelerating voltage of 20 kV. Average particle sizes were calculated by

measuring all distinct particles within 1 mm² areas and averaging. If this proved impossible particle sizes were measured over larger areas of the obtained images.

2.9.2.(v) Surface area analysis.

Surface area measurements were obtained from 12–30 mg quantities of precipitated silica obtained after 168 hours reaction. Single point measurements and full BET isotherms were obtained using a fully automated Micromeritics Tristar 3000 (Ineos Silicas, Warrington). Samples were degassed at 403 K for a minimum of 16 hours before analysis at liquid nitrogen temperatures. The specific surface area was obtained via the BET method where nitrogen is assumed to have a crosssectional area of 0.16 nm². Pore size distributions were calculated by the application of BJH theory to the desorption branch of the isotherms.

2.9.2.(vi) Thermogravimetric analysis (TGA).

The organic material associated with the sedimentable silica was detected by thermogravimetric analysis. Analysis was performed under nitrogen using a Stanton Redcroft TG 760 furnace, balance controller and UTP temperature controller with a heating rate of 10 K min⁻¹ with data being sampled every 30 seconds. Entrained organic content was calculated by comparison of weight loss between 400 and 800 K relative to the silica produced from the benzenediolato complex alone.

2.9.2.(vii). Fourier transform infrared spectroscopy (FTIR).

Samples were suspended in a potassium bromide disk prepared by grinding approximately 1mg of sample with 200mg of potassium bromide to give a fine powder. The mixture was then fused by pressing in a stainless steel die at 10 tonnes under reduced pressure. The spectra of the suspended samples were then recorded in the mid IR range (4400-200cm⁻¹).

2.9.3 Experimental details for chapter 5.

2.9.3.(i) Reagents.

1,2 diaminoethane (DA2), 1,4 diaminobutane (DA4), 1,6 diaminohexane (DA6), 1,8 diaminooctane (DA8) and 1,10 daminodecane (DA10) were purchased from Sigma Aldrich chemicals ltd. All were reported as 98% pure or better and were used without further treatment. All other reagents where used were as per chapter 4.2.1. Listed in 2.9.2 above.

2.9.3.(ii). Deviations from 2.9.2

The mole ratio of amine groups to silicon was maintained at 1:1 and the gas adsorption analysis was conducted with a quantasorb 3400E analyser which operates on the same principle as the Micromeritics Tristar 3000 used previously. All other operating conditions were as section 2.9.2.

2.9.4. Experimental details for chapter 6.

2.9.4.(i) Reagents.

Monoethyleneamine (MEDA), diethylenetriamine (DETA), triethylenetetramine (TETA), tetraethylenepentamine (TEPA), pentaethylenehexamine (PEHA), spermidine (SPDNE), spermine (SPNE) were all purchased from the Sigma-Aldrich company Ltd. Material quality was checked by ¹HMR spectroscopy and all were used as purchased without further treatment.

2.9.4.(ii) Deviations from 2.9.2

The amines were introduced to the model system with a Si:N ratio of 1:1. Additional experiments were undertaken in which the amine levels were varied at N ratios of 0.1 – 2:1 to silicon.

For thermal treatment, samples of silica were heated at 10°C/minute to 650°C in a furnace and held for 2 hours under an air atmosphere. The silica appeared colourless after this treatment indicating that all organic components had been removed. Additionally in order to perform silica quantitation, sedimentable silica was isolated at the times listed and washed as before from a predetermined volume of the condensing systems. The isolated silica was then allowed to redissolve in 2M sodium hydroxide at room temperature until a clear solution was obtained. Aliquots of these solutions were then sampled by the molybdenum blue assay method and the silica quantified by comparing with a set of standards prepared from a 10ppm stock solution of monosilicic acid. Entrained polyamines were determined by ^1H NMR spectroscopy of the sodium hydroxide solutions measuring the integral height of the amine signals against that of the chemical shift reference and comparing with a set of standards prepared using known amounts of polyamine measured under the same solution conditions against the same chemical shift reference. For ^1H NMR spectroscopy, all samples were measured in 5mm glass NMR tubes from aliquots taken directly from the experiments with no sample preparation. Spectra were accumulated from 32 scans with a pulse delay time of 1s using a Jeol JNM-EX270 Fourier transform nuclear magnetic spectrometer. A tube insert containing sodium 2,2 dimethyl-2-silapentane-5-sulphonate (DSS) in D_2O provided the chemical shift reference and deuterium lock signal with the DSS dimethyl signal also being employed as a reference for quantification purposes.

All other operating conditions were as section 2.9.2.

General references.

Molybdenum blue assay method.

J.D.H. Strickland, - *J.Am.Chem.Soc.*, 1952, 74, 862-876.

F.A. Cotton, G. Wilkinson, - *Advanced Inorganic Chemistry*, 5th edition. 1988. Wiley and sons, New York 811-818

G.B. Alexander, - *The polymerisation of Orthosilicic acid.*, 1953. *J.Am.Chem.Soc.*, 75, 2094-2096.

R.K. Iler, - *The Chemistry of silica.*, 1979, John Wiley and sons, New York.

J.B. Mullin, J.P..Riley, *Anal Chim Acta.*, 1955, 12, 162-170

Photon correlation spectroscopy.

B. J. Berne, R. Pecora, *Dynamic light scattering : with applications to chemistry, biology and physics.*, 1976, Wiley, New York,London.

Beckman coulter training course workbook 9914796-A

Gas adsorption analysis.

S. Brunauer, L.S. Deming, W.S. Deming, E. Teller, *JACS.*, 1940, 62, 1723.

J. H. de Boer, "The Structure and Properties of Porous Materials", p. 68, Butterworths, London, (1958).

S. Brunauer, P. H. Emmett and E. Teller, *J. Am. Chem. Soc.*, 1938, 60, 309.

E. P. Barrett, L. G. Joyner and P. P. Halenda, *J. Am. Chem. Soc.*, 1951, 73, 373.

Quantasorb, NOVAWin2 / 2-P Ver. 2.1 Operation Manual P/N 05079

Nuclear magnetic resonance spectroscopy.

J. W. Hennel and J. Klinowski, *Fundamentals of Nuclear Magnetic Resonance.*, 1993, Harlow Longman Scientific & Technical.

P. Kebarle and L. Tang, *Anal .Chem.*, 65, 972A (1993).

R.J. Pfeifer, C.D. Hendricks., *AIAA J.* 1968; 6: 496.

Mass spectrometry.

R. B. Cole, Some Tenets Pertaining to Electrospray Ionization Mass Spectrometry., *J. Mass Spectrom.* 35, 763–772 (2000)

R. G. Cooks, R. M. Caproli, Editorial: Special Feature on Electrospray Ionization., *J. Mass Spectrom.* 35, 761 (2000)

S. J. Gaskell, Electrospray: Principles and practice., *J. Mass Spectrom.*, 32, 677-688 (1997)

R. E. March, An Introduction to Quadrupole Ion Trap Mass spectrometry., *J. Mass Spectrom.*, 32, 351-369 (1997)

H. Wollnik, Ion Optics in Mass Spectrometers., *J. Mass Spectrom.* 34, 991–1006 (1999)

Scanning electron microscopy.

J. Goldstein, D.E. Newbury, P. Echlin, D.C. Joy, A.D. Romig Jr, C.E. Lyman, C. Fiori, E. Lifshin, Scanning electron microscopy and X-ray microanalysis : a text for biologists, materials scientists, and geologists., 1981, New York, London, Plenum.

Infrared spectroscopy.

R.K. Iler, – The Chemistry of silica., 1979, John Wiley and sons, New York.

Chapter 3.

3.1 The model system.

Various systems have been employed in the investigation of silicifying systems including the use of alkoxysilanes¹⁻⁴, sodium silicate solutions⁵, silica sols⁶ and a range of silicon 1,2 dihydroxybenzene complexes^{7,8}. In nature the source of soluble silicon is monosilicic acid at a few parts per million and at higher than 100ppm concentrations this spontaneously condenses to silica. In order to study the earliest stages of the condensation process only the monomeric silica species should be present. Any other oligomeric or particulate species present will result in problems with redissolution of species and condensation with already formed silicates all of which exhibit various kinetics traits and mechanisms with oligomer reorganisations involved, and as a consequence the system becomes too complex to analyse meaningfully. The use of alkoxysilanes is clearly problematic as the initial stage involves the hydrolysis of alkoxysilane bonds which results in a mixture of partially hydrolysed and partially condensed species in solution. The use of silica sols prevents any analysis of the early condensation stages as they represent pre-condensed stabilised species where only aggregative effects can be studied, and basic solutions of sodium silicate contain stabilised oligomeric species which form the nuclei for further condensation again clouding the early condensation stages.

1,2-dihydroxybenzene precursors however are stable forming basic aqueous solutions which on neutralisation with acid rapidly form supersaturated solutions of monosilicic acid which immediately begin to condense. Additionally such hypervalent silicon complexes have been implicated in the biosilicification process^{11,12} possibly as a mechanism for the transport of silicon at concentrations exceeding the solubility of monosilicic acid. The use of these complexes was therefore the chosen basis for the model system.

Silica condensation in natural systems occurs by necessity in an environment in which many other species are present which may or may not play a direct role in the deposition of the mineral form. A simpler system producing material over a realistic time scale is required for the purposes of meaningful analysis. To this end 50mmoldm⁻³ dipotassium tris(1,2-benzenediolato-*O,O'*)silicate.2H₂O systems have previously been employed^{8,9,10} to produce on the reduction of pH to 7 rapidly

condensing solutions of monosilicic acid which contain in addition only potassium and chloride ions and 1,2 dihydroxybenzene and reach equilibrium within 24 hours. The mechanisms and critical parameters of this model were investigated.

3.2 Inherent difficulties with the model.

The process of neutralisation of the dipotassium tris(1,2-benzenediolato-*O,O'*)silicate.2H₂O complex using small volumes of concentrated hydrochloric acid to attain a pH of 7 results in a level of error in the final concentrations not only of monosilicic acid in solution but also of residual complex. The residual complex dissociates differentially in the molybdenum blue assay depending on the level of monosilicic acid also present and conversion factors have to be determined based on the addition of known amounts of complex during the condensation process. Experiments have shown that between 60% and 90% of the complex dissociates to form the silicomolybdic acid complex, the lower values of conversion found at higher monomer concentrations. Attempts to eliminate this conversion factor determination by modifying the conditions of molybdenum complex formation have proven unsuccessful so herein the alternative solution of minimising the residual complex levels was attempted.

3.2.1 Attempts to eliminate the conversion factor.

The mechanism of complex dissociation with HCl was first investigated by titrimetry. 10cm³ of a 50mmoldm⁻³ solution of dipotassium tris(1,2-benzenediolato-*O,O'*)silicate.2H₂O was prepared and titrated against 2M HCl and the pH monitored throughout (figure 3.1).

The requirement was for 2 moles of acid to fully dissociate the complex and since the production of 3 molar equivalents of 1,2 dihydroxybenzene and 1 molar equivalent of monosilicic acid results there is a further requirement for 4 molar equivalents of water. So the dissociation process becomes:



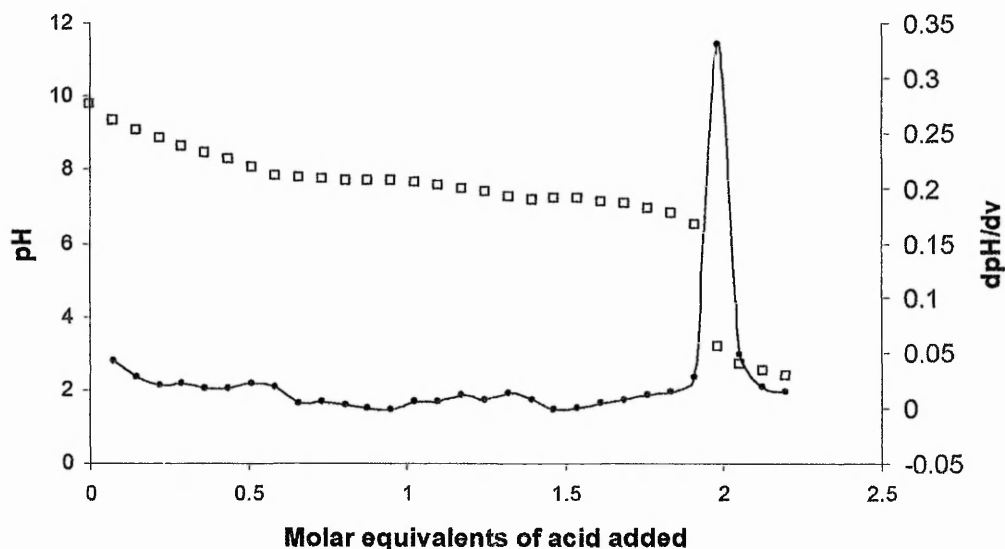


Figure 3.1 Titration of 10cm^3 of a 50mmoldm^{-3} dipotassium tris(1,2-benzenediolato-*O,O'*)silicate. $2\text{H}_2\text{O}$ with 2Mdm^{-3} solution of HCl.

The necessity for only 2 molar equivalents of acid indicates the expected collapse of the octahedral complex structure. The expansion of the d orbitals following the removal of the first 1,2 dihydroxybenzene group results in reduced orbital overlap which favours the tetrahedral structure which is unable to accommodate the steric requirements of the remaining ligands which are then easily hydrolysed by water releasing monosilicic acid and 2 further molar equivalents of 1,2 dihydroxybenzene. It is also clear from titrimetry that the pH can be maintained at around 7 when in excess of 95% of the complex has been dissociated. There therefore seems to be some opportunity to perform the condensation experiments almost in the absence of residual complex thereby obviating the need to use conversion factors in the calculation of monosilicic acid concentration. To investigate the possibilities of this, experiments were carried out on a set of solutions of the silicon complex with varying stoichiometric levels of acid added. The pH was monitored and the level of dissociation was measured by ^1H NMR spectroscopy. The use of deuterated solvents is usually a requirement of ^1H NMR spectroscopy but here the presence of the water signal did not interfere with the signals from either the complex or the 1,2 dihydroxybenzene ligand.

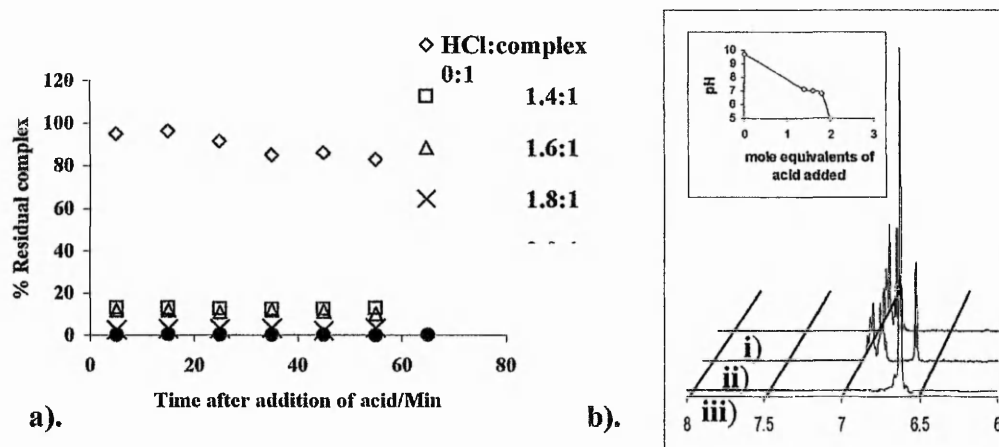


Figure 3.2 a). molar % of residual complex after acid treatment (b). Example ^1H NMR spectra. Singlet signal at 6.6ppm is complexed ligand ring protons and the multiplet at 6.8ppm is the free 1,2 dihydroxybenzene ring protons. Mole ratio of acid added to complex (i) 2:1 (ii) 1.6:1 (iii) 0:1.

It was possible therefore to conduct experiments in ordinary deionised water with an insert containing D_2O and sodium-3-trimethylsilylpropionate-2,2,3,3,- d_4 (TSP) to supply lock signal and chemical shift reference respectively.

The level of residual complex was proportional to the molar equivalents of acid added and the pH of the solutions varied from 7.1 to 6.8 over the H^+ :complex ratio range of 1.4 to 1.8. ^1H NMR of a controlled 1.9:1 molar additions of acid to complex (figure 3.2) showed less than 2 mol% of residual complex within 5 minutes of the acid addition (the time taken to complete the first spectrum acquisition), this level remaining practically constant for over 24 hours. The pH as measured after 24 hours was 6.8.

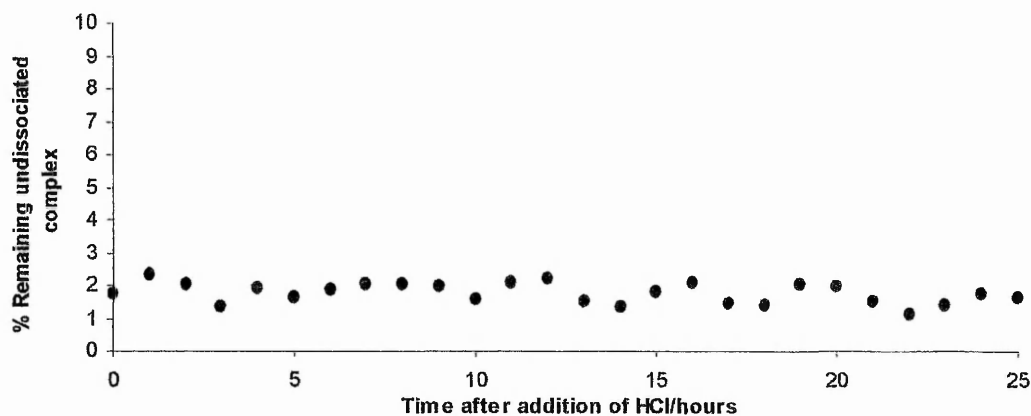


Figure 3.3 Level of residual complex measured by ^1H NMR after a 1.9:1 molar addition of acid to 50mMdm^{-3} complex solution.

Initial experiments with practically fully dissociated 50mmoldm^{-3} solutions resulted in difficulties in recognising the early kinetic domains when monitoring with the molybdenum blue method due to the relatively high levels of monosilicic acid released, (previously only around 50% of the available complex was dissociated). In order to extend this region to allow time for a meaningful number of measurements to be made the concentration of complex was reduced to 30mmoldm^{-3} and subjected to the same stoichiometry of acid addition prior to analysis with the molybdenum blue assay method.

3.2.2 Experimental details of the molybdenum blue method.

Molybdic acid reagent: Ammonium molybdate tetrahydrate (20g) was dissolved in deionised water (500ml). Concentrated hydrochloric acid (60ml) was added and diluted to 1000ml with deionised water after cooling.

Reducing reagent: Oxalic acid (20g), 4-Methylaminophenolsulphate (6.67g) and sodium sulphite (4g) were dissolved in deionised water (500ml). Concentrated sulphuric acid (100ml) was added and the solution diluted to 1000ml with deionised water after cooling.

Standard calibration graph:

1.5ml of molybdic acid reagent was diluted with sufficient deionised water to give a total volume of 16.5ml when 1 – 10ml of 10ppm aqueous solution of SiO_2 was added. The silicomolybdic acid complex was allowed to develop for 15 minutes before addition of 8.0 ml of the reducing reagent. The absorbance at 810nm in clear polymethacrylate cells (path length 10mm) was measured after between 2 and 24 hours after the addition of the reducing reagent. A plot of concentration as Si(OH)_4 against absorbance was plotted to determine the concentration/absorbance relationship and that it was linear over the range of concentrations of the samples expected.

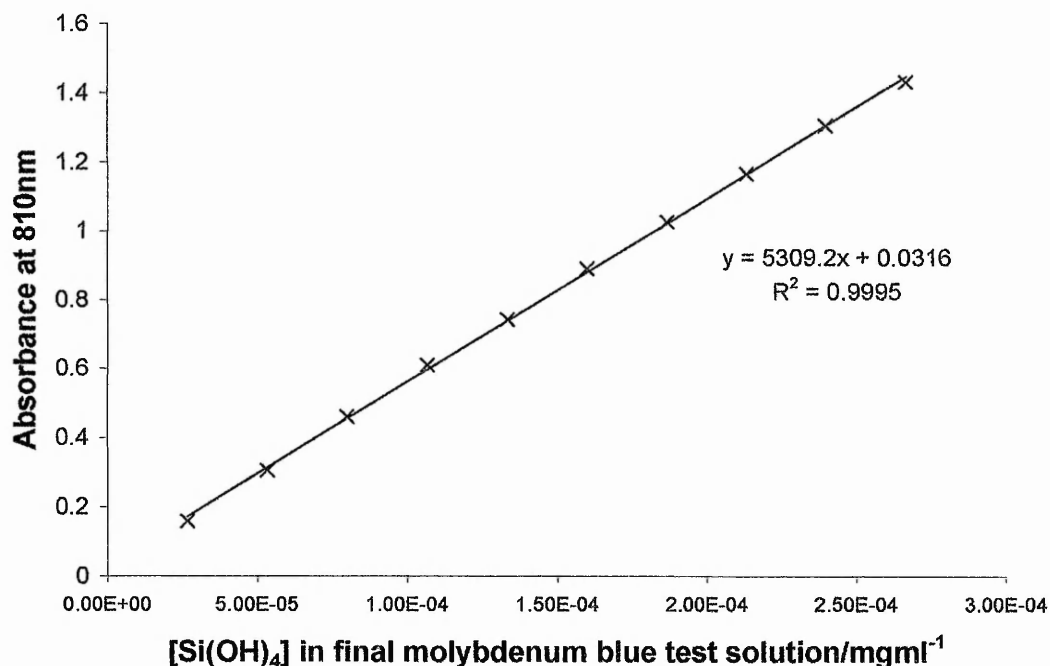


Figure 3.4 Calibration graph for modified molybdenum blue assay.

Sample analysis.

Measured aliquots of the condensing system under investigation were added to 1.5ml of molybdic acid reagent diluted with 15ml of deionised water. The timing and volume of reducing reagent addition and absorbance monitoring were as above. The concentration as Si(OH)_4 was then determined from the relationship determined by the standard calibration plot.

3.2.3 Statistical analysis of the standard model system.

30×10^{-5} mol of dipotassium tris(1,2-benzenediolato-*O,O'*)silicate.2H₂O was dissolved in sufficient deionised water to give a final volume of 10.0cm³ when a sufficient volume of 2M HCl had been added to effect a 1.9:1 molar equivalent addition of acid to the complex. 10 μ l aliquots of the condensing silicic acid system were then taken at known times for the molybdenum blue assay (detailed above) and the concentration of molybdenum active species (as monomer) determined. The data was analysed as per Harrison and Loton⁸ to isolate the different kinetic domains and the 3rd order rate constants determined. Four repeat analyses were conducted giving a value of $1.16 \times 10^{-6} \pm 8.21 \times 10^{-8} \text{ mM}^{-2} \text{ dm}^6 \text{ s}^{-1}$ for the third order rate constant, based on a

95% t test confidence meaning that any sample analysed under the conditions used only has a 5% chance of falling outside of these values by chance alone.

3.3. Solution species.

During the condensation process under the conditions used the formation of dimers to trimers is thought to be followed by the rapid formation of higher oligomers and particles which are inactive with respect to the molybdenum blue method. The presence of species which are active in that they dissociate in the time frame of the experiment would clearly interfere with the kinetic analysis conducted. Higher oligomers dissociate more slowly in the Molybdic acid reagent and should therefore show up as changes in the rate at which the silicomolybdic acid complex forms. A series of experiments were therefore conducted to establish whether any changes in the profile of the complex development indicated the formation of such slower dissociating species during the course of the condensation.

The model system was prepared as before and 10 μ l aliquots taken after increasing condensation times and added to the molybdic acid reagent. The development of the silicomolybdic acid complex was then monitored for each aliquot over a period of 30 minutes at 370nm. 1st derivative analysis was then carried out on the data to ascertain if any obvious changes in the colour development with time could be observed.

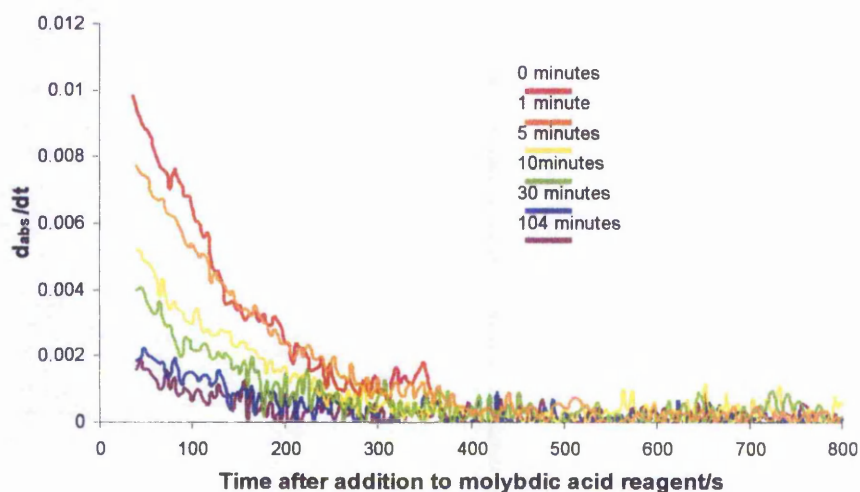


Figure 3.5 Rate of change of complex development with time for samples taken from the condensing model system at increasing condensation times.

Inspection of the data showed no obvious zonal changes in the complex development indicating that if slower reacting species were remaining in the condensing system for any length of time they were at concentrations not likely to affect the kinetic analysis. However, analysis of a solution of silica dissolved in 12.5% aqueous tetramethylammonium hydroxide which is known to stabilize cubic octamer silicate species also showed the same complex formation profile. This would be expected as these species are only stable in basic solution so one would expect rapid dissociation in the acidic conditions employed in the molybdic acid reagent, but it does highlight the possibility that other species could exist without necessarily being noticed. To clarify this situation a mass spectroscopic and ^{29}Si NMR study was carried out. Work by Bussian et al¹³ showed that it was possible to study silicate speciation in stable systems by electrospray mass spectrometry (ESI), the various species surviving the ionization and mass analysis conditions. In addition, for stable systems the long nuclear magnetic resonance experiments required for ^{29}Si analysis can be conducted. Since the transfer of methodologies between mass spectrometric systems can be problematic, a brief feasibility study was undertaken.

3.3.1 Stabilised silica solution.

A solution was prepared of a fumed silica (60mg) dissolved in a 12.5% tetramethylammonium hydroxide solution in water/methanol 3:1(20cm³). The silica dissolved readily at 40°C (within 30 minutes) to give a clear and colourless solution.

3.3.2 ^{29}Si Nuclear Magnetic Resonance investigation.

^{29}Si NMR analysis was conducted on the solution in a 10mm plastic NMR tube using an insert containing d₆ acetone and tetramethylsilane (TMS) to provide lock and reference signals respectively. A total of 1000 scans were accumulated overnight and a delay of 6 seconds between pulses employed to ensure full relaxation.

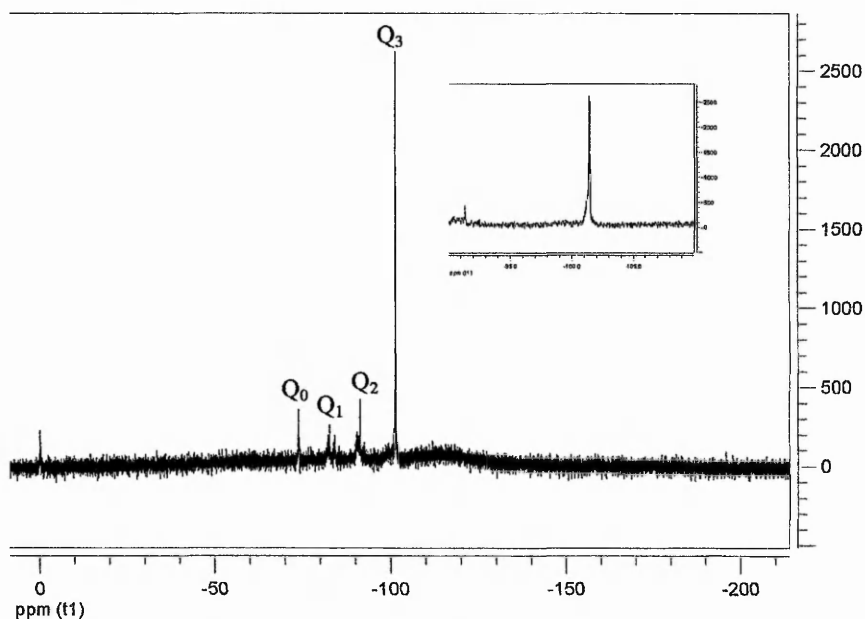


Figure 3.6 ^{29}Si NMR spectrum of TMAOH stabilized silicate species. Silica concentration was 3mgml^{-1} . The insert is an expansion of the region from -90 to -110ppm i.e. the Q_3 region.

The dominant species observed had a chemical shift relative to the TMS reference correlating to that of Q_3 species¹². Expansion of this region showed some broadening of the signal indicating the presence of more than one species. It was likely therefore that the solution contained more silicate cage structures than merely the cubic oligomer.

In addition the solution was seen to contain significant levels of monosilicic acid, Q_0 and Q_1 species which indicated some linear (or partially linear) species. The presence of a signal compatible with that of Q_2 species was evidence of branched or cyclic structures. The system therefore contained all the condensation levels of silicate structures which could be encountered and as such provided an excellent tool for mass spectral investigations.

3.3.3 Mass Spectrometric investigation.

The stabilized oligomer solution was introduced into the electrospray source using a syringe pump through 0.17mm ID peek tubing at a flow rate of $7\mu\text{lmin}^{-1}$. The analysis was conducted in negative ion mode. The capillary voltage was maintained at 3.5kv, the ion energy at 2.0, a source temperature of 100°C and a nitrogen flow rate of 400lhr^{-1} . The cone voltage was adjusted to obtain the optimum ionization of the

silicate species. Mass separation was achieved using a single quadrupole mass analyzer and an electron multiplier detector. Data analysis was carried out with the Mass lynx v 3.5 spectral analysis software.

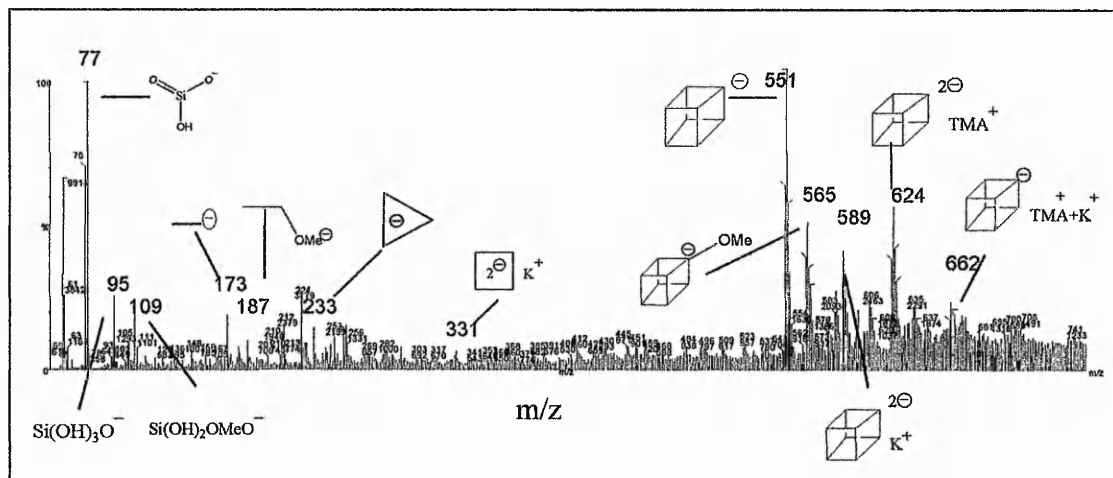


Figure 3.7 Negative ion mode mass spectrum of silicate solution species.

The spectrum obtained was dominated by silicate cage species (Q_3) as had been predicted by the ^{29}Si NMR data and most of the Q_2 species were cyclic as predicted by modeling studies.¹⁴ All of the species anticipated by the ^{29}Si NMR analyses were found and interestingly the cage species were not dominated by TMAOH stabilized ions indicating the ability of this method to successfully transfer the aqueous species to the gas phase without change possibly even from unstable systems. The next challenge was therefore to apply this method to samples of the model system.

3.3.4 Mass spectrometry of the model system.

Freshly condensing model system solutions were prepared as before and immediately introduced to the electrospray by syringe pump at $7\mu\text{lmin}^{-1}$. Operational conditions were as used for the investigative work carried out on the TMAOH stabilized samples. In addition to the condensing model samples, solutions of 1,2 dihydroxybenzene and dipotassium tris(1,2-benzenediolato-*O,O'*)silicate. $2\text{H}_2\text{O}$ were also analysed to give an indication of non silicate species likely to be encountered.

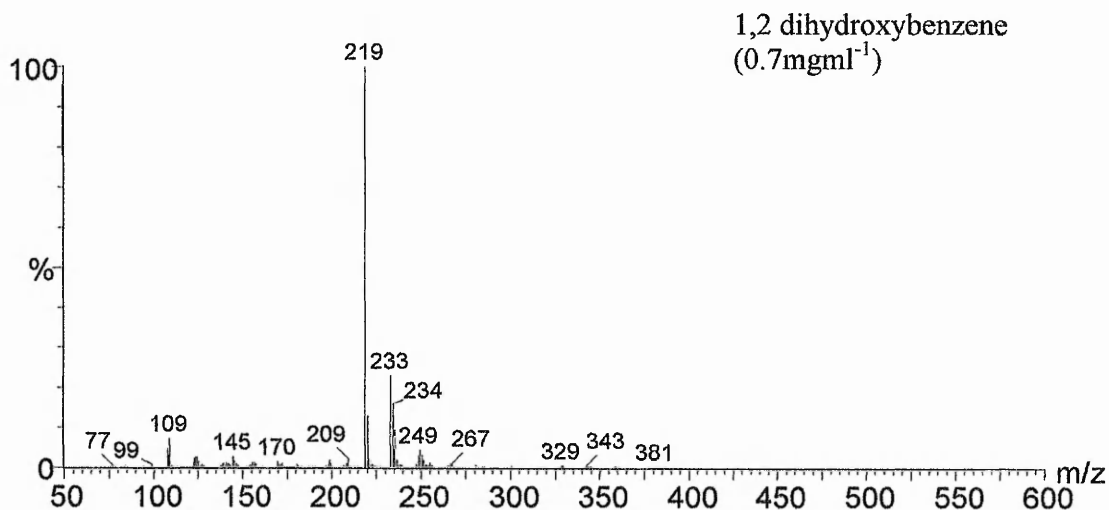


Figure 3.8 Mass spectrum of 1,2-dihydroxybenzene (90 mM dm⁻³).

The mass spectrum of 1,2-dihydroxy benzene was dominated by the 219 ion which probably represents a bimolecular adduct ion $[C_6H_4(OH)_2]_2 - H^+$. The small 109 ion represents the molecular ion $[C_6H_4(OH)_2] - H^+$. Unfortunately the presence of the ion m/z 233 will interfere with any occurrence of cyclic trimer which is regarded as a key feature in the early stages of silica condensation. The origin of the ion here is uncertain.

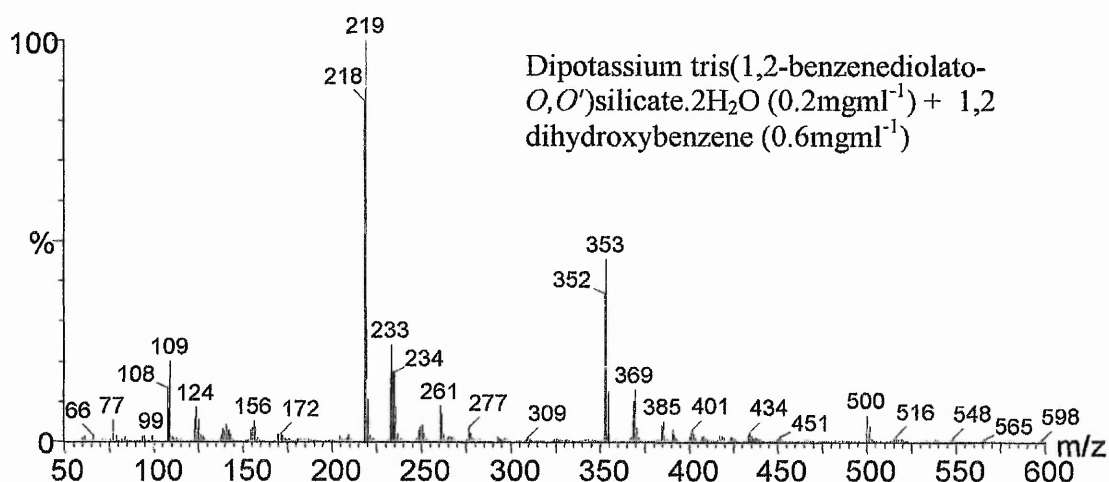


Figure 3.9 Spectrum of a mixture of dipotassium tris (1,2-benzenediolato-*O,O'*) silicate.2H₂O + 1,2-dihydroxybenzene (mole ratio of 1:9) recorded in negative ion mode.

The ion of m/z 353 was the molecular ion stripped of potassium ions $[\text{Si}(\text{C}_6\text{H}_4\text{O}_2)_3]^{2-} \text{H}^+$. Again a strong feature of the spectrum is the 1,2 dihydroxybenzene bimolecular adduct ion. Happily there was no interference at m/z 95 which would be expected to be fairly conspicuous in the spectrum of the model system ($[\text{Si}(\text{OH})_3\text{O}]$).

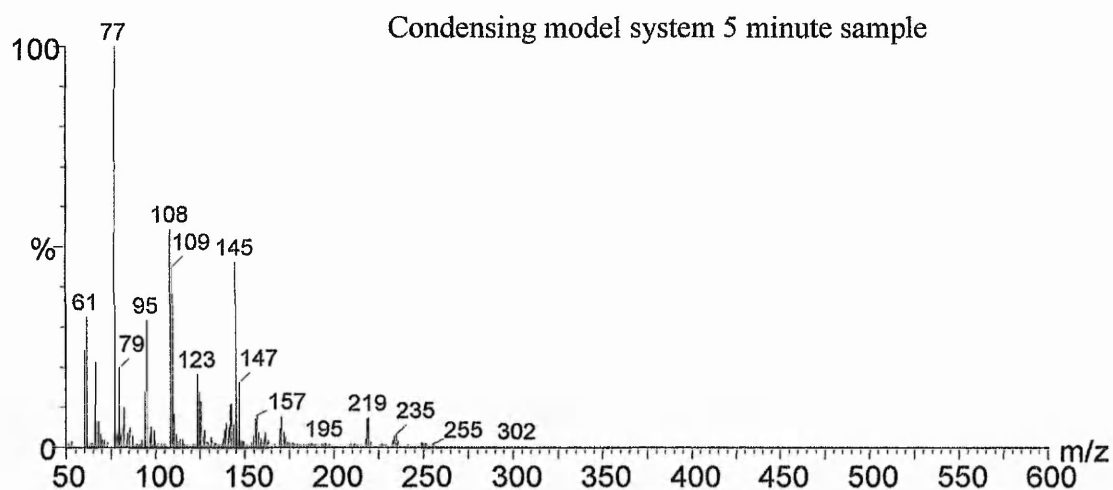


Figure 3.10 Spectrum of the model system after 5 minutes condensation.

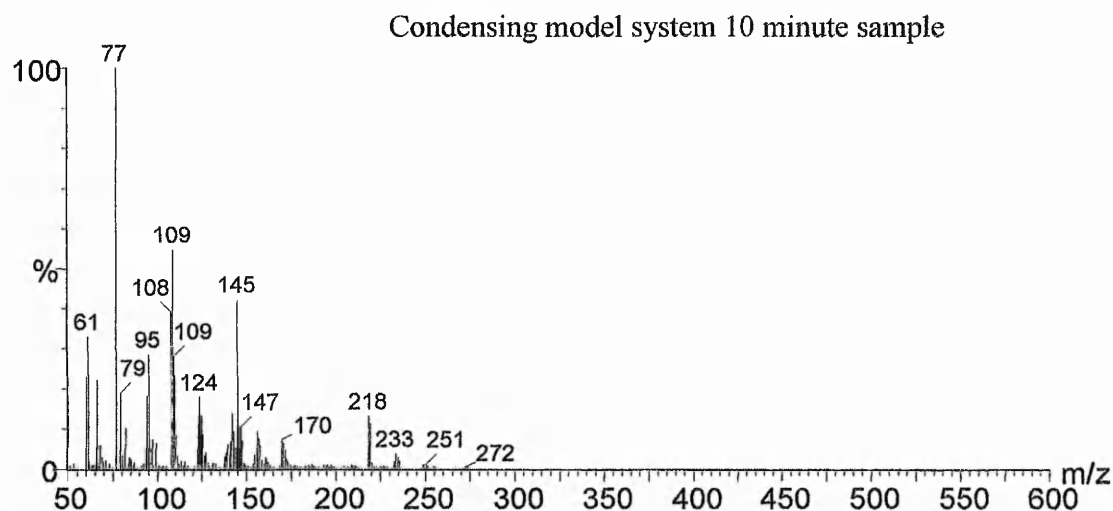


Figure 3.11 Spectrum of the model system after 10minutes condensing.

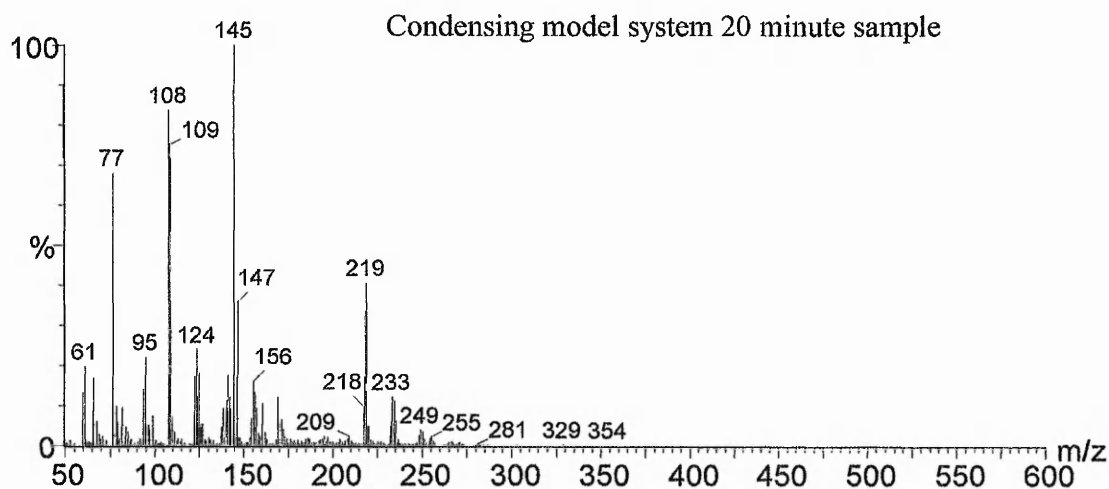


Figure 3.12 Spectrum of the model system after 20minutes condensing.

Immediately noticeable in these spectra was the almost complete absence of the 353 ion of the silicon complex reinforcing the fact that hydrolysis on pH adjustment was rapid and practically complete. The presence of the m/z 77 and 95 ions here are indicative of monosilicic acid anion and dehydration product. No evidence was found for the presence of dimeric species or fragments but as the trimerisation stage is no longer dominant after 5 minutes according to molybdenum blue analysis then any residual monomer populations, which are clearly represented here, would be expected to preferentially co-condense with trimers and larger oligomeric species resulting in a rapid depletion of the smaller oligomers. As the analysis continued from 5 – 10 – 20 minutes there was a noticeable increase in the level of 1,2-dihydroxybenzene related species. Rather than this being due to an increase in such species it is probably an indication of reduction in the level of monosilicic acid with time and therefore a reduction in the ion suppression caused by it. No evidence was found for the presence of solution species larger than the monomer in the model system.

Finally the rate of dissociation of the complex on pH adjustment required clarifying in order to justify rate constants determined from data collected only shortly after the adjustment. Initially the plan had been to use the mass spectrometer in conjunction with fast flow techniques, but unfortunately the necessary use of ultra small ID tubing proved prohibitive in conjunction with the viscosity and surface tension of the aqueous solutions employed resulting in very high back pressures beyond the

performance of a syringe pump. Instead the dissociation rate was investigated by the analysis of quenched solutions by ^1H NMR.

3.4 The rate of dissociation of dipotassium tris(1,2-benzenediolato-*O,O'*).2H₂O complex upon pH adjustment.

It was necessary to assess whether or not the complex was fully dissociated at the earliest times that sampling was conducted for the molybdenum blue method (within 30 seconds).

Solutions of dipotassium tris(1,2-benzenediolato-*O,O'*).2H₂O were prepared to give a final concentration of 30mmoldm⁻³ on addition of 2moldm⁻³ HCl. Different levels of acid were added to determine whether there was any evidence of slow down in the dissociation process at less than stoichiometric additions of acid to the complex. The dissociation process was quenched at known times by adding aliquots to sufficient levels of 1moldm⁻³ potassium hydroxide solution to return the pH to above 8.

Sample details:

In all cases 140mg ± 0.1mg of dipotassium tris(1,2-benzenediolato-*O,O'*).2H₂O was weighed. 820μl aliquots of the pH adjusted solutions were then quenched with 180μl of 1moldm⁻³ potassium hydroxide solution.

Volume of water added/cm ³	Volume of 2moldm ⁻³ HCl added/cm ³	pH after acid addition	pH after quenching
9.75	0.25	2.3	9.7
9.77	0.23	6.4	9.7
9.78	0.22	7.1	9.8
9.79	0.21	7.2	9.8

Table 3.1 Details of the complex dissociation quenching experiments.

The ^1H NMR spectra of all solutions were then recorded using an insert containing D₂O and sodium-3- trimethylsilyl propionate-2,2,3,3-d₄ (TMP). 16 scans were accumulated each with a pulse delay time of 1 second.

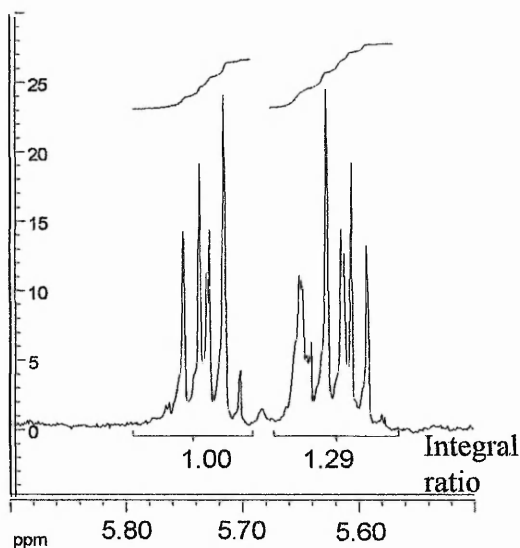


Figure 3.13 Example NMR spectrum of quenched dissociated complex.

Figure 3.13. shows a typical spectrum of a quenched dissociated complex. The chemical shifts are affected by the pH and hence we now have overlap of the complex and 1,2-dihydroxybenzene ring protons. Since 1,2-dihydroxybenzene is symmetrically substituted with no further coupling other than between the aromatic protons then it is correct to assume that the integrals for both the up and downfield proton pairs will be the same. The contribution to the right hand signal from the residual complex (centred at 5.65ppm) will be the difference in the measured integrals (in this case 0.29). The mol % of complex was calculated from this at each sample time.

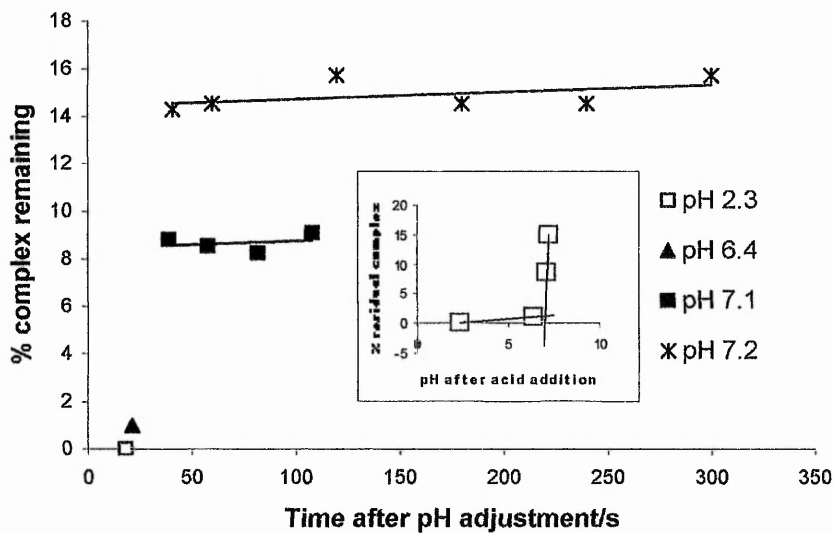


Figure 3.14 Plot of residual complex with dissociation time for samples treated with increasing amounts of acid. Insert shows the relationship between pH and residual complex.

Only the first sample time was analysed for the samples at low pH since the complexes had practically completely dissociated within 20 seconds. The samples with a lower molar equivalent of acid added showed an immediate (within the first sample time) reduction in residual complex level which remained unchanged throughout the duration of the experiment. The dissociation of the complex was therefore as required for the kinetic analysis *viz* practically immediate and leaving stable residue when insufficient acid has been added for complete dissociation. The relatively minor change in the pH of the solutions for reasonably extensive differences in complex composition also highlights the importance in monitoring the levels of residual complex by ^1H NMR during all kinetic analyses.

The effects of controllable parameters on the model system kinetics were then investigated.

3.5 The effects of changing controllable parameters on the kinetics of the model system.

Concentration, temperature and pH are all known to affect the kinetics of reactions. Knowing how these specifically affect the model system should allow us to gather more information and extend the flexibility of it and enable us to use data from experiments which didn't initially fall within the condition parameters set.

3.5.1 Temperature dependence.

Solutions of dipotassium tris(1,2-benzenediolato-*O,O'*)silicate.2H₂O were prepared to give a final concentration of 30mmoldm⁻³ on addition of 2moldm⁻³ HCl and held in a water bath at the experiment temperature to equilibrate. Temperatures for the experiments were 0, 10, 20, 30, 40 and 50°C. After acid addition 10μl aliquots were taken at timed intervals for the molybdenum blue assay. Data was treated as outlined in Chapter 2.1.

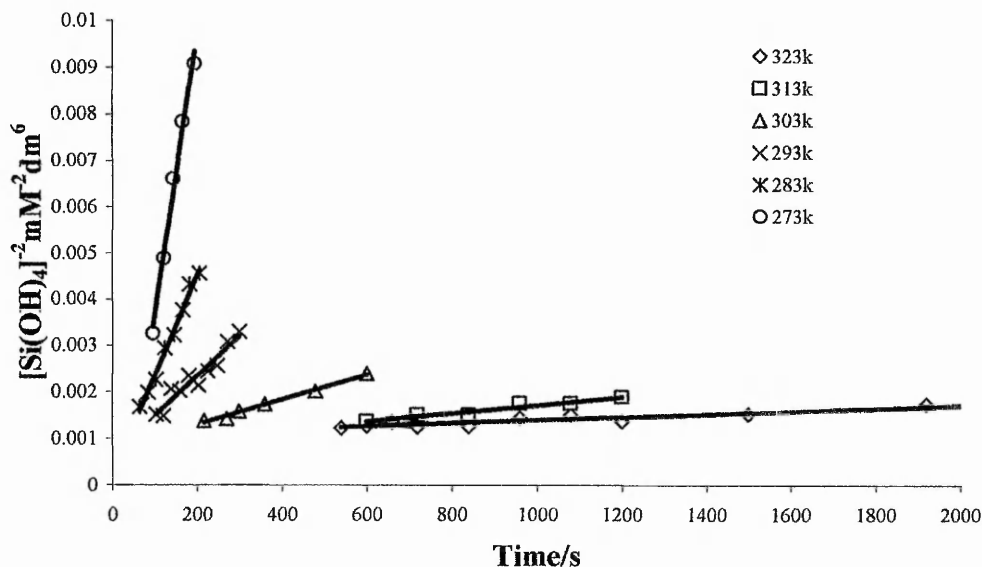


Figure 3.15 Isolated 3rd order kinetic regions for the range of temperatures 0- 50°C.

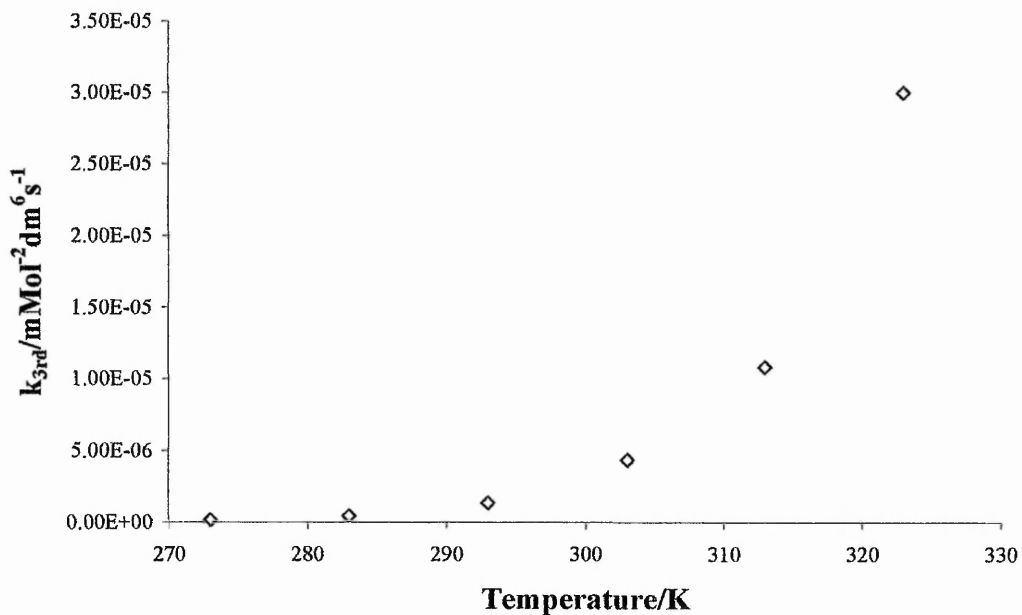


Figure 3.16 Effect of temperature on the 3rd order rate constants.

The increase in the third order rate constant, k^{3rd} with temperature highlights the need to conduct experiments with strict temperature control. A discrepancy of only $\pm 2^\circ\text{C}$ results in approximately a $\pm 20\%$ variation in k^{3rd} . Onset and cessation of the third order domain were similarly moved to shorter time frames. Application of the

Arrhenius equation to the data (a plot of $\ln k^{3rd}$ against $1/T(k)$) gave a linear plot (figure 3.16.) emphasising the correct selection of the time frames for determining the individual rate constants. The Arrhenius equation relates the rate constant with the temperature, the activation energy of the process and includes a term which relates to the collisional frequency of the reacting species and the likelihood that they will be in the correct orientation to react:

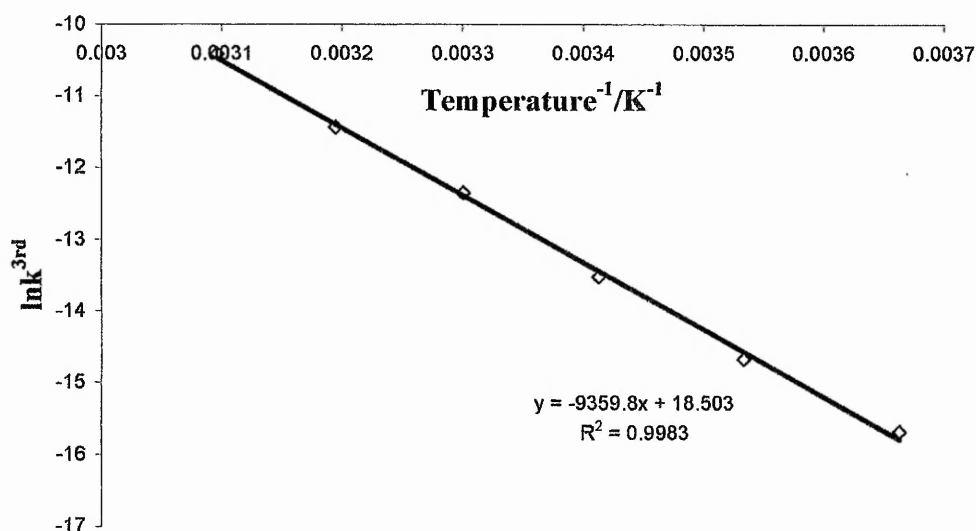


Figure 3.17 Arrhenius plot of k^{3rd}

The Arrhenius equation:

$$k = Ae^{-\frac{Ea}{RT}}$$

Where k = the rate constant

A = the frequency factor which is a measure of the collisional frequency and species orientations

Ea = the activation energy for the process

R = universal rate constant

T = temperature (k)

In logarithmic form this becomes:

$$\ln k = \ln A - \frac{Ea}{RT}$$

The frequency factor is therefore the intercept with the y axis and $-E_a/R$ is the slope. The value for E_a obtained from the data was 77kJmol^{-1} .

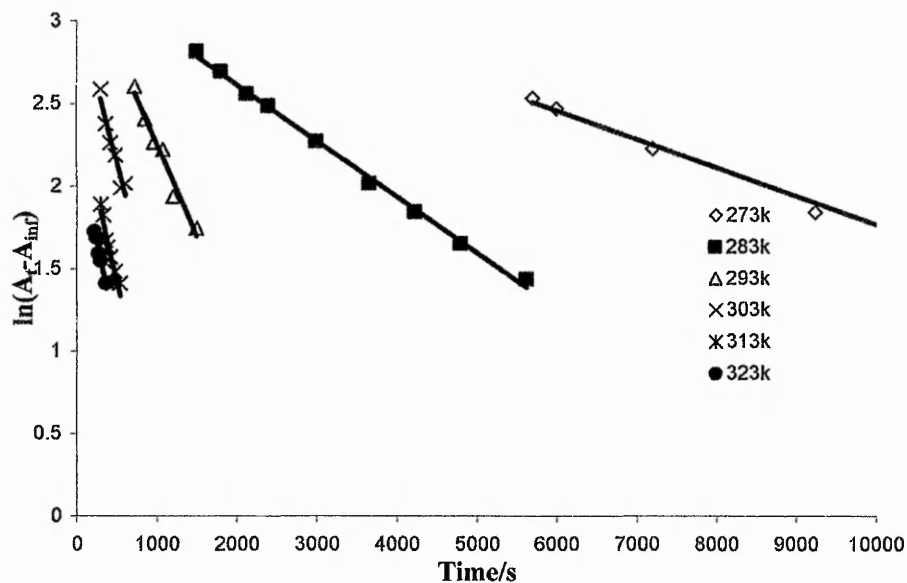


Figure 3.18 Isolated reversible 1st order domains at 0-50°C.

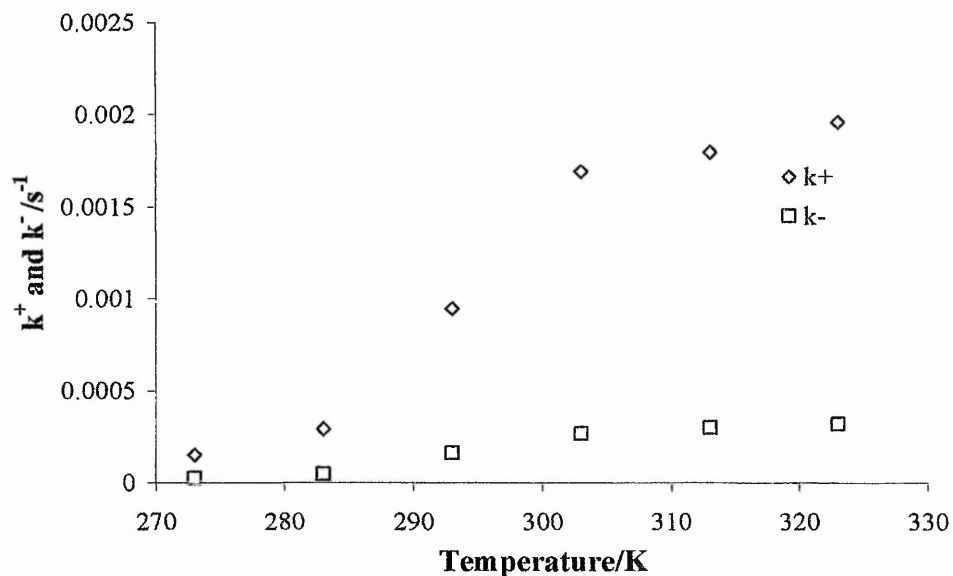


Figure 3.19 Affect of temperature on 1st order forward and reverse rate constants.

The effect of temperature on the first order reversible kinetics showed that both the forward and reverse rates were increased. The ratio of forward to reverse rate

constants did not indicate any appreciable detectable increase in the solubility of the silicate species ranging from 5.8 to 6.3 over the range but showing no specific trend.

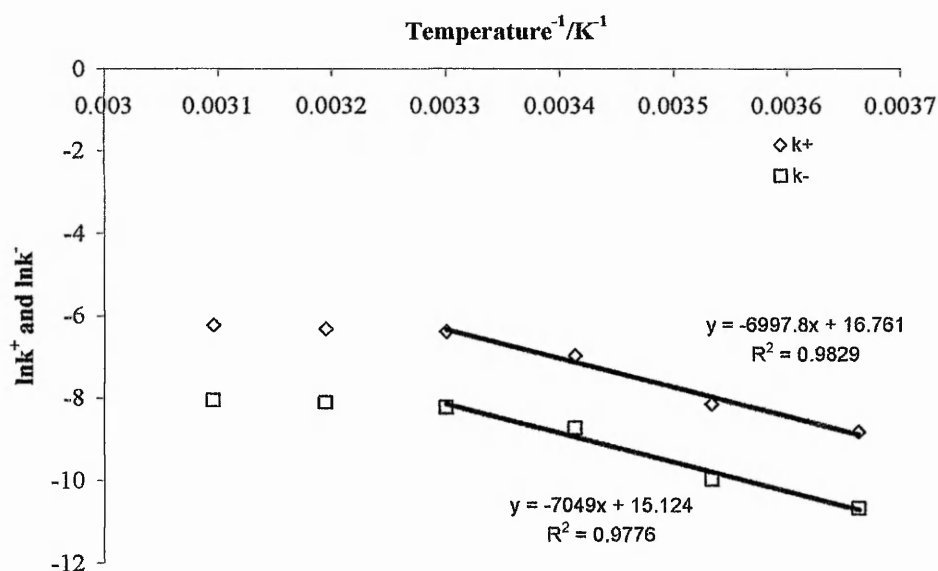


Figure 3.20 Arrhenius plot for 1st order forward and reverse rate constants.

Arrhenius treatment of the data showed a distinct activation energy change. From 0 to 30°C values for the forward and reverse activation energies were 55.0 and 58.6 kJmol⁻¹ respectively. This is in good agreement with the results obtained by Harrison and Loton who found the activation energy to be 58 kJmol⁻¹ but didn't separate the forward and reverse rates for the determination. Other reported determinations for the activation energy gave values of between 13 and 85 kJmol⁻¹.^{8,15,16} Above 30°C considerably lower activation energies were observed. It is believed that this may be a reflection of the selection of the time frames for the determination of the first order domain. At higher temperatures the onset of the first order domain occurs increasingly at earlier times and for a much decreased period making the transition between the kinetic domains more difficult to determine. The decreased activation energies observed were possibly a result of measuring the first order domain where the condensation of monosilicic acid on to particulate species as well as oligomers was also occurring. This would be a consequence of the increasing ease of deprotonation of the silicate species due to their increased acidic nature with increased condensation. Furthermore the activation energy determined for the third order domain was higher (77 kJmol⁻¹) reflecting that protons are most difficult to remove from this uncondensed species.

3.5.2 Concentration dependence.

Solutions of dipotassium tris(1,2-benzenediolato-*O,O'*)silicate.2H₂O were prepared to give a final concentrations of between 10 and 50mMdm⁻³ on addition of 2Mdm⁻³ HCl and held in a water bath at 20°C for 10minutes for temperature equilibration. After acid addition 10μl aliquots were taken at timed intervals for the molybdenum blue assay. Data was treated as in Chapter 2.1.

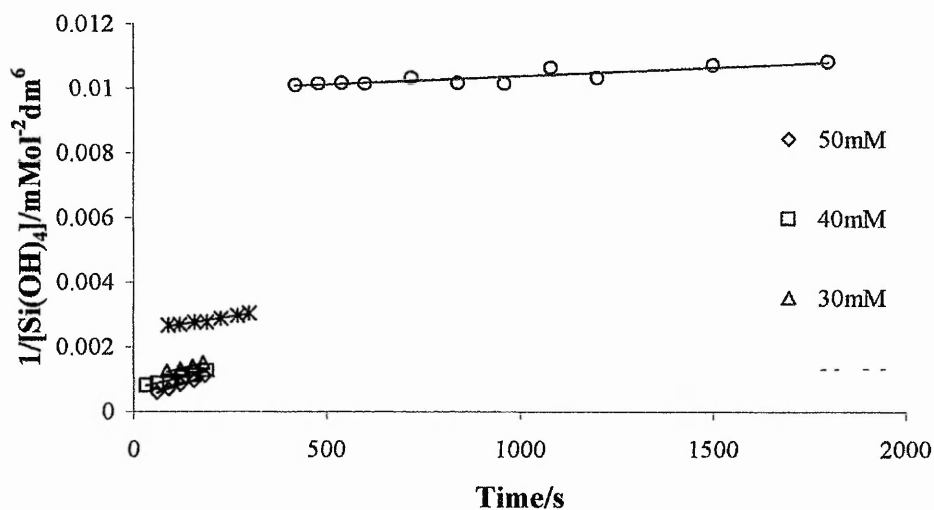


Figure 3.21 3rd order rate domains with increasing concentration.

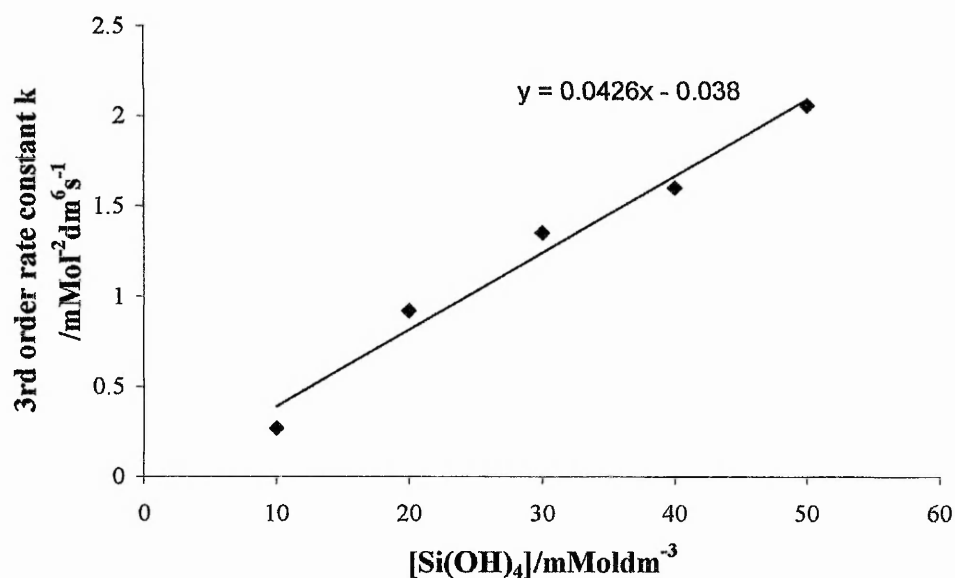


Figure 3.22 Increase in 3rd order rate constant with increasing [Si(OH)₄].

Solutions of dipotassium tris (1,2-benzenediolato-*O,O'*)silicate.2H₂O for experiments conducted throughout were made up by weighing out 140.0mg ± 0.2mg. The significance of this margin of allowed error can now be determined in terms of rate constants. The margin of error allowed in the weight of complex was calculated to result in an uncertainty of ±0.001 for a rate constant of 1.260 mmol²dm⁻⁶s⁻¹. The error margin allowed for the weight of complex taken can therefore be regarded as resulting in negligible effect on the 3rd order rate constant observed.

Extrapolation of the 3rd order rate data to zero gives a concentration of 0.9mmoldm⁻³ which is the equilibrium concentration for this reaction. Due to the forward reaction dominating at the concentrations of monosilicic acid usually used for the model system this reaction stage is treated as non reversible. This result reinforces the reversibility of the reaction step and puts a limit of 86ppm on the solubility of silica in the conditions of the experiment which is in line with other estimates.¹⁷

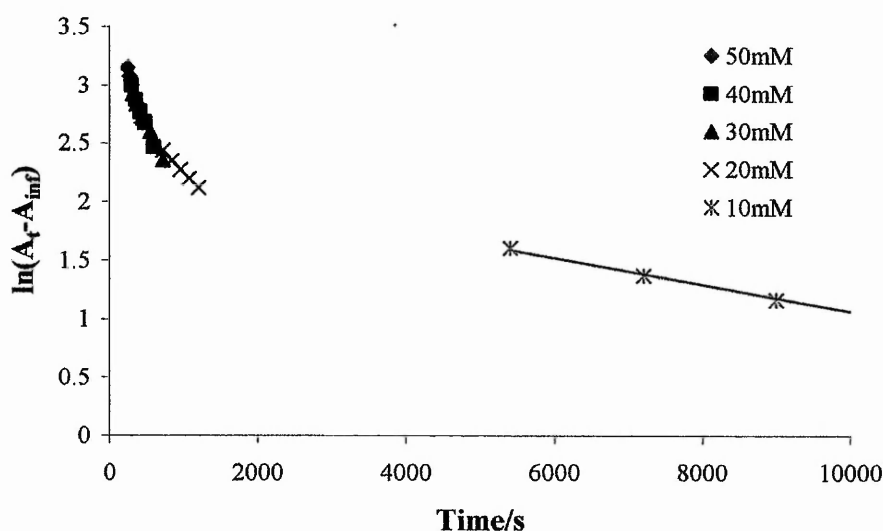


Figure 3.23 Reversible 1st order kinetic domains at increasing [Si(OH)₄].

For the 1st order data the forward and reverse rates showed a convergence at around 8mMdm⁻³ for the equilibrium concentration suggesting that at lower concentration the oligomers will dissolve. This is at odds with reported solubility of silica particles in water which is lower at 100- 200ppm. However it does reinforce the observed trend for solubility of particles decreasing with increasing size.

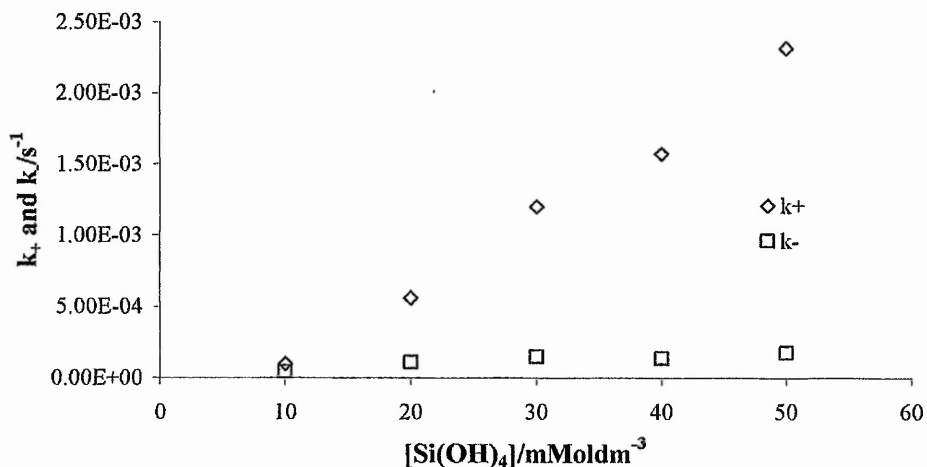


Figure 3.24 Reversible 1st order rate constants for condensation of monosilicic acid on to oligomers at increasing concentration.

3.5.3 pH dependence.

Solutions of dipotassium tris(1,2-benzenediolato-*O,O'*)silicate.2H₂O were prepared to give a final concentration of 30mmoldm⁻³ on addition of 2moldm⁻³ HCl and held in a water bath at the experiment temperature to equilibrate. Acid additions were varied to give final solution pH's of 3.4 – 6.8. After acid addition 10μl aliquots were taken at timed intervals for the molybdenum blue assay. Data was treated as outlined in Chapter 2.1

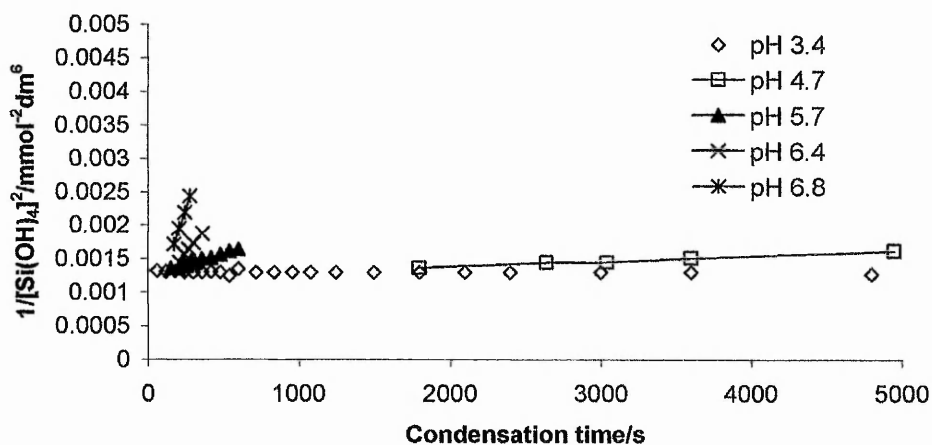


Figure 3.25 3rd order rate domains for monosilicic acid condensations carried out at varying pH. No evidence of 3rd order kinetics was observed at a pH 3.4, hence no trend line is shown.

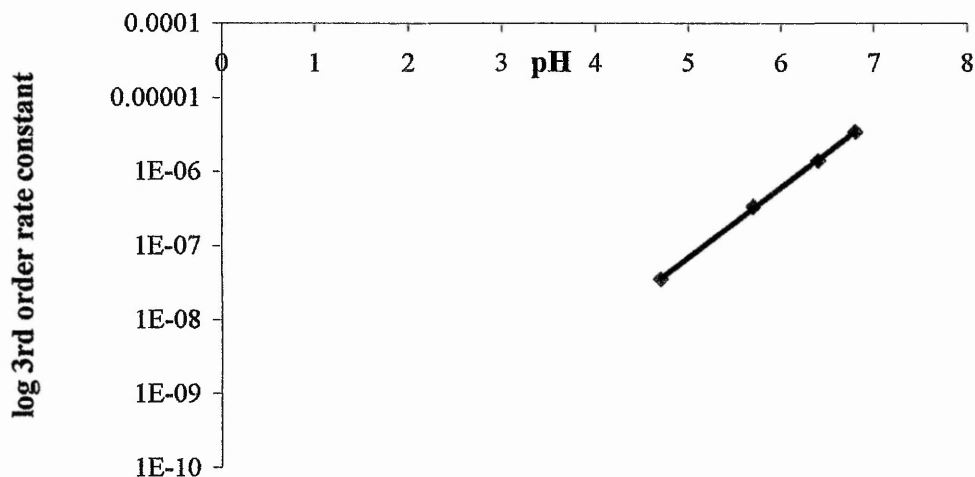


Figure 3.26 Plot of log 3rd order rate constants against pH.

The significant change in 3rd order rate constant with pH reinforces the importance of carefully controlling the acid addition to obtain meaningful data from the model system. A discrepancy of ± 0.2 either side of pH 7 results in a range of $\pm 20\%$ in the measured rate constant. At a pH of 3.4 no evidence of condensation was observed in the first 24 hours of measurement. After 7 days the level of monosilicic acid had fallen to $\sim 9.0 \text{ mmoldm}^{-3}$. The fact that condensation was observed after 7 days indicates that changing the pH of the model system allows us to observe the dimerisation stage, a kinetic domain not accessible under the normal model conditions. Also by being able to monitor kinetic domains over extended time periods in this way would allow us to explore the cross over to other techniques such as NMR and mass spectrometry, techniques that are much less time intensive in terms of labour time of the analyst compared to the molybdenum blue method.

The effect of increasing the pH was to greatly increase the condensation rate. As detailed in chapter 1, the condensation mechanism for monosilicic acid involves the presence of anionic species. As the pH rises the population of these anionic species rises due to the increased deprotonation of silanol groups, and as a consequence the rate of condensation rises. The log of the 3rd order rate constant shows a linear response with pH, i.e. with $[\text{H}^+]$. Reversible first order rates also increased (both forward and reverse) with increasing pH. However the increases appear to approach a limit as the pH increases further (figure 3.29) not observed for the 3rd order data.

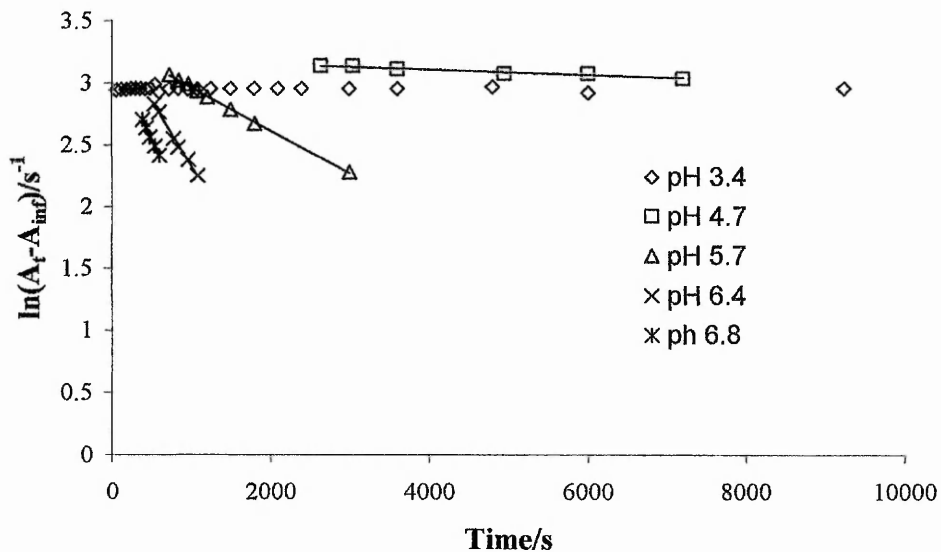


Figure 3.27 Reversible 1st order domains at pH's ranging from 3.4 to 6.8. At pH of 3.4 there was no evidence for a 1st order kinetic domain.

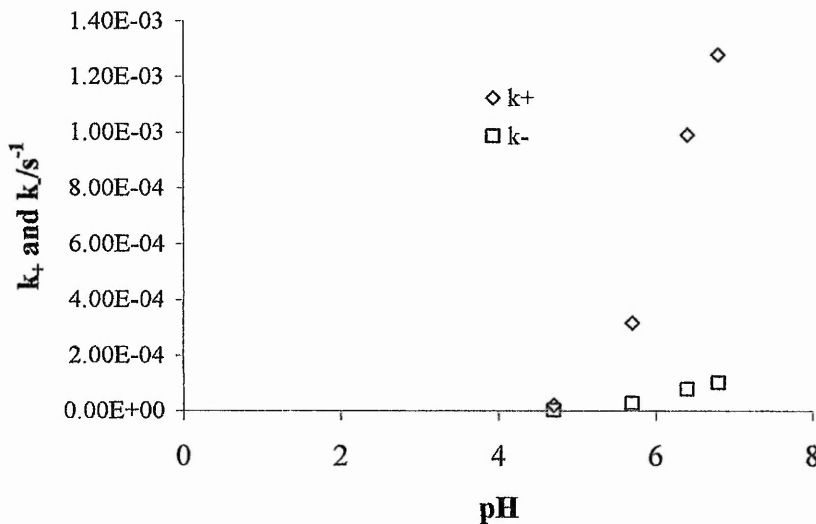


Figure 3.28 1st order forward and reverse rate constant variation with pH.

This can be explained by comparing these results with the the pKa of monosilicic acid and particulate silica and its influence on the level of deprotonation of the silanol groups.¹⁸ The pKa of monosilicic acid is around 9.8 making it a very weak acid. Removal of protons from the silanol groups is therefore difficult and even at pH 8 less than 2% of the silanols are deprotonated (figure 3.30), but over the range of pH 5 – 8 the deprotonation of silanol groups follows a linear trend. By comparison colloidal

silica particles are stronger acids with a pKa of 6.8 and at a pH of 8 ~94% of silanol groups are deprotonated. As the level of deprotonation increases so the difficulty in deprotonating the remaining ones increases and the pH has to be increasingly raised. As a consequence of this the change in the rate of condensation increase becomes exponential. This is not observed for the 3rd order rate as at less than 1% anionic molecules there is no increased resistance to deprotonation.

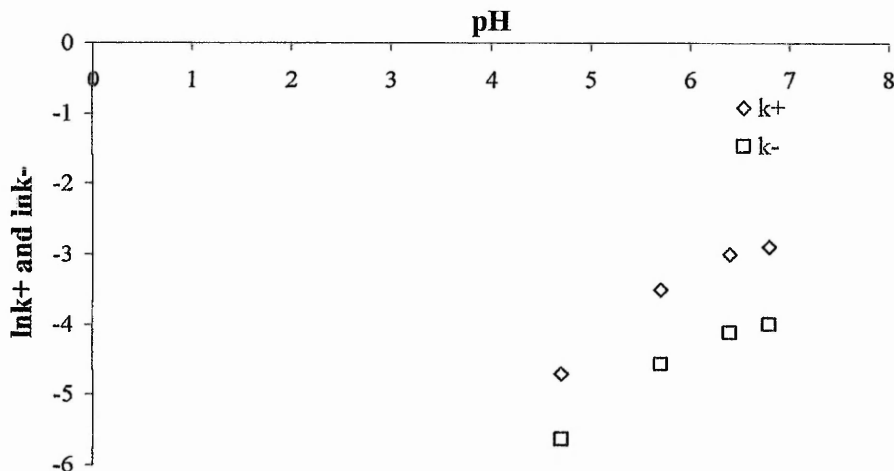


Figure 3.29. Log forward and reverse 1st order rate constant variation with pH.

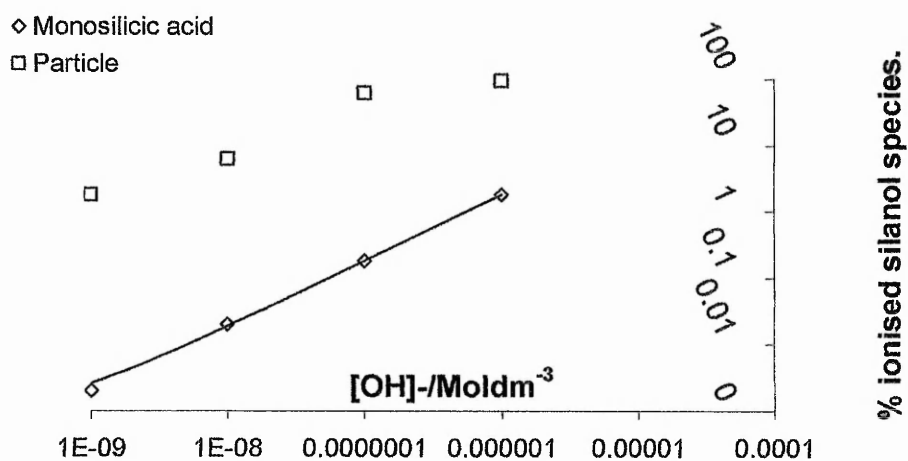


Figure 3.30. Affect of hydroxide ion concentration on silanol ionisation in monosilicic acid and particulate species.

Summary.

In this study of the model system the elimination of the necessity to construct conversion factors tables for the residual complex was achieved by careful control of acid addition aimed at dissociating in excess of 95% of the silicon complex but maintaining the pH at 7.0.

The study of solution species by ^{29}Si NMR and ESIMS and the silicomolybdic acid method found no evidence of interfering species with the 3rd and 1st order reversible but did indicate the potential for mass spectroscopy to analyse these models, possibly in conjunction with NMR particularly at reduced pH. The complex was shown to dissociate as required within the time of sample data acquisition for the molybdenum blue kinetic analyses. Statistical analysis conducted on the model system showed that the control of variable parameters were successful. The importance of the control of pH, temperature and to a lesser extent the concentration of the model system was emphasised by kinetic analyses and enabled the determination of activation energies for the 3rd order trimerisation step and the reversed 1st order phase of condensation. These were found to be in agreement with published data. Stability concentration limits were estimated at both the kinetic phases studied suggesting agreement with published effects on particle size and condensation rates were shown to increase with pH but increases were shown to be limited by the increased difficulty of deprotonation caused by charge density. The possibility of transferring technologies was also raised by the pH analysis of the model system by slowing down the kinetic domains sufficiently to allow longer timescale analytical techniques such as NMR spectroscopy to be used.

References.

- 1) N. Kroger, S. Lorenz, E. Brunner and M. Sumper, *Science*, 2002, 298, 584.
- 2) S. V. Patwardhan and S. J. Clarson, *Silicon Chem.*, 2002, 1(3), 207.
- 3) L. Sudheendra and A. R. Raju, *Mater. Res. Bull.*, 2002, 37, 151.
- 4) J. N. Cha, G. D. Stucky, D. E. Morse and T. J. Deming, *Nature*, 2000, 403, 289.
- 5) T. Coradin and J. Livage, *Colloids Surf. B*, 2001, 21, 329.
- 6) T. Coradin, O. Durupthy and J. Livage, *Langmuir*, 2002, 18, 2331.
- 7) T. Mizutani, H. Nagose, N. Fujiwara and H. Ogoshi, *Bull. Chem. Soc. Jpn.*, 1998, 71, 2017.
- 8) C. C. Harrison (now Perry) and N. Loton, *J. Chem. Soc., Faraday Trans.*, 1995, 91, 4287.
- 9) C. C. Perry and T. Keeling-Tucker, *Colloid Polym. Sci.*, 2003, 281, 652.
- 10) C. C. Perry and T. Keeling-Tucker, *Chem. Chemmun.*, 1998, 2587.
- 11) A. Hertzog and A. Weiss, *Biochemistry of silicon and related problems*, Plenum press, New York., 1978, 108-128.
- 12) S.D. Kinrade, A.M.E Gillson, C.T.G. Knight., *J. Chem. Soc., Dalton Trans.* 2002, 307-309.
- 13) P. Bussian, F. Sobott, B. Brutschy, W. Schrader, F. Schuth., *Angew.Chem.Int.Ed.* 2000,39,21,3901-3905.
- 14) M.J. Mora-Fonz, C. Richard, A. Catlow, D.W. Lewis., *Angew.Chem.Int.Ed.* 2005,44,3082-3086.
- 15) H.P Rothbaum, A.G Rhode, *J. Colloid Interface Sci.*, 1990,73,345
- 16) W.A House, L.A Hickenbottom, *J. Chem Soc., Faraday Trans.*, 1992,88,2021
- 17) R.K Iler, "The chemistry of silica," Plenum Press, NewYork, 1979.
- 18) C.C Perry, D.Belton, K. Shafran, in "Progress in Molecular and submolecular biology", ed W.E.G Muller, Springer-Verlag, Berlin Heidelberg,2003,33,277.

Chapter 4.

The effects of amino acids on the condensation and aggregation of silica in the model system.

4.1 Introduction

Proteins and peptides have been found intimately associated with biosilica, presumably encased during the condensation process. It is believed that these proteins/peptides are involved in the generation of well regulated biosilica structures. A major source of interaction of proteins/peptides with silica and silicic acids will be their side chain functionalities which show a range of physicochemical properties. It is necessary to understand the contribution of these components, singly and in combination, in order to gain some understanding of the interactions taking place in the biosilicification process. To this end a systematic study of the effect of amino acids and small peptide oligomers on silica formation from aqueous solution was conducted. The amino acids chosen were selected in order to cover as much as possible the range of properties exhibited by the naturally occurring amino acids found associated with plant biosilica (equisetum species).^{1,2} To this end the following were selected:

Amino acid (all L isomers)	Isoelectric point (pI)	Classification	Side chain functionality
Glutamic acid	3.22	Polar -ve charge (acid)	Acid
Asparagine	5.41	Polar uncharged	Amide
Threonine	5.64	Polar uncharged	Hydroxyl
Glutamine	5.65	Polar uncharged	Amide
Tyrosine	5.66	Aromatic	Phenolic
Serine	5.68	Polar uncharged	Hydroxyl
Glycine	5.97	Non polar	None
Alanine	6.00	Non polar	Methyl
Proline	6.30	Polar uncharged	Condensed cyclic

Amino acid	Isoelectric point (pI)	Classification	Side chain functionality
Lysine	9.59	Polar +ve charge (base)	Amine
Arginine	11.15	Polar +ve charge (base)	Guanidine

This selection allowed the study of the effects of a wide range of side chain isoelectric points (3.22 – 11.15), polarities and side chain functionalities. Following early results it was also decided to examine the effect of small chain homopeptides of L-lysine. Homopeptides with 1-5 repeat L-lysine groups were therefore used in addition to a polylysine sample of 150 repeat units, a species which has been shown to affect silica morphology in vitro using other precursors.

4.2 Experimental.

Experiments were conducted as detailed in Chapter 2. Amino acids were added at a mole ratio of 1:2 amino acid to silicon and lysine oligomers at the same ratio based on amino acid units.

4.3 Results.

4.3.1 Solution chemistry.

The residual un-dissociated complex for reactions performed in the presence of a 1 amino acid : 2 silicic acid molar ratio after 24 hours reaction varied from 0.2–0.6 mmoldm⁻³, corresponding to an initial orthosilicic acid concentration for the condensation experiments of 29.4 to 29.8 mmoldm⁻³ (98–99%). The pH of all solutions was in the range 6.8 ± 0.2. Silicic acid concentrations were monitored from 30 seconds after initiation of the reaction (by lowering of pH or mixing) until 24 hours of reaction had elapsed.

Figure 4.1 shows plots of silicic acid concentration with time in the presence of amino acids. The data for the blank model sample is shown for comparison.

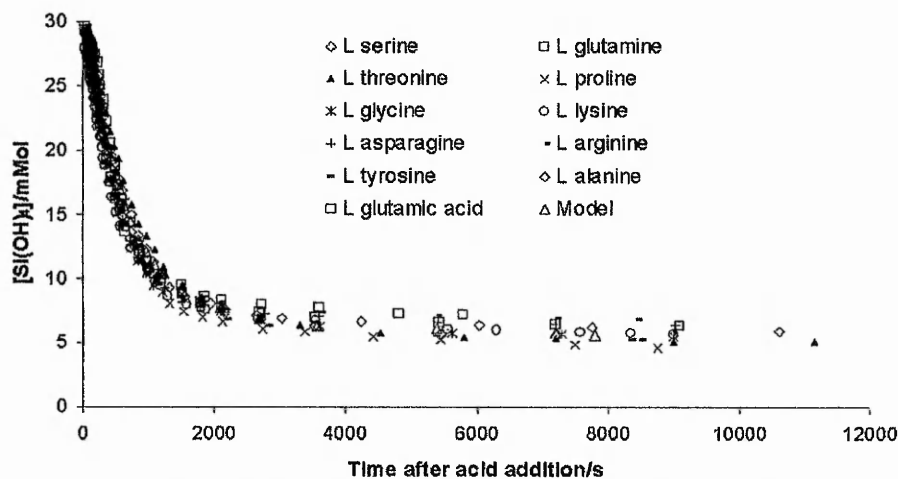


Figure 4.1 Changes in orthosilicic acid concentration with time following initiation of the reaction by pH reduction to 7.0 for a 30 mmol dm^{-3} solution of $\text{K}_2[\text{Si}(\text{Cat})_3] \cdot 2\text{H}_2\text{O}$ in the presence of 15 mmol dm^{-3} of selected amino acids.

None of the experiments showed a dominant dimerisation phase where no loss in silicic acid with time was observed. The region of 3rd order dominance occurred during the first 3 minutes of condensation for reaction with all the amino acids studied. Increased rates of condensation were observed for arginine, asparagine, lysine and glutamine and slower rates of condensation, compared to the blank system for reactions performed in the presence of threonine and glutamic acid (Fig. 4.2).

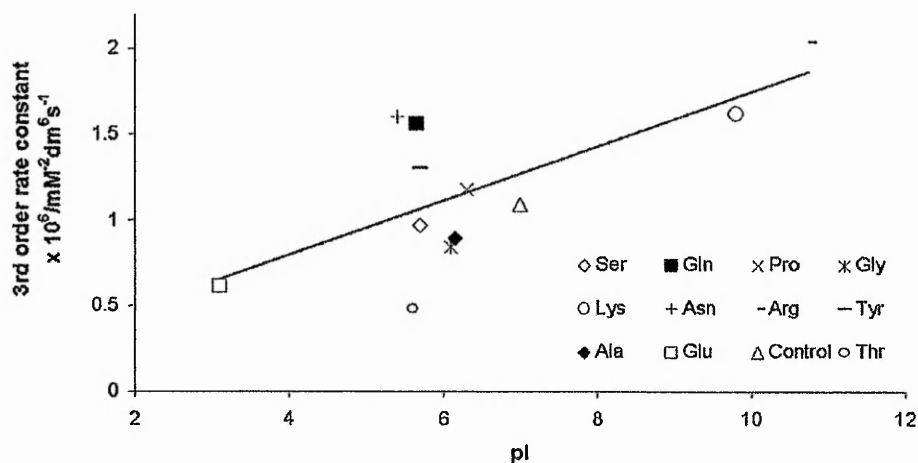


Fig 4.2 The relationship between the 3rd order rate constant for the formation of trimers from monomer and dimer of orthosilicic acid and isoelectric point of selected amino acids. The line shows the trend only.

The reversible 1st order region dominated from about 4 to 12 minutes in each of the experiments but with less influence of the amino acids when compared with the 3rd order region. By the end of the reversible 1st order region (after ~12 minutes) between 50 and 60% of the available orthosilicic acid had condensed to trimers or larger oligomers. All of the systems showed a continued reduction in orthosilicic acid over the 24 hour period investigated with a range of rates between $1.2\text{--}2.1 \times 10^{-3} \text{ mmoldm}^{-3} \text{ min}^{-1}$. Final orthosilicic acid concentrations ranged from 3.5 to 5.0 mmoldm^{-3} . At the end of the 24 hour period all but proline had formed a clear weak gel which could be broken by very gentle agitation. In the case of experiments performed in the presence of proline, a grainy sediment was formed as observed by the naked eye. For reactions performed in the presence of L-lysine homopeptides the residual undissociated complex varied from 0.1 to 0.7 mmoldm^{-3} , corresponding to an initial orthosilicic acid concentration of 29.3 to 29.9 mmoldm^{-3} (98–99%). The pH of the solutions prepared using the shorter peptides was 6.8 ± 0.2 , but that of reactions performed in the presence of poly L-lysine was 6.4. On addition of poly-lysine to the complex an immediate precipitate was formed. This was not thought to be silica as a molybdenum blue assay of the homogenised mix still gave an orthosilicic acid concentration of ca. 30 mmoldm^{-3} . It is suggested that the precipitate may have been the complex cationically exchanged with poly-lysine amine side chains in place of potassium. Separation of the precipitate from the supernatant immediately after mixing resulted in a reduction of orthosilicic acid being detected commensurate with about 20% of the available silicon being associated with the poly-lysine. This factor was responsible for the reduced condensation rates and a lower pH being observed during the early stages of reaction. When the precipitate was allowed to remain in the reaction mixture it was observed to slowly re-dissolve during the course of the experiment and the final orthosilicic acid concentration measured at the end of the experiment was found to be in line with all other experiments. The 3rd order rate constant was observed to increase with increasing lysine oligomer chain length from $2.2 \times 10^{-6} \text{ mmol}^2 \text{ dm}^{-6} \text{ s}^{-1}$ for the monomer to $3.2 \times 10^{-6} \text{ mmol}^2 \text{ dm}^{-6} \text{ s}^{-1}$ for the tetramer and pentamer. This compares with a value of $1.3 \times 10^{-6} \text{ mmol}^2 \text{ dm}^{-6} \text{ s}^{-1}$ for reactions conducted in the absence of lysine and its oligomers, Fig. 4.3.

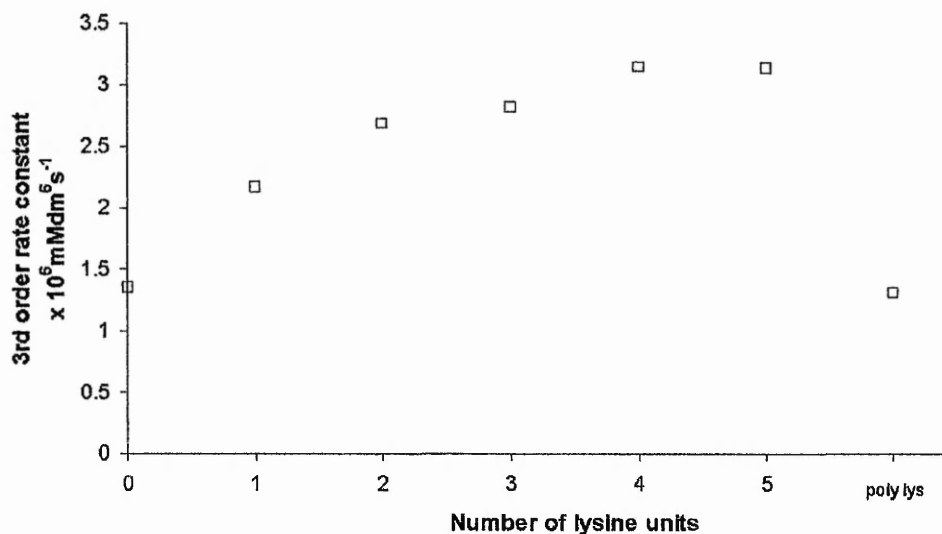


Fig 4.3 The effect of the number of lysine units per molecule on the 3rd order rate constant for the formation of trimers from a monomer and dimer of orthosilicic acid.

Increasing glycine oligomer length, on the other hand, showed little effect on the 3rd order rate constant ($0.8 \times 10^{-6} - 1.0 \times 10^{-6} \text{ mmol}^2 \text{ dm}^{-6} \text{ s}^{-1}$). The onset of the 3rd order region appeared to be slightly delayed with increasing oligomer chain length. The effect of the additives on the reversible 1st order region was less well defined, but suggested a slight increase in the rate of the forward reaction with increased oligomer length. First order kinetics dominated from around 5 to 12 minutes in all systems, during which time the available orthosilicic acid concentration fell to around 40% for the short oligomers. Over the course of 24 hours of reaction the concentration of orthosilicic acid fell to between 4.0 and 6.7 mmol dm^{-3} which were values in excess of those monitored for the blank system. At the end of the 24 hour period the samples were homogenous but had become increasingly cloudy with increasing homopolymer length but with no visible sedimentation although a sediment could be formed on gentle agitation of the solutions.

4.3.2 Photon correlation spectroscopy (PCS).

Data obtained by photon correlation spectroscopy are presented in figure 4.4 and 4.5 for experiments conducted in the presence of amino acids and oligomers of lysine

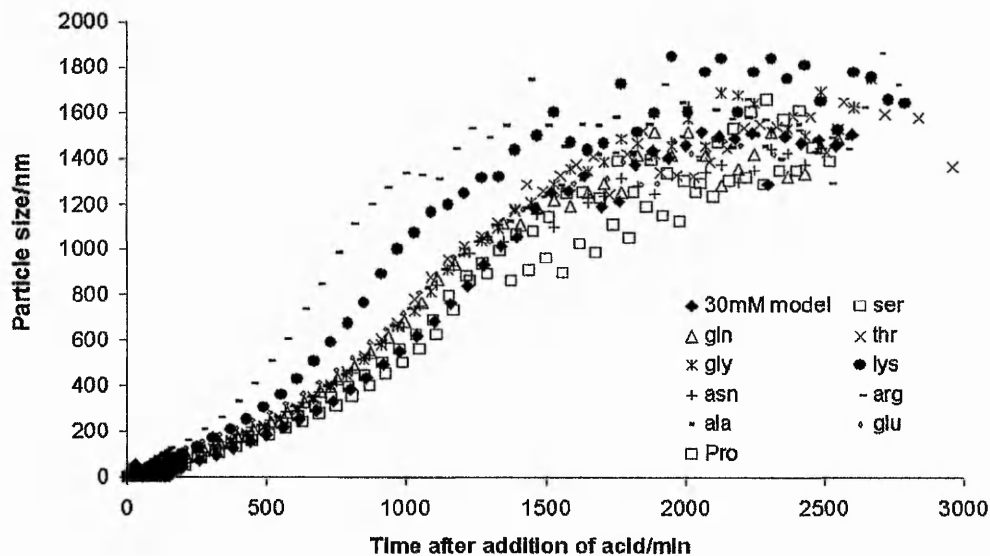


Figure 4.4 Photon correlation spectrometry of silica aggregating in the presence of selected amino acids.

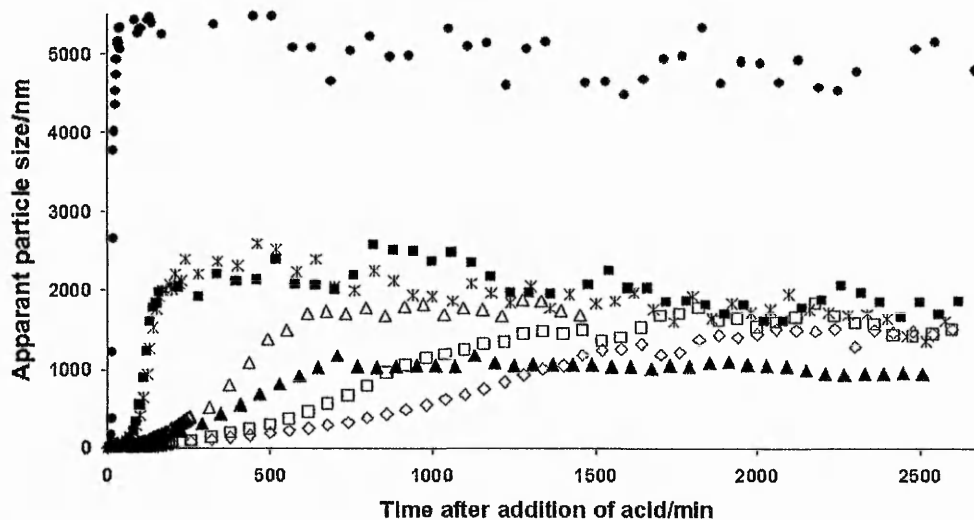


Figure 4.5 Photon correlation spectrometry of silica aggregating in the presence of (lys)_n where the total concentration of the lysine functional groups is 15 mmoldm³.

respectively. Rates of aggregation are compared by analysis of the maximum growth rates in terms of volume increase of apparent particle size with time, figure 4.6 and 4.7. For experiments conducted in the presence of amino acids, maximum aggregation rates

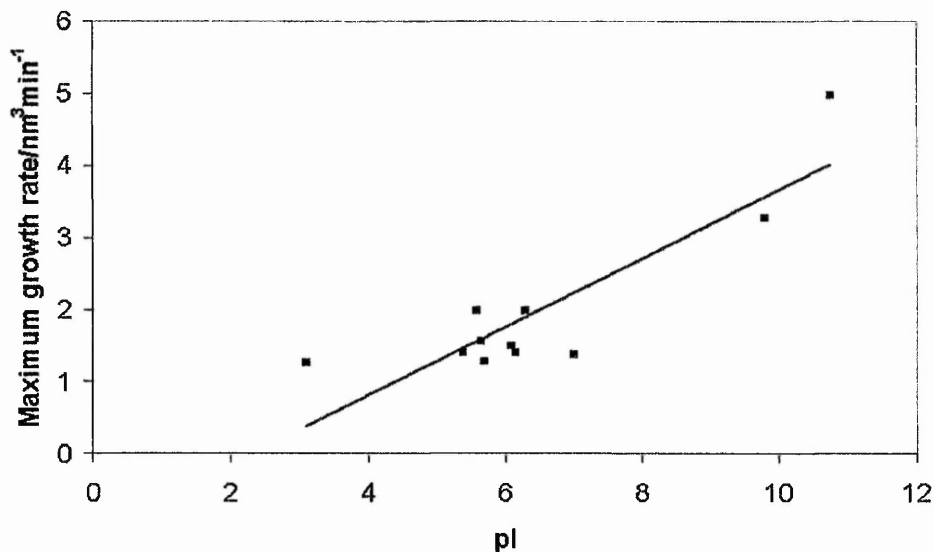


Figure 4.6 Maximum growth rate of the structures as measured by photon correlation spectroscopy in relation to the isoelectric points of the side chain functional groups of selected amino acids. The line shows the trend only.

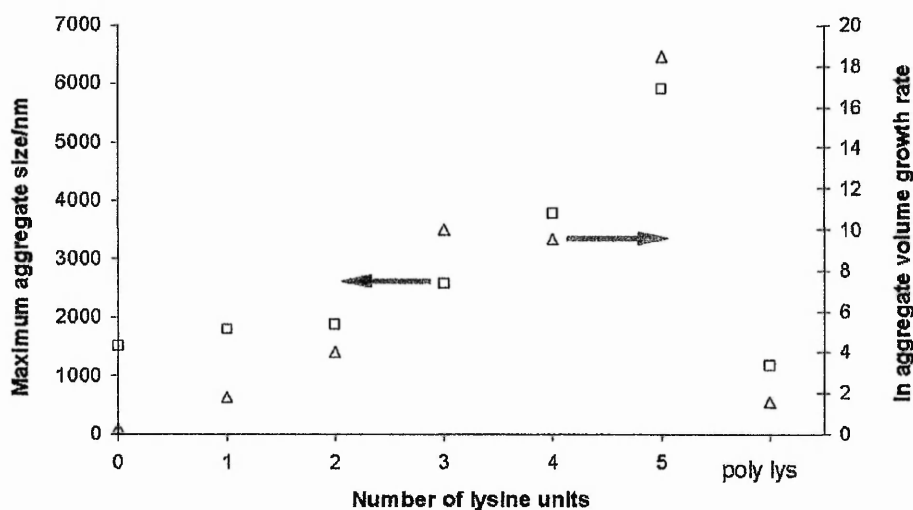


Figure 4.7 Maximum growth rate and maximum apparent particle size for silica aggregating in the presence of lysine oligomers.

were observed for L-arginine and L-lysine (5.0 and $3.3 \text{ nm}^3 \text{ min}^{-1}$ respectively) compared to a value of $1.4 \text{ nm}^3 \text{ min}^{-1}$ for the blank alone. The lowest rate was observed for L-glutamic acid of $1.3 \text{ nm}^3 \text{ min}^{-1}$. For all systems a maximum aggregate size was attained

after which an increased scatter in the data occurred which was also marked by a decrease or cessation in the aggregation growth. The shortest times for this boundary were observed for L-arginine and L-lysine (1000 and 1300 min respectively), for all others the time was between 1500 and 1600 min. The rates and boundary times were found to be largely in line with the isoelectric points of the amino acids and were shown to be most significant where the amino acid side chains were expected to be charged at the pH of the experiments, figure 4.6. For precipitation experiments performed in the presence of L-lysine homopeptides, aggregation rates were dramatically increased with lysine units from $3.3 \text{ nm}^3 \text{ min}^{-1}$ to $103 \times 10^6 \text{ nm}^3 \text{ min}^{-1}$ for the range mono to penta L-lysine, figures 4.5 and 4.7. Apparent maximum particle size increased from mono to penta L-lysine from 1800 nm to 5900 nm, figure 4.7. The boundary times decreased with increased L-lysine number from 1640–40 minutes and were followed by a period of contraction observed for di L-lysine to penta L-lysine but not for reactions carried out in the presence of the monomer or for the control reaction. Glycine oligomers showed little change in the aggregation rate ($1.5\text{--}2.6 \text{ nm}^3 \text{ min}^{-1}$), boundary times were all ~ 1500 min and no subsequent contraction was observed.

4.3.3 Residual organic material in sedimented silica.

Residual organic material entrained within the sedimentable silica (not removed on washing with distilled water) was determined as the weight lost during thermogravimetric analysis over the temperature range 400–800 K after subtraction of the underlying loss of weight through silanol condensation over the same range (i.e. for the blank system), figures 4.8 and 4.9. This temperature range corresponded to the thermal decomposition of organic compounds and resulted in the loss of CO_2 , H_2O , NH_3 and some short chain volatile rearrangement products. In the experiments carried out under nitrogen, darkening of samples was observed, which is indicative of the presence of residual organic matter (as graphite). For silicas condensed in the presence of amino acids, only material prepared in the presence of L-tyrosine showed a significant weight loss over the temperature region highlighted. This was thought to be due to its low water solubility

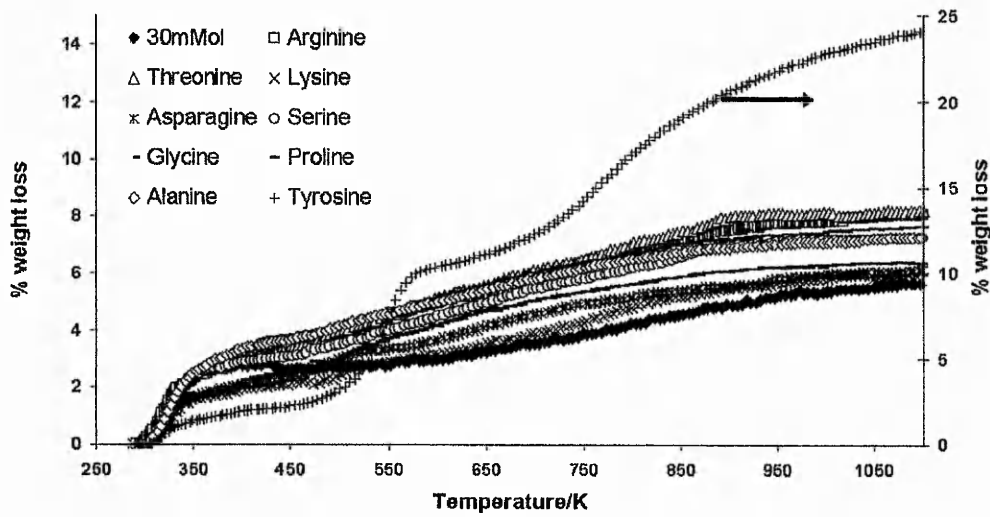


Fig 4.8 Thermo-gravimetric analysis of silicas condensed in the presence of selected amino acids.

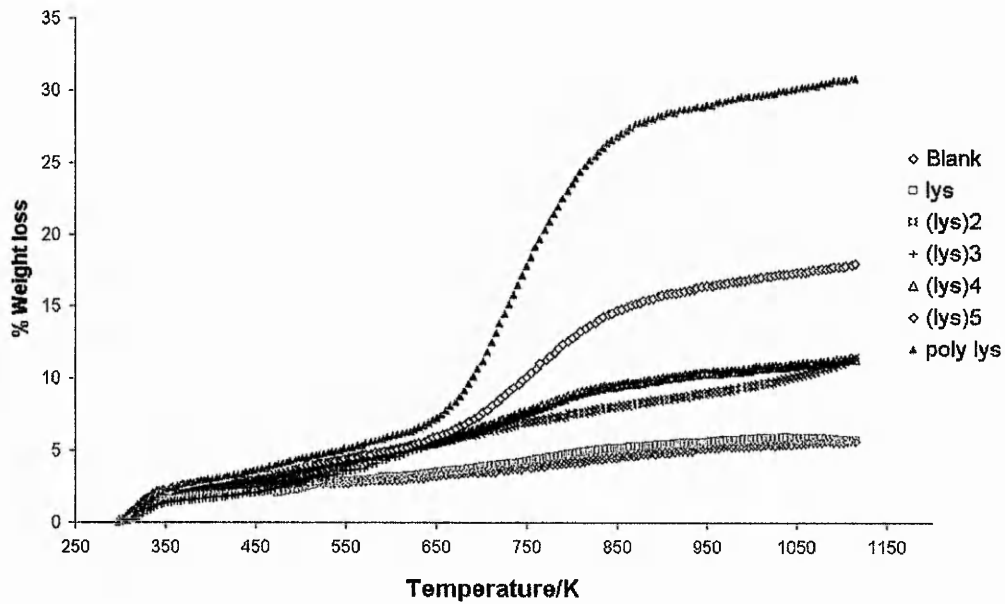


Fig 4.9 Thermo-gravimetric analysis of silicas produced in the presence of $(lys)_n$.

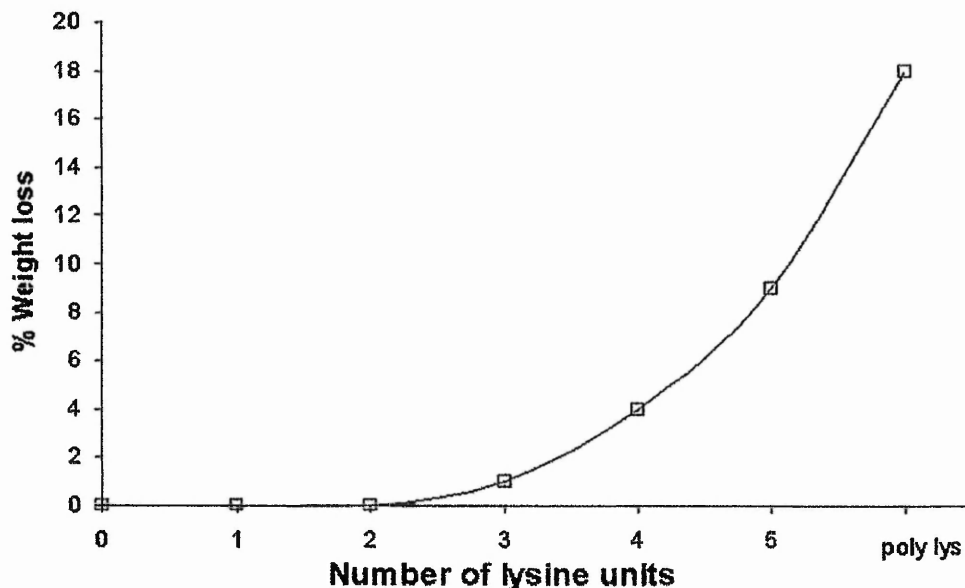


Fig 4.10 Relationship between % weight loss from silica with number of lysine units in homopeptide.

rather than its incorporation into the silica matrix. The L-lysine homopeptides showed increasing incorporation with increasing chain length with 9% penta L-lysine retained and 18% poly L-lysine retention, figure 4.10. Glycine oligomers by comparison showed little organic component in the silica produced—the maximum found was ~0.5% in pentaglycine .

4.3.4 Gas adsorption analysis.

Silica samples produced in the presence of amino acids gave type IV isotherms with type A hysteresis typical of micro/ mesoporous materials according to the classifications of Brunauer, Deming, Deming and Teller (BDDT)³ and deBoer⁴ respectively. Surface areas were determined by the application of BET⁵ isotherms and pore volumes and size domains were determined by the BJH method.⁶ Surface area analysis by the BET method gave values between 538 and 730 m² g⁻¹. A correlation between surface area and side chain hydrophobicity was observed, figure 4.11, the most hydrophobic amino acids

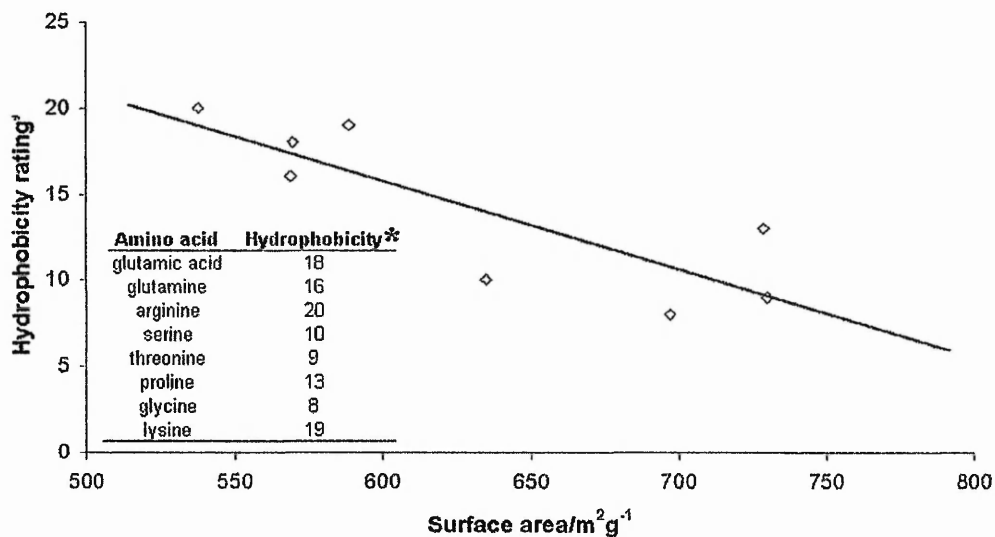


Fig 4.11 Relationship between surface area and order of hydrophobicity of selected amino acids for silica condensed in their presence. The line shows the trend only. The order of hydrophobicity was based on physicochemical properties of amino acid side chains.

producing the largest surface areas. Values of hydrophobicity were arbitrarily assigned as 1–20 for the most hydrophobic to the least hydrophobic functional side chain. Adsorption/desorption isotherms for the silicas prepared in the presence of the small (1-3) lysine oligomers gave type IV isotherms with type A hysteresis typical of micro/mesoporous materials. For silicas prepared in the presence of the larger peptides the hysteresis was observed to shift to higher partial pressures. A decrease in surface area was observed with increasing chain length, figure 4.12. Increases in average pore diameter but little change in pore volume were also observed. There was a general trend towards reduced micropore volumes and increasingly disperse and enlarged mesopores with increasing lysine peptide chain length, figure 4.13. The material changed from predominantly mesoporous to predominantly macroporous as the peptide length increased from 3 to 5, figure 4.14.

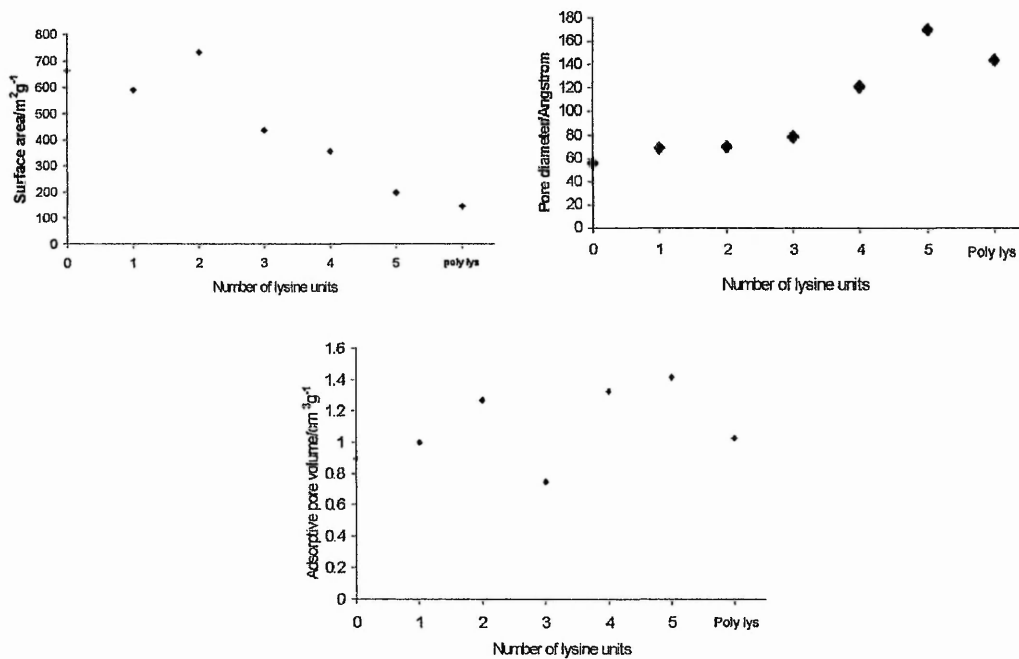


Fig 4.12 Surface area, pore volume and average pore diameters for silicas produced in the presence of $(\text{lys})_n$.

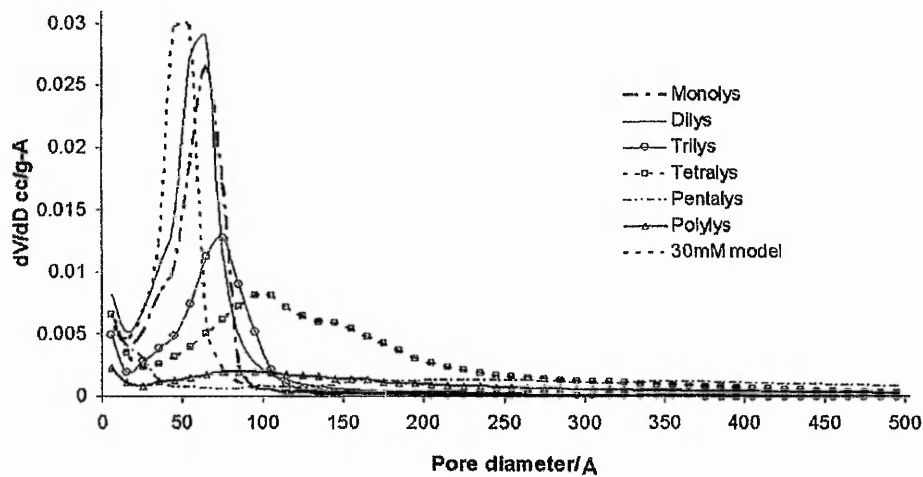


Fig 4.13 Pore size distributions for silicas produced in the presence of $(\text{lys})_n$.

For silica prepared in the presence of polylysine a range of both mesoporous and macroporous pores was observed, perhaps due to silica being deposited at different time

periods in the silica precipitation reaction due to the initial presence of the polylysine-silicon complex aggregate that was observed to form.

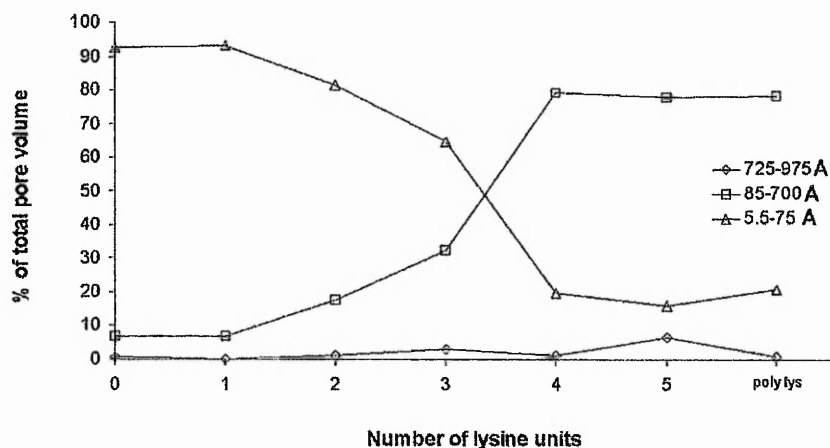


Fig 4.14 Relative pore volumes of different size domains of pores in silicas produced in the presence of $(lys)_n$.

4.3.5 Scanning electron microscopy (SEM).

In the case of silica formation without any additive, the typical average particle size as observed by SEM was 77 nm (micrograph H in figure 4.15). The material is however made up of primary particles in the order of a few nanometers so these particles represent the formation of localised aggregates. In the presence of the nitrogen containing amino acids considered here, larger aggregates were observed. In particular, the average aggregate size in the case of arginine (micrograph A, figure 4.15) was 123 nm and that for asparagine (micrograph B, figure 4.15) was 175 nm. All silicas synthesised in the presence of nitrogen-containing amino acids produced materials with granular appearance. Silica prepared using lysine and glutamine (micrographs G and E respectively in figure 4.15) contained aggregates of average size of 108 and 140 nm respectively. Furthermore, addition of lysine and glutamine to the reaction medium were also found to alter the macroscopic morphology of the silica. As shown in the inserts of micrographs E and G in figure 15, it can be seen that both amino acids produced silica with sharp edges, while no such morphologies were observed in the other samples.

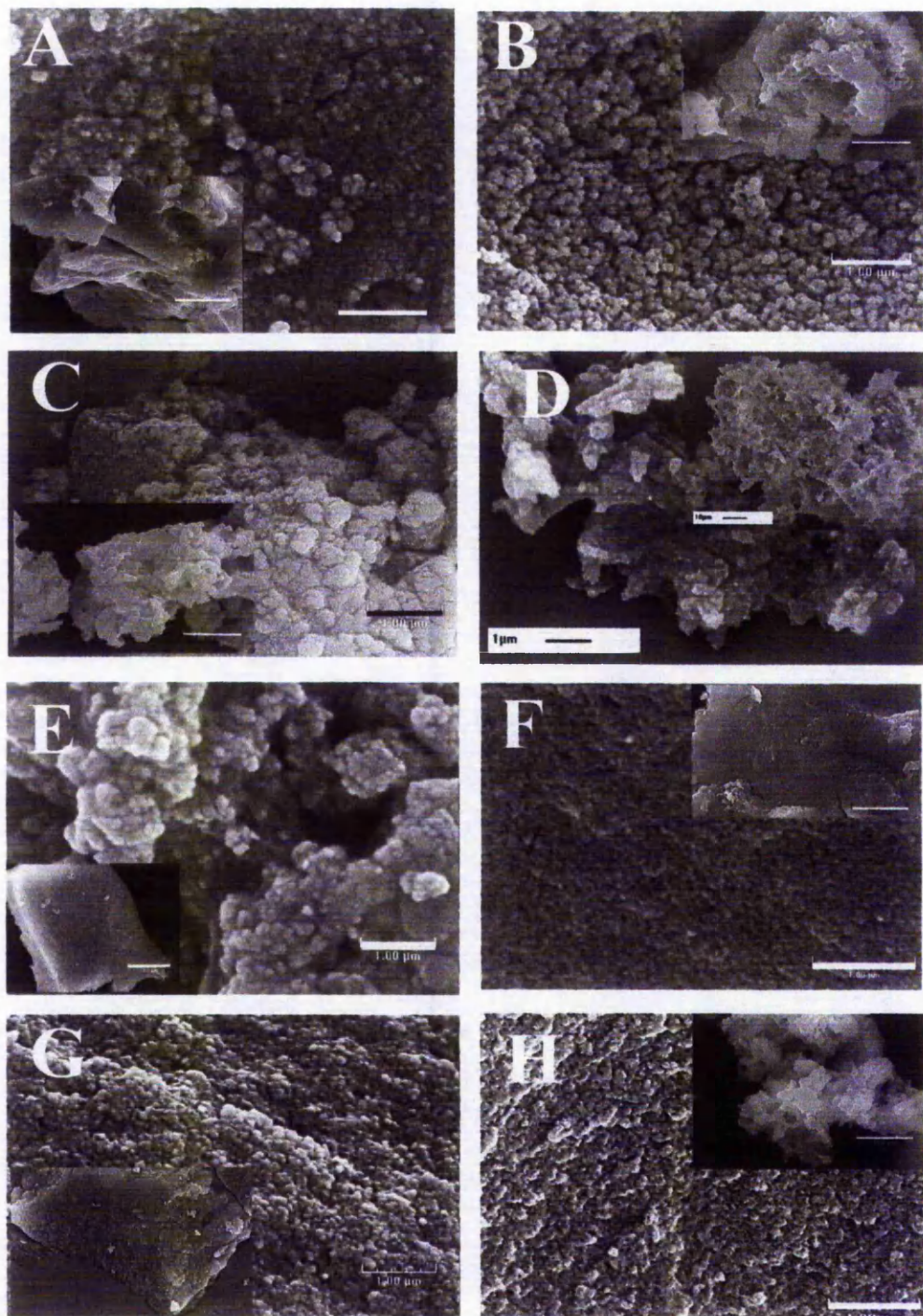


Figure 4.15 Scanning electron micrographs of silicas produced in the presence of selected amino acids. A). Arginine, B). Asparagine, C). Glutamic acid, D). Glycine, E). Glutamine, F). Alanine, G). Lysine, H). Blank. Scale bars represent 1 μ m. Inserts 10 μ m.

The presence of proline in the reaction medium produced a granular silica with average particle size of 114 nm, (micrograph A of figure 4.16).

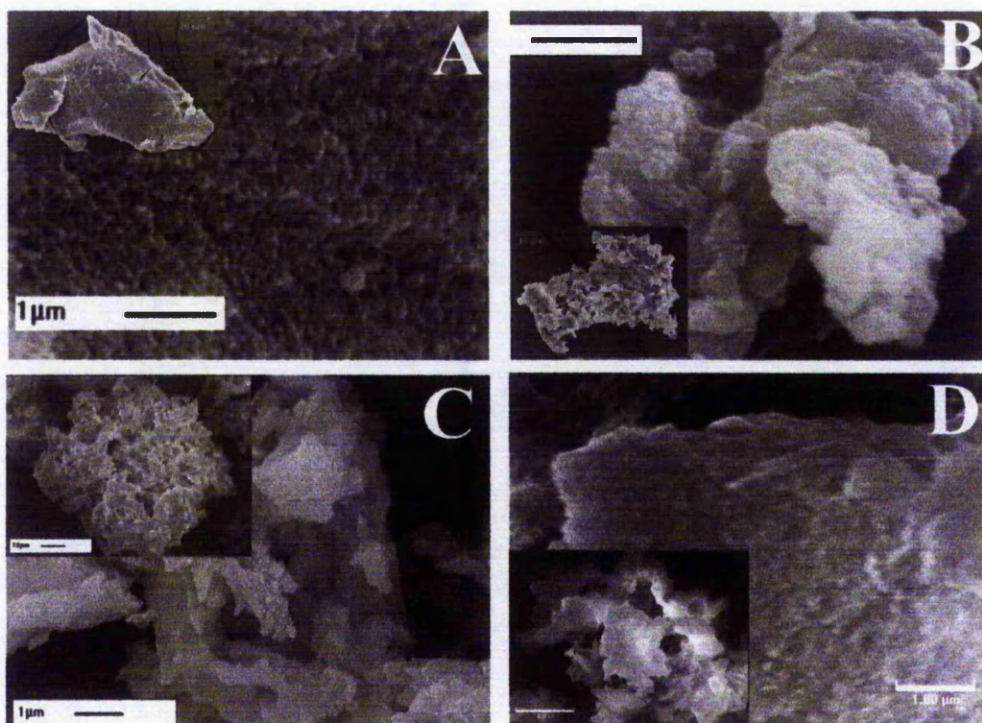


Fig 4.16 Scanning electron micrographs of silicas produced in the presence of selected amino acids. A. proline, B. serine, C. threonine acid, D. tyrosine. Scale bar represents 1 μm (inserts 10 μm).

Hydroxyl containing amino acids decreased the granular appearance of the silica produced. Serine, threonine and tyrosine were found to produce silica with “smooth” surface morphology (micrographs B, C and D in figure 4.16). These amino acids affected the macroscopic nature of silica to a limited extent. Finally, glycine and alanine had little effect on the silica produced in their presence. The average particle sizes of silica synthesized in the presence of glycine and alanine were 84 and 48 nm respectively and more open flaky structures were formed. Although glutamic acid did not affect the particle formation on the microscopic scale, various large aggregates were observed (see micrograph C in figure 15). Based on the data presented herein on the role of amino acids in silica formation, it is clear that all the nitrogen-containing amino acids investigated

have an effect on the aggregation of silica particles. Silica formation was also examined in the presence of di-, tri-, tetra-, penta- and poly-lysine samples. The representative SEM data of silica synthesized in the presence of lysine oligomers (figure 4.17). The formation of distinct silica aggregates was observed in the presence of lysine oligomers. The average aggregate sizes of silica particles formed using di-lysine, tri-lysine, tetra-lysine, penta-lysine and poly-lysine where the concentration of side chain functionalities was kept constant were respectively 108, 139, 85, 109, 122 and 467 nm. Comparatively larger particles were formed when poly-lysine was used as an additive. It should be noted that silica particles of similar sizes have been previously synthesized in the presence of poly-L-lysine using various other silica precursors such as tetramethoxysilane, ethylene glycol modified silane and water glass.^{8,9,10} In previous experiments on silica precipitation using bio-extracts isolated from horsetail ferns, it was found that these bio-extracts were able to direct the formation of crystalline domains within the siliceous material.^{1,2} In order to assess any similar structure direction in the current investigation, X-ray diffraction and selected area electron diffraction studies were performed. In the investigated samples, there was no evidence for the presence of any crystallinity.

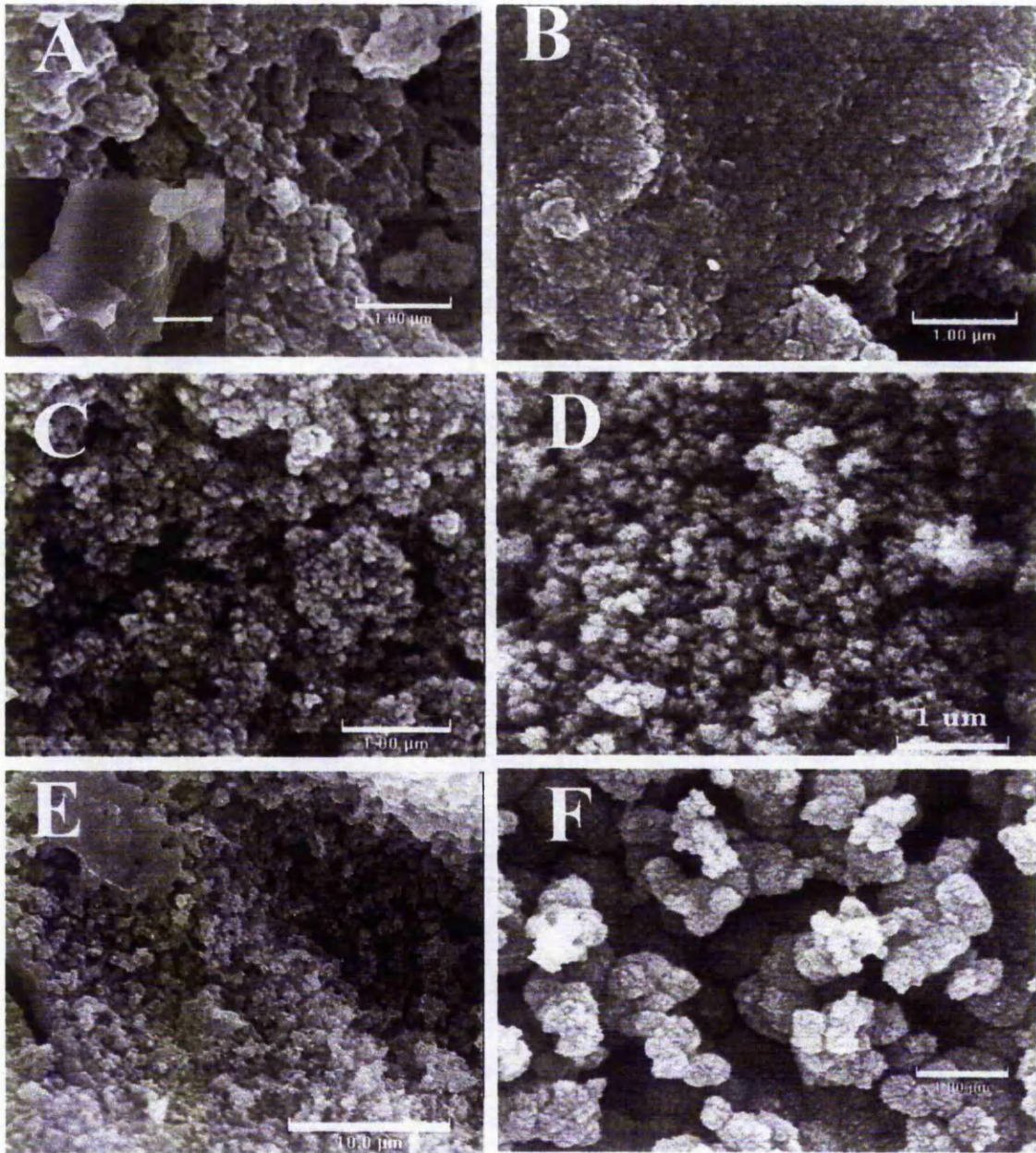


Fig4.17 Scanning electron micrographs of silicas produced in the presence of $(lys)_n$ A. $(lys)_2$ B. $(lys)_3$ C. $(lys)_4$ D. $(lys)_5$ E. and F, poly-lysine.

Scale bars represent 1 μm for A-D, F and 10 μm for E and insert in A.

4.4 Discussion.

Solutions of orthosilicic acid at a concentration of 30mmoldm^{-3} were rapidly formed at circumneutral pH by the acid dissociation ($\sim 98\%$ complete) of the complex $\text{K}_2[\text{Si}(\text{C}_6\text{H}_4\text{O}_2)] \cdot 2\text{H}_2\text{O}$. This allowed the early stages of condensation of orthosilicic acid in an aqueous environment to be followed in the absence of interference from continued hydrolysis of organosilicon species. This is in direct contrast to model studies using organosilane precursors such as tetramethoxysilane where a complex mixture of oligomers (some alkoxylation is still present) is generated within 15 minutes of its hydrolysis with only 20% of the initial silicic acid available for reaction with any additives that are introduced at this point into the reaction environment.^{11,12,13} The initial dimerisation stage of the process is not detected by the molybdenum blue method since the dimer dissociates within the time of the silicomolybdic acid complex development so no apparent loss of orthosilicic acid is detected. This has sometimes been referred to as the induction period. During the next (3rd order) stage monomers and dimers condense so that the apparent reduction in orthosilicic acid concentration is the combined effect of monomer and dimer loss. Beyond this region, since monomer condensation on to existing oligomers occurs in preference to oligomer co-condensation, reversible 1st order kinetics are observed as a competing dissolution of monomer back in to solution occurs. The rate constant measured for the trimerisation stage was increased by the addition of nitrogen containing amino acids, particularly L-arginine and L-lysine, and was reduced for reactions performed in the presence of L-glutamic acid. This effect highlights the dependence of the early stages of condensation on the presence of anionic species since rates at neutral pH are controlled by relatively small populations of them;



Enhancement of anion formation in the presence of L-arginine and L-lysine, and suppression in the presence of L-glutamic acid would be expected and it appears to be the case. In addition to L-lysine and L-arginine, L-asparagine and L-glutamine were also able to affect the kinetics in the early stages of silicic acid condensation. The role of these

uncharged nitrogen side chains in accelerated condensation remains unclear as the nitrogen groups are not protonatable at the pH encountered.

The importance of positively charged nitrogen functional groups in regulating amorphous silica production was reinforced when increasing chain lengths of L-lysine homopeptides were used. Onset and cessation of the trimer stage were delayed slightly. The delay in the onset of the time period when third order kinetics dominated, assuming complex dissociation and dimerisation were unaffected would result in a higher population of the dimer at the onset of 3rd order kinetics and therefore higher rates of condensation if the process is largely dependent on the presence of anionic dimers.

In studies of condensation of silicic acid prepared from sodium silicate solutions, a dramatic increase in condensation rates in the presence of lysine and arginine homopeptides has been reported.¹⁴ These solutions were allowed to condense for 10 minutes prior to introduction of the peptides so would be expected to contain a significant population of silica oligomers. In this study amino acids and lysine homopeptides were added to a rapidly dissociating complex providing supersaturated monomeric silicic acid. The condensation rates in the early stages were found to be enhanced only moderately by comparison (approximate doubling of the 3rd order rate constant observed with (lys)₅). Co-addition of poly-lysine and acid to the complex resulted in no observed immediate loss of molybdate active species, any precipitate formed was attributed to the formation of a cation exchanged poly-lysine silicon catecholate complex with lower solubility than the potassium analogue. The indication was therefore that immediate silica precipitation previously reported was due to oligomer aggregation. Aggregation rates of the condensing silica observed by photon correlation spectroscopy showed increases for L-arginine and L-lysine. Although below neutral pH silica particles become less charged and tend to aggregate there is nonetheless a noticeable effect suggesting that residual surface charges are neutralised by the presence of the basic amino acid side chains. This effect was much more prominent for the aggregation of silica in the presence of the L-lysine homopeptides and suggests that these can cause bridging between particles similar to that described previously.^{1, 8, 14} The importance of the basic side chain on these homopeptides was demonstrated by the failure of L-glycine homopeptides to produce any effect discounting homopeptide chain length alone as a contributory factor. The increased

apparent particle size observed with increased peptide chain length suggests that this bridging effect is strong enough to produce extended structures in solution but that they are too weak to survive the isolation process demonstrated by the absence of similar large scale structural changes observed by SEM. The growth cessation and onset of size irregularities observed in the PCS data are thought to occur at the stage where a continuous network of silica aggregates forms throughout the sample. The size fluctuations observed beyond this point are, we believe, due to structural inhomogeneities within this network. The subsequent general decrease in aggregate size in the systems involving lysine homopeptides could be a consequence of the bridging effect resulting in continued inter-particle silanol condensation brought about by the more proximate neighbouring aggregates or merely precipitation of some of the larger aggregates. Complete removal of organic material by washing was achieved with all of the amino acid condensed silicas with the exception of L-tyrosine due to its relative insolubility in water. However increasing amounts of organic material were found in the lysine homopeptide condensed silica with increased peptide chain length. That this is due in part to entrainment of the homopeptides in the pores formed as the silica particles condense together is in no doubt, but the failure of the glycine oligomers to be retained in the material to the same degree suggests a more involved role for the L-lysines, possibly in the formation of more inter-particle condensation brought about by extended contact times between the reacting species resulting in partial pore closure and entrapment of the lysine oligomer. Changes in surface areas, pore volumes and average pore diameters obtained for silicas prepared in the presence of the L-lysine homopolymers are also indicative of a change in the structure of the siliceous materials produced as the oligomer chain length increased. A reduction in the surface area with increasing chain length occurs whilst at the same time the volume contribution from small pores also decreases, (figure 4.14). The silicas change from being predominantly mesoporous to largely macroporous as the additives increase in length from tri L-lysine to penta L-lysine. Again this could be due to blocking of smaller pores by organic residues or through closure of pores through increased inter-particle condensation. It is also possible that some contribution to the measured porosity of the samples arises from pores present within aggregates. The surface areas of the amino acid condensed silicas could in general be

related to the hydrophobicity of the amino acid side chains with the more hydrophobic amino acids producing silicas with higher surface areas. The more hydrophobic amino acids appeared to reduce inter-particle interaction and condensation resulting in more open framework structures being produced. Increasing the chain length of the homopeptide from 1 to 5 resulted in material with smaller surface areas but pore volumes which showed no general trend, which is in line with the data reported in the literature.¹⁴ The pore size domains however became more disperse with a trend towards a larger average diameter. SEM data show an increase in granularity of the materials with the nitrogen containing amino acids suggesting an ability to stabilise aggregates. Silica condensed with L-lysine oligomers also showed this granularity with no change in average granule size observed with increasing chain length. Poly L-lysine however produced spherical porous spheres of up to 1.5 μm which appeared to be made up of smaller aggregates. The aggregation of small aggregates into larger ones could be accomplished by the formation of chains of aggregates connected by entrained poly L-lysine strands. These would tend to form spheres through entropic effects once the charge on the lysine side chains becomes reduced by the presence of silica. The absence of such large scale structures for silicas produced in the presence of L-lysine oligomers shows that merely being able to electrostatically bridge the aggregates is insufficient. Previous silicification studies using silicon catecholate complexes as the silica precursor, have shown that the counter ions of the complex have a profound effect on the kinetics and the final product properties.⁴ In particular, the ions (NH_4^+ , Et_3NH^+ , etc.) get associated with the surfaces of silica oligomers/particles by electrostatic attractions and produce silicas with vastly reduced surface area as found in the current study using lysine oligomers. It should be noted that all these precursors, including the one used in this study were water soluble and dissociate to produce orthosilicic acid upon neutralisation, unlike their organosilane counterparts.

4.5 Conclusions.

The purpose of this study was to understand the role of biomolecules in biosilicification via individual and oligomeric amino acid effects on in vitro silicification. Individual amino acids variously reduced or accelerated the early kinetics of condensation and aggregation and produced silicas with surface areas which varied according to the isoelectric point of the amino acid. Introduction of (lys)_n produced a slightly increased enhancement of the early kinetics but dramatically increased aggregation rates as silica condensation progressed, suggesting that aggregation may be a major influence on biosilica formation. Surface areas of the silicas were affected by the amino acids according to their hydrophobicities and a degree of control over both surface area, average pore size and size dispersity were exerted by the addition of lysine homopeptides of varying lengths. Effects on the morphologies of the silicas was observed even with individual amino acids, and with nitrogen containing amino acids producing granular materials.

References.

- 1 C. C. Perry and T. Keeling-Tucker, *Colloid Polym. Sci.*, 2003, **281**, 652.
- 2 C. C. Perry and T. Keeling-Tucker, *Chem. Chemmun.*, 1998, 2587.
- 3 S. Brunauer, L.S. Deming, W.S. Deming, E. Teller, *JACS.*, 1940, **62**, 1723.
- 4 J. H. de Boer, "The Structure and Properties of Porous Materials", p. 68, Butterworths, London, (1958).
- 5 S. Brunauer, P. H. Emmett and E. Teller, *J. Am. Chem. Soc.*, 1938, **60**, 309
- 6 E. P. Barrett, L. G. Joyner and P. P. Halenda, *J. Am. Chem. Soc.*, 1951, **73**, 373.
- 7 J. Kyte., R. Doolite, *J. Mol. Biol.*, 1982, **157**, 105.
- 8 S. V. Patwardhan, N. Mukherjee, M. Steinitz-Kannan and S. J. Clarson, *Chem. Commun.*, 2003, **10**, 1122
- 9 S. V. Patwardhan and S. J. Clarson, *J. Inorg. Organomet. Polym.*, 2002, **12**, 109.
- 10 S. V. Patwardhan, C. Raab, N. Hüsing and S. J. Clarson, *Silicon Chemistry*, 2005 **2**, 5-6, 279-285.; S. V. Patwardhan and S. J. Clarson, unpublished data.
- 11 N. Kroger *et al.*, *Science*, 2002, **298**, 584.
- 12 N. Poulsen, M. Sumper and N. Kroger, *Proc. Natl. Acad. Sci. USA*, 2003, **100**, 12075.
- 13 M. Sumper, S. Lorenz and E. Brunner, *Angew. Chem. Int. Ed.*, 2003, **42**, 5192.
- 14 T. Coradin, O. Durupthy and J. Livage, *Langmuir*, 2002, **18**, 2331.
- 15 C. C. Harrison (now Perry) and N. Loton, *J. Chem. Soc., Faraday Trans.*, 1995, **91**, 4287.

Chapter 5.

The importance of non covalent interactions of diamines on the condensation and aggregation process in silica.

5.1 Introduction.

Following on from Chapter 4, where a significant effect on the condensation and aggregation of silica in a condensing system was observed to be exerted by a combination of electrostatic (through pK_a) and hydrophobic effects, the possible role of non covalent interactions was investigated. The presence of diamines in nature is common with species such as putrescine and cadaverine occurring in the cells of most organisms^{1,2} so there is a likelihood that they will be present in the cell contents of silicifying organisms. Using terminal n-alkyldiamines with various carbon chain separations to cover the range of amine separations observed with the homopeptides used in Chapter 4 as additives to the model system, the effects on condensation, particle growth and aggregation and silica morphologies were investigated.

5.2 Experimental.

Experiments were conducted as detailed in Chapter 2.

5.3 Results and discussions.

5.3.1 Solution chemistry.

The rates of trimerisation (a third order reaction with respect to monomer concentration; rate constant k_3) and further oligomerisation (a first order reversible reaction; rate constants k_+ , k_- (Figure 5.1)) were monitored by the molybdenum blue assay as previously described (Chapter 2, modifications detailed in Chapter 3).

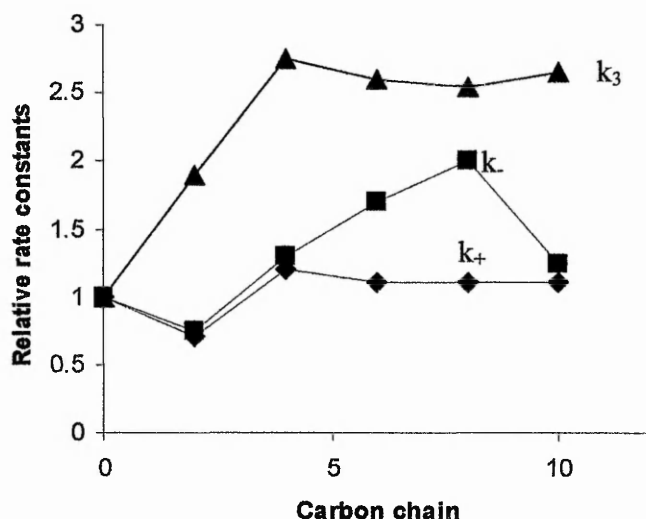


Figure 5.1 Relative rate constants for the early stages of monosilicic acid condensation

The rate constants for the formation of trimers from monomer and dimer were found to increase by *ca.* two fold for the 1,2 diaminoethane system and *ca.* 2.5 times for the longer chain diamines when compared with the blank (with no trend observed over these latter samples). Increases in the third order rate constants were found to be statistically significant, exceeding two standard deviations calculated using four 'blank' data-sets. The next stage of the reaction involves the reversible addition of orthosilicic acid to already formed oligomers and showed less variation for the silicas prepared in the presence of diamines. Previous work on silicic acid condensation in the presence of Group 1 cations has shown a rate dependency related to the size of the hydration sphere of the cations.⁴ Here the cationic species and concentration were constant and only the hydrophobic portion of the additive varied as the chain length of the diamine increased.

5.3.2 The hydrophobic effect⁵.

Due to the differences in the electronegativities of hydrogen and oxygen atoms in water molecules a dipole is formed with the oxygen atom carrying a small negative charge and the hydrogen atoms a small positive one. This gives rise to strong attractive forces between neighbouring water molecules through the formation of hydrogen bonds (Figure 5.2).

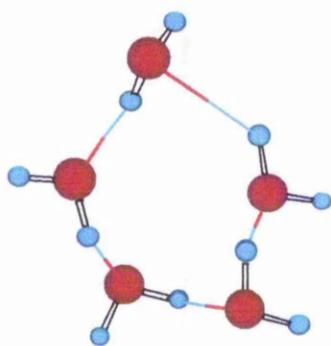


Figure 5.2 Hydrogen bonding between water molecules (shown as coloured lines).

In ice each molecule hydrogen is bonded to 4 other molecules but in liquid water due to greater thermal motions which disrupt, distort, and occasionally break hydrogen bonds each molecule is on average hydrogen bonded to approximately 3.4 other water molecules, so there is a dynamic state set up where hydrogen bonds are continually being formed and broken but where their presence fundamentally affects the properties of the bulk medium resulting in unexpected behaviour such as high boiling point and heat capacities, etc. When polar solutes are dissolved in water, hydrogen bonds may be alternatively formed with them and so the flux of rearranging hydrogen bonds is not disturbed. If on the other hand a non polar hydrophobic molecule is caused to dissolve, hydrogen bonding is not possible with it. In order to reduce the number of non hydrogen bonded water molecules they rearrange to form a cage like structure (Figure 5.3), in which as few pendant non hydrogen bonded species as possible occur around the solute, which sits at the centre of the cavity.

The free energy of transfer of a non-polar compound from some reference state, such as an organic solution, into water, ΔG_{tr} , is made up of an enthalpy, ΔH , and entropy, $-T\Delta S$, term:

$$\Delta G_{tr} = \Delta H_{tr} - T\Delta S_{tr}$$

but because the enthalpy of transfer from organic solution into aqueous solution is negligible the interaction enthalpies are the same in both cases. The formation of the cage cavities around the solute however introduces order into the system so the entropy term is negative. This entropic change in the system will affect the bulk properties of water resulting in a reduction in other relatively ordered sites such as

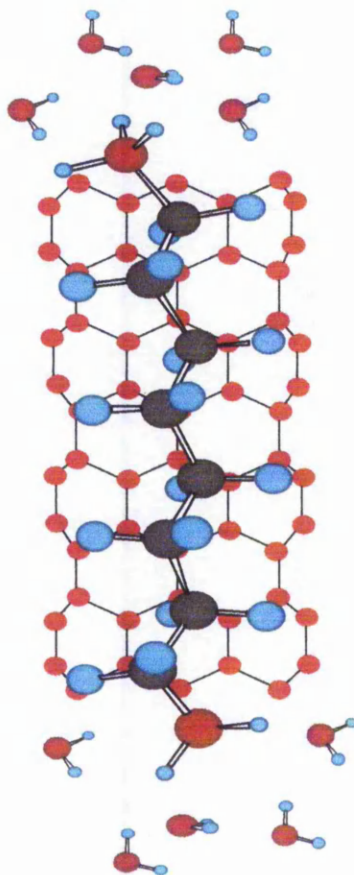


Fig 5.3 Formation of hydrogen bonded water cage around hydrophobic section of molecule. Only Oxygen atoms (red) shown.

those of ion solvation rendering these solvated ions more susceptible to chemical attack (Figure 5.4a). The increase in the early kinetics observed as the hydrophobic nature of the added diamine increases is thought to be a product of this since anionic silicate species are the central to silica condensation (Figure 5.4b). As the hydrophobic domains increase further however the increasing entropic effects are minimised by the aggregation/micellisation of the diamines to minimise the hydrophobic surface exposed to water and the amount of ordered water around them and hence further increase in the early kinetics is prevented for diamines with carbon chain lengths greater than around four (Figure 5.4c).

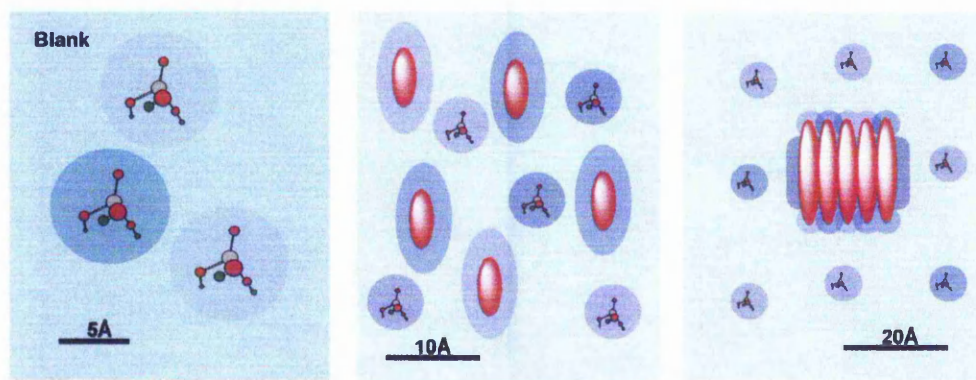


Figure 5.4 Results of the hydrophobic effect on localised water structure. a). Monosilicic acid in blank showing the solvation sphere barrier to condensation. b). Ordered water structure around hydrophobic domains of shorter (eg 1,4) diamines and reduced solvation sphere around monosilicic acid. c). Formation of micelles to minimise hydrophobic surface in contact with water. Hydrophobic domains shown in red shade, ordered water as darker blue shade.

5.3.3 Particle growth and aggregation.

Once the stable nuclei are formed, particle growth and aggregation can occur. This process was monitored using photon correlation spectroscopy (PCS) (Figure 5.5). Duplicate analyses were conducted for each sample to confirm the reproducibility of the data. The relative growth rates in the presence of diamines determined as the maximum growth rate observed during each experiment were enhanced up to *ca.* 15000 times as the carbon chain length increased. In addition, there was a distinct step change in the relative growth rate between the additives 1,4 diaminobutane and 1,6 diaminohehexane (Figure 5.6).

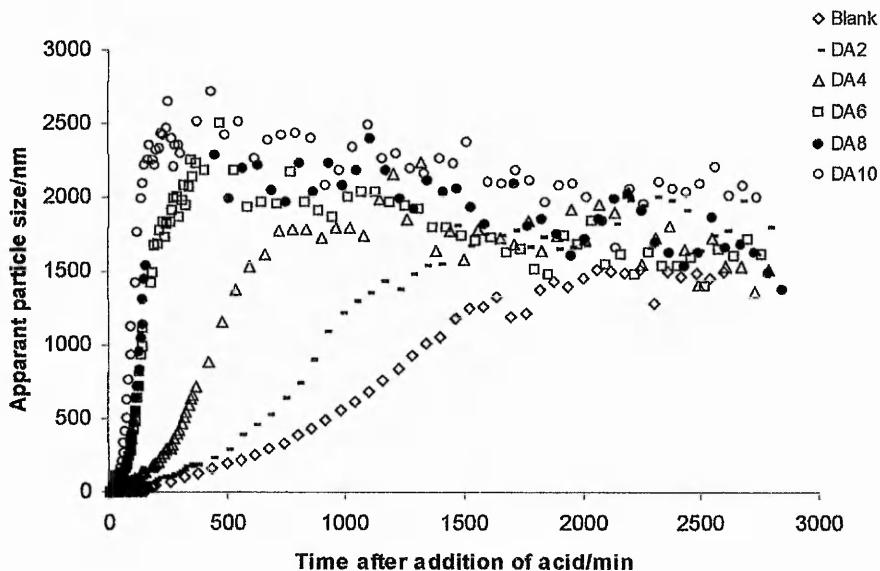


Figure 5.5 Particle growth/aggregation (values measured are hydrodynamic radii) as determined by photon correlation spectroscopy.

Gelation times decreased with diamine chain length and also showed the step change in behaviour between the same diamines. Comparison of orthosilicic acid concentration with PCS data (Figure 5.7) shows that it is particle aggregation and not particle growth that is being monitored, as in excess of 80% of monomer is already condensed before significant growth is observed by this technique (*ca.* 23 min for 1,10 diaminodecane).

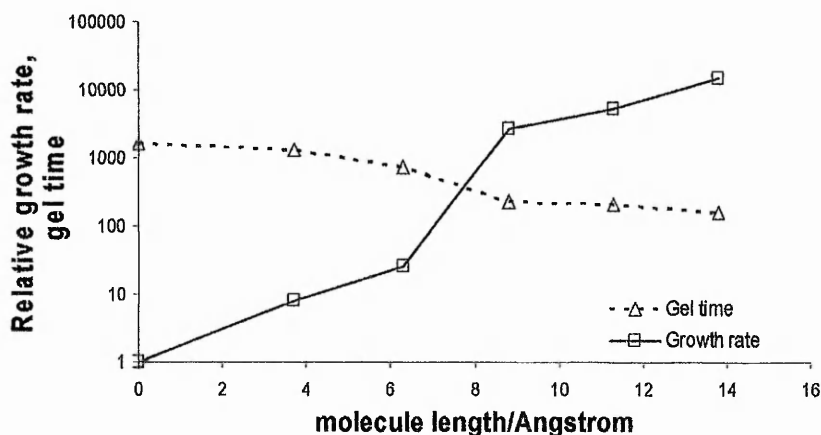


Figure 5.6 Relative growth rates and gel times for silica particles in the condensing in the presence of n-alkyldiamines.

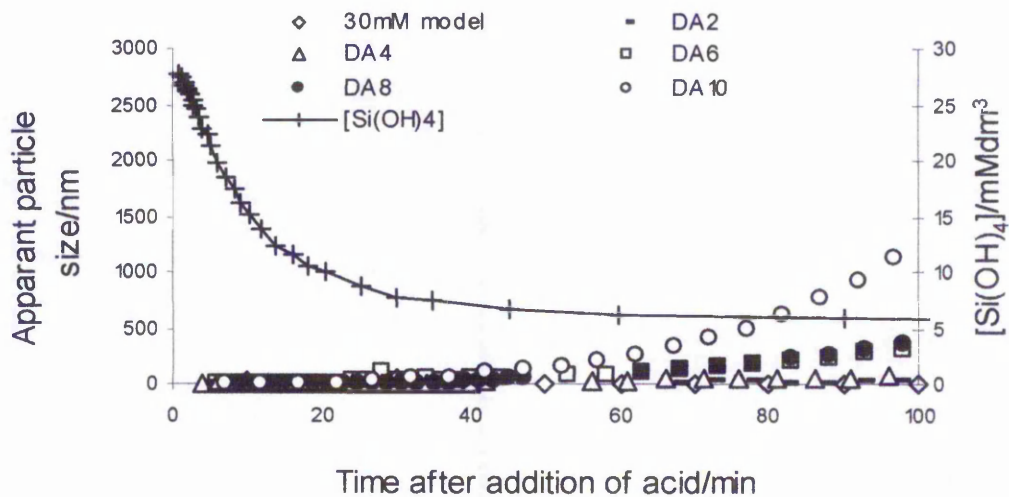


Figure 5.7 comparison of particle growth/aggregation with the decrease in monosilicic acid concentration through condensation.

5.3.4 Electrostatic effects

The observed behaviour can be explained in terms of electrostatic effects. At pH 7 and below silica particles become increasingly negatively charged as the silanols become increasingly acidic on increased condensation. There is a tendency for charged species to be attracted to or repelled from the silica particle-solution interface. This gives rise to a separation of charge, and the layer of solution with

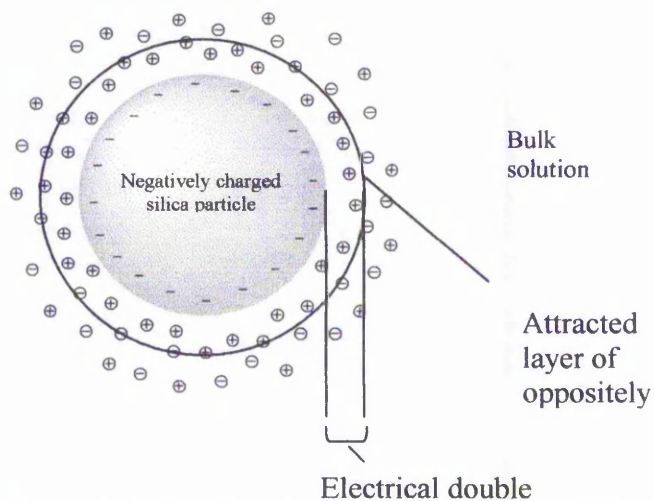


Figure 5.8 Formation of electrostatic double layer around negatively charged silica particle

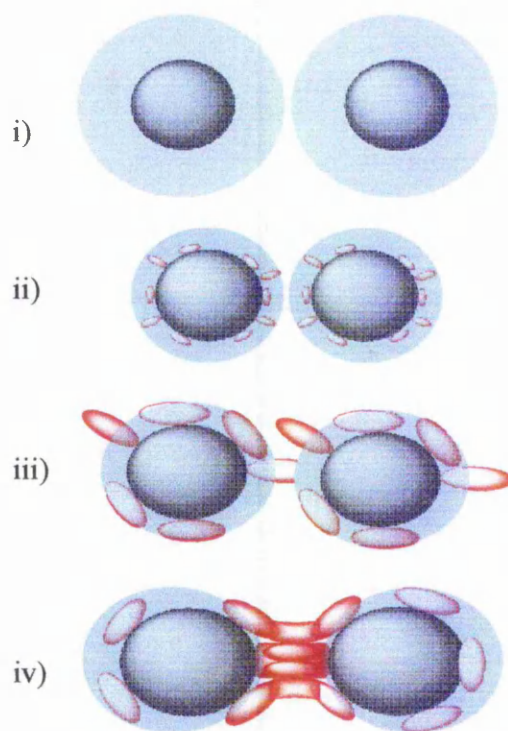


Figure 5.9 Electrostatic and hydrophobic effects on the aggregation of silica particles. i) Particles showing double layer ii) reduced boundary layer caused by steric charge reduction iii) Increased aggregation through particle bridging iv) Coacervation through the hydrophobic effect.

different composition from the bulk solution is known as the electrostatic double layer (Figure 5.8), and it is this layer which acts as a barrier to particle aggregation. Reduction of the thickness of this double layer can be achieved by charge neutralisation of the particle surface through the adsorption of diamines to the surface by the uncharged hydrocarbon domains sterically displacing other counter ions. As a consequence particles are able to aggregate more easily through random collisions as observed with 1,2 diaminoethane (Figure 5.9(i) and (ii)). As the diamines increase in length they are able to extend beyond the double layer and at some point penetrate the double layer of neighbouring particles to form bridges (Figure 5.9(iii)). At this point the aggregation rates increase more quickly as inter-particle collisions occur more often and this can explain the step rate change in apparent growth observed between 1,4 diaminobutane and 1,6 diaminohexane. Further increases in the carbon chain length result in the formation of a hydrophobic layer on the surface of the silica particle and this further effects aggregation by coacervation, another entropic effect whereby the hydrocarbon surface exposed to water is minimised by the aggregation of

the hydrophobic surfaces (Figure 5.9(iv)). This is shown by the continued increase in apparent growth rates from 1,8 diaminooctane to 1,10 diaminodecane.

5.3.5 Silica maturation.

The process of maturation and evolution of structure, in the presence of diamines, was studied using nitrogen gas adsorption and electron microscopy.

5.3.5.(I) Nitrogen gas adsorption analysis.

Adsorption/desorption isotherms typically showed type iv isotherms with type A hysteresis (according to Brunauer, Deming, Deming and Teller (BDDT)⁶ and de Boer⁷ respectively), typical of mesoporous materials with cylindrical pores (figure 5.10).

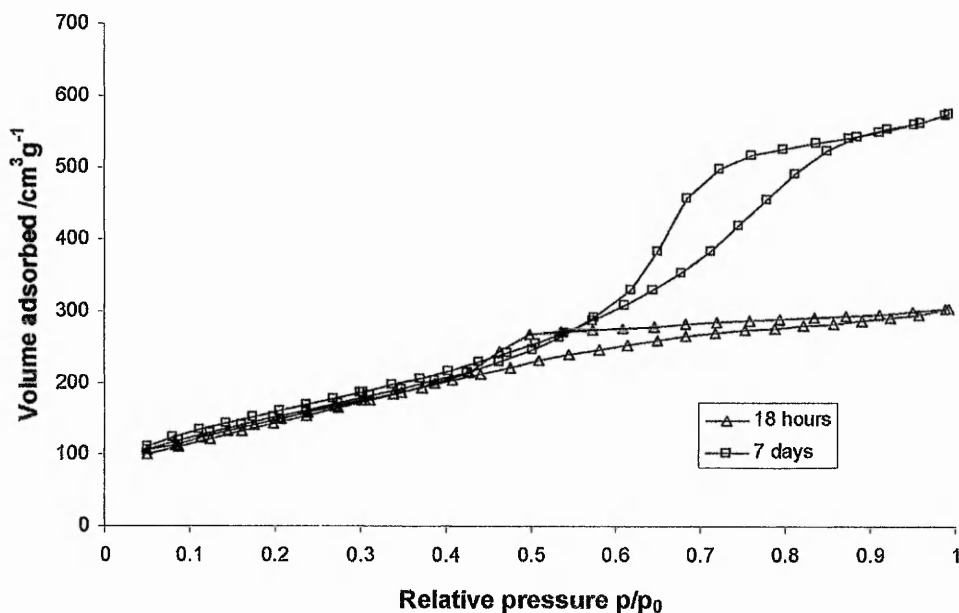


Figure 5.10 Typical adsorption/desorption isotherms for silica isolated at $t_{\text{gel}}^{1/2}$ and after 7 days maturation. Data shown here was for silica precipitated in the absence of added diamines.

Surface areas determined by the BET method decreased with time of reaction and with increasing chain length of the additives (Figure 5.11).

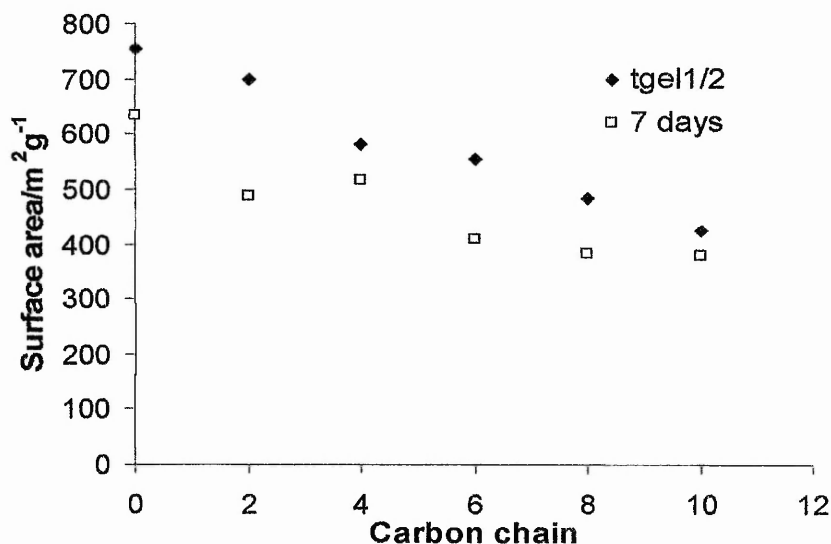


Figure 5.11 Surface areas of sedimentable silica determined by the BET method taken at $t_{gel}^{1/2}$ and 7 days maturation times

Surface area reduction with time is the expected consequence of Ostwald ripening as smaller particles redissolve and precipitate on to larger ones. Reduction of surface area with increasing diamine chain length in silicas isolated at shorter maturation times may be a consequence of the degree of condensation of the silicas produced since pore radii in the isolated material were unaffected (Figure 5.12).

Measurements of pore radii (Figure 5.12) show the beginning of the permanent structure after 1 day (before 1 day pore radii were around 20 Å for all silicas. By 7 days this resulted in pore radii of up to 50 Å possibly representing a templating effect of micelles, and 37Å for 1,10-diaminodecane. The reduced pore radii of the material produced with 1,10-diaminodecane is thought to be a function of greater flexibility of the diamine compared with the other diamines used as more flexible hydrophobic molecules use folding as an internal mechanism for minimising entropic effects, thus promoting some degree of coiling of the hydrocarbon chains to produce smaller micelles. Pore volumes followed the same trends; material with larger pores had larger pore volumes, *i.e.* some conservancy of overall pore populations.

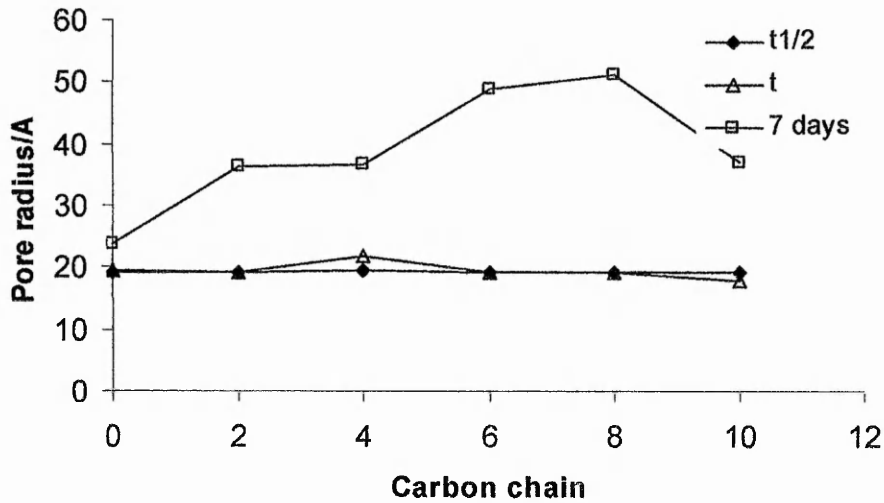


Figure 5.12 Affect of maturation times and carbon chain length on pore radii as determined by the BJH method.

5.3.5.(II) Thermogravimetric analysis.

Thermogravimetric analysis on samples isolated after different periods of reaction showed a virtual absence of significant levels of entrained organic material after up to one day of maturation. However after 7 days maturation (Figure 5.13) the level of organic entrainment increased with the additive chain length due to the increasingly

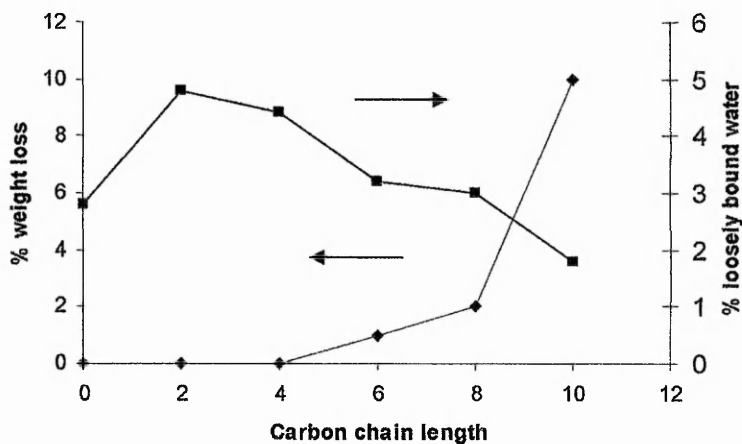


Figure 5.13 Results from thermogravimetric analysis of isolated silica highlighting the two distinct weight loss domains of <373k for physisorbed (loosely bound) water and 500-900k for the removal of entrained organics.

condensed silica matrix. The percentage of loosely bound water determined as the weight loss below 373 K decreased with increasing diamine carbon chain length and therefore increasing hydrophobicity. The presence of hydrophobic groups associated with the aggregating silica particles would be expected to squeeze out water between the forming pores and during coacervation.

5.3.5.(III). Scanning electron microscopy.

Scanning electron microscopic data (Figure 5.14) showed an ordering of silica structure with time for all samples. In particular, the silica prepared in the presence of

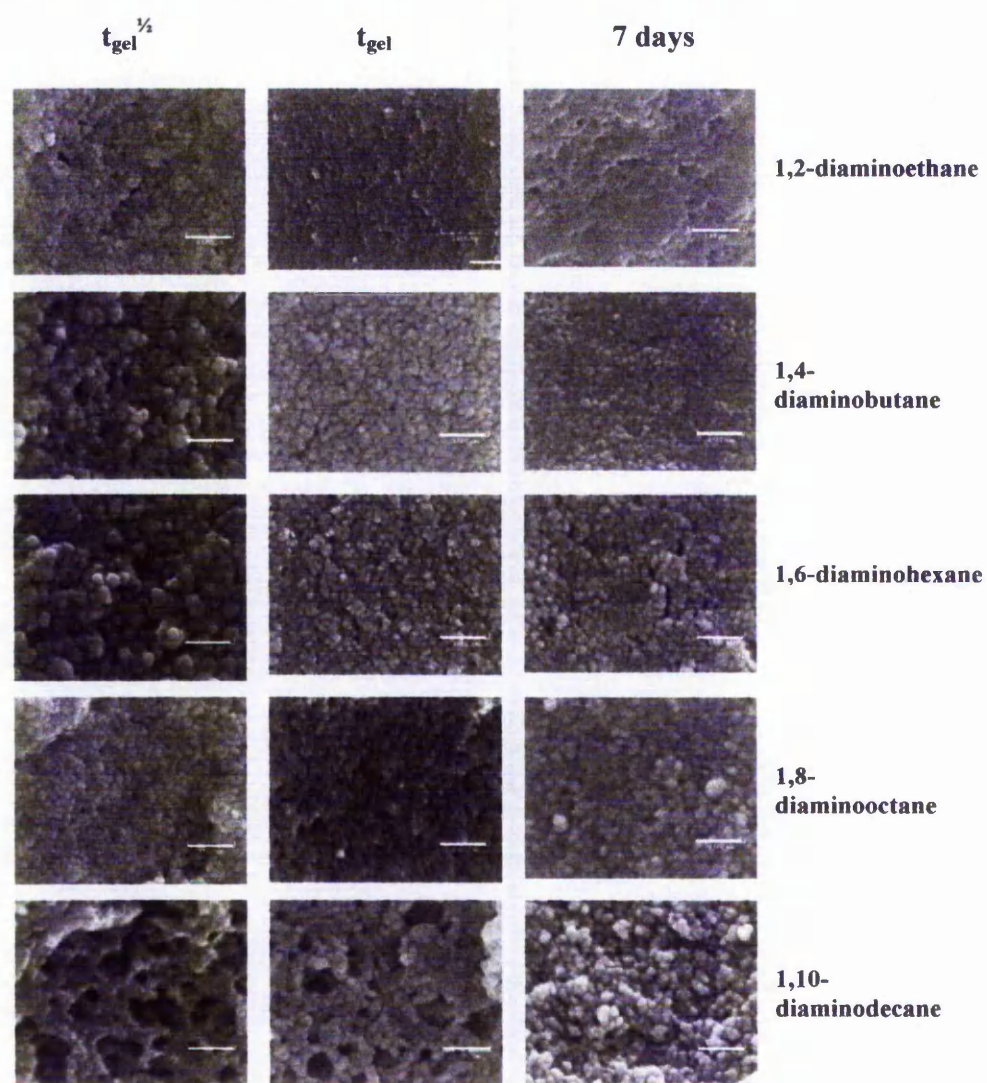


Figure 5.14 Scanning electron micrographs of silica condensed in the presence of diamines and isolated at different maturation times. Scale bar 0.5 μ m except 1,2 diamine 7 day - 1 μ m

1,10-diaminodecane, had a very open structure due to very rapid aggregation allowing little time for packing rearrangements, but became more ordered and close packed during the Ostwald ripening phase. Increasingly large aggregates with increasing diamine chain length was also observed. Primary particles measured after 7 days maturation by TEM were slightly bigger (5–7 nm) when compared with the blank sample (4 nm) but with no specific trend. Confirmation that the structures observed were siliceous was made by EDS and FTIR analyses. Selected area electron diffraction carried out on selected samples showed no evidence of ordering on the atomic or molecular scale, confirming the amorphous nature of the silica produced.

References.

- 1) N. Bagni, R. Pistocchi., 1992, Polyamine metabolism and compartmentation in plant cells. In "Nitrogen Metabolism of Plants" (K Mengel, DJ Pilbeam eds), Clarendon Press, Oxford, 229-248.
- 2) T.A. Smith, N. Bagni, D.S. Fracassini., 1979, The formation of amines and their derivatives in plants. In (EJ Hewitt, CV Cutting eds) "Nitrogen Assimilation of Plants", Academic Press, New York, 557-570.
- 3) R. K. Iler, *The Chemistry of Silica*, John Wiley & Sons, New York, 1979.
- 4) C. C. Harrison (now Perry) and N. Loton, *J. Chem Soc. Faraday Trans.*, 1995, **91**, 4287.
- 5) C. Tanford, *The Hydrophobic Effect. Formation of Micelles and Biological Membranes*. J Wiley and Sons, New York, (1980).
- 6) S. Brunauer, L.S. Deming, W.S. Deming, E. Teller, *JACS*, 1940, **62**, 1723.
- 7) J. H. de Boer, "The Structure and Properties of Porous Materials", p. 68, Butterworths, London, (1958).

Chapter 6.

The importance of interamine spacing in polyamines on the silica condensation process.

6.1 Introduction.

The diatom silaffin proteins are relatively enriched with lysine residues that are modified by the attachment of long chain polypropylamines to the side chain. Similar polypropylamines terminated by a putrescine group are also found in isolation.¹ These polyamines appear to be a homologous group synthesised as a continuation of the putrescine, spermidine and spermine metabolic pathway all common naturally occurring polyamines.² Due to their prevalence in nature it is therefore possible that the utilisation of these polyamines may be an adventitious one and that, at least *in vitro*, other polyamines with different amine separations may cause similar effects to those observed for the molecules isolated from diatoms. The possibility of using similar molecules that are cheaper and readily available to produce superior silica products under more benign conditions is desirable.

A considerable body of work already exists on the chemical and biomimetic effects of amine species on the condensation of silicic acid systems and characterisation of the harvested silica³ but any mechanistic differences between the chemical and biological approaches are still poorly understood. A range of amines and polyamines have shown catalytic effects and generated unusual *in vitro* silica structures from a range of precursors.^{3,4} Studies of the effects of amino acids and homologous peptides with a range of silica precursors (dipotassium tris(1,2-benzenediolato-*O,O'*)silicate, sodium silicate and tetraethoxysilane) showed enhanced condensation, aggregation and harvestable silica yields⁵ and the formation of silica spheres was shown to occur with the addition of poly-L-arginine.⁶ Silica sphere and hexagonal silica production of varying sizes and dispersities has been shown to occur in poly-L-lysine/tetramethoxysilane (TMOS) systems and mechanical effects (e.g. shear) leading to the production of platelets and elongated fibre-like structures for these systems have also been reported.^{7,8} In addition,

studies using polyallylamine hydrochloride have shown similar sphere formation control⁹ and transformation from sphere to honeycomb structure when the precursor was changed from TMOS to a polyamine stabilized silica sol.¹⁰ Silica formation in the presence of polyethyleneimine functionalised porphyrin rings and benzene rings, and linear polyethyleneimines has generated complex structures such as filamentous aster, fibrillar sponge and leaf morphologies where electron microscopy has shown that the silica fibres consist of a coating of silica particles around an axial polyethyleneimine filament, highly analogous to the formation of sponge spicules where silica coats an axial protein filament.¹¹ The unmodified R5 peptide derived from silaffin proteins involved in diatom biosilicification has been investigated for structure directing effects. R5 has been found to produce 400-700 nm spheres and 100-300 nm diameter fibres when subjected to shear stress.¹² Both silaffin proteins and the polyamines isolated from diatom biosilica have been shown to influence silica morphologies at circumneutral pH and are thought to be key to the formation of many of the structures observed in diatoms through sol stabilisation and flocculation at aqueous interfaces. In addition to peptides and (bio)macromolecules, relatively simpler additives have been investigated for their influence on silica formation. Addition of diethylenetriamine, triethylenetetramine and pentaethylenhexamine to silicifying reaction mixtures were previously studied by Mizutani *et al.* and it was found that these amines increase the rate of gelation of silica, but further extensive characterisation leading to the amines exact role were not performed.¹³ Furthermore, tripropylenetetramine and pentapropylenehexamine were able to precipitate *ca.* 400 nm particulate silica from a solution of hydrolysed TMOS.¹⁴ Studies using small amines – cysteamine, ethanolamine, 2-(dimethylamino)ethanethiol, 2-(ethylthio)ethylamine and propylamine facilitate the hydrolysis and condensation of alkoxysilanes at near-neutral pH, cysteamine being the most effective additive.¹⁵ A recent study on the roles of putrescine homologues on silicification was reported and it was found that electrostatic forces between additive and silicic acid, and the hydrophobic behaviour of the additives are both important not only in controlling solution chemistry (kinetics and aggregation) but also in generating tailored silicas.¹⁶ This chapter therefore concerns the effects of naturally occurring polyamines – spermidine and spermine – and a series of linear ethyleneimine homologues (EAs) of between 1 and 5 repeat

ethyleneimine units on a model silica condensing system. The chain length, inter amine separation and amine basicity effects have been investigated.

6.2 Experimental

6.2.1 Reagents.

Monoethyleneamine (MEDA), diethylenetriamine (DETA), triethylenetetramine (TETA), tetraethylenepentamine (TEPA), pentaethylenehexamine (PEHA), spermidine (SPDNE), spermine (SPNE), tetramethoxysilane (TMOS) and Dipotassium tris(1,2-benzenediolato-*O,O'*)silicate were all purchased from the Sigma-Aldrich company Ltd. Hydrochloric acid (37%) was purchased from Fisher scientific, and deuterated water and NMR standards from Goss ltd.

6.2.2. Methods.

Experimental methods used were as indicated in Chapter 2 unless otherwise stated.

The amines were introduced to the model system with a Si:N ratio of 1:1.

For thermal treatment, samples of silica were heated at 10°C/minute to 650°C in a furnace and held for 2 hours under an air atmosphere. The silica appeared colourless after this treatment indicating that all organic components had been removed. Additionally in order to perform silica quantitation, sedimentable silica was isolated at the times listed and washed as before from a predetermined volume of the condensing systems. The isolated silica was then allowed to redissolve in 2M sodium hydroxide at room temperature until a clear solution was obtained. Aliquots of these solutions were then sampled by the molybdenum blue assay method and the silica quantified by comparing with a set of standards prepared from a 10ppm stock solution of monosilicic acid. Entrained polyamines were determined by ¹H NMR spectroscopy of the sodium hydroxide solutions measuring the integral height of the amine signals against that of the

chemical shift reference and comparing with a set of standards prepared using known amounts of polyamine measured under the same solution conditions against the same chemical shift reference. All samples were measured in 5mm glass NMR tubes from aliquots taken directly from the silica dissolution experiments with no sample preparation. Spectra were accumulated from 32 scans with a pulse delay time of 1s using a Jeol JNM-EX270 Fourier transform nuclear magnetic spectrometer. A tube insert containing sodium 2,2 dimethyl-2-silapentane-5-sulphonate (DSS) in D₂O provided the chemical shift reference and deuterium lock signal with the DSS dimethyl signal also being employed as a reference for quantification purposes.

6. 3 Results.

The effects of naturally occurring polyamines – spermidine and spermine – and a series of linear ethyleneimine homologues (EAs) of between 1 and 5 repeat ethyleneimine units on a model silica condensing system have been studied. The physical characteristics of the amines used in this study, intra-amine distances are listed in **Table 1**.

N	Name	ℓ	ℓ_1	ℓ_2	ℓ_3	ℓ_4	ℓ_n
2	MEDA	3.78	3.78				
3	DETA	7.36	3.75	3.75			
3	SPDN	11.17	5	6.23			
4	TETA	11.1	3.75	3.76	3.78		
4	SPN	16.1	5	6.24	4.96		
5	TEPA	14.72	3.75	3.76	3.76	3.76	
6	PEHA	18.45	3.75	3.76	3.76	3.76	3.78

Table 6.1 Terminal nitrogen separation and interamine distances for the polyamines used in this study.

N = number of amines per molecule, ℓ = end-to-end distance of molecules. ℓ_i = distance between i^{th} and $i+1^{\text{th}}$ amines.

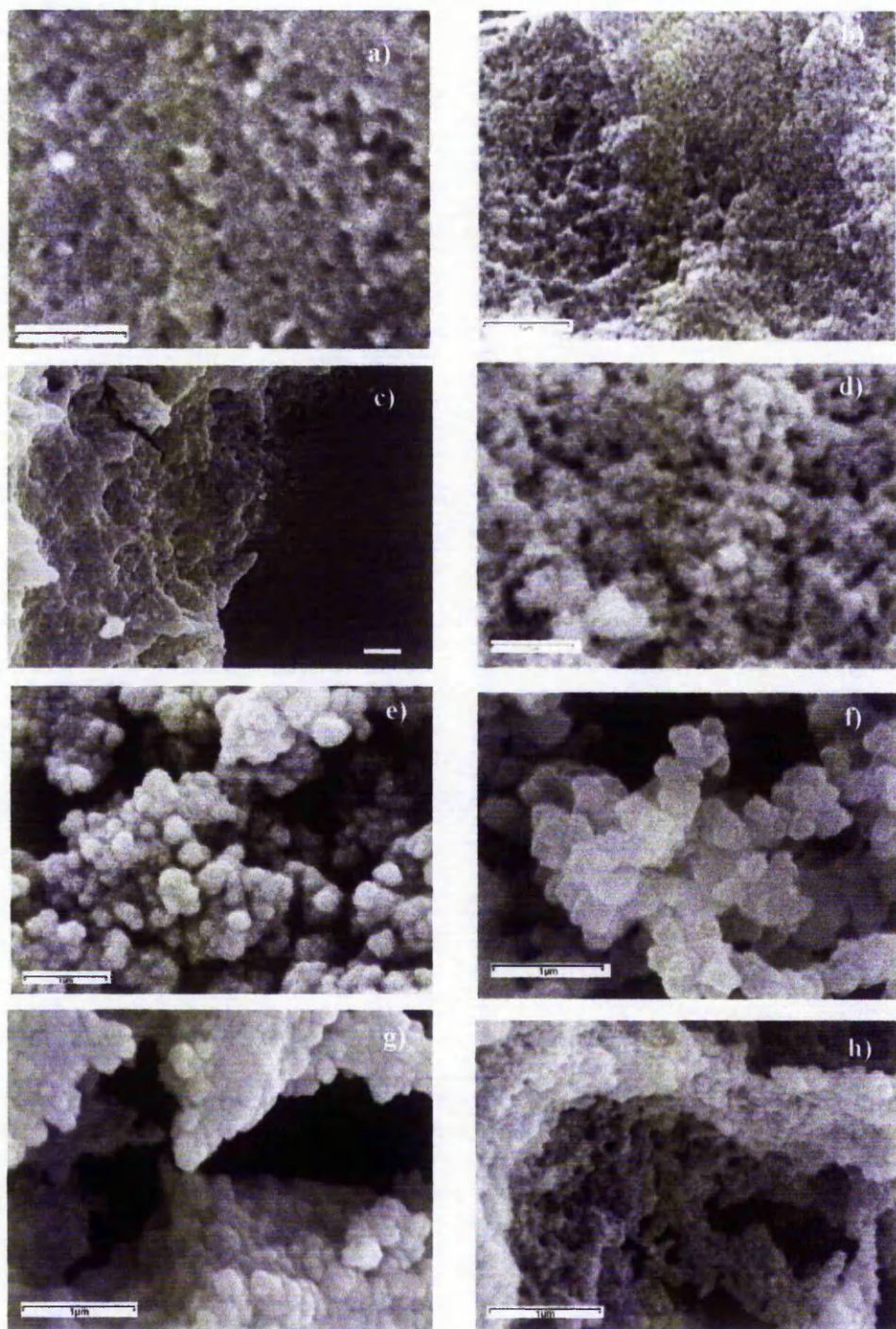


Figure 6.1 Scanning electron micrographs of silica condensed in the presence of a) Blank b) MEDA, c) DETA, d) TETA, e) TEPA, f) PEHA, g) SPDNE, h) SPN. Scale bars 1 μ m.

Silica samples prepared in the presence of amines were collected after seven days, dried and their morphology studied. SEM images obtained on silica condensed in the presence of the homologous ethyleneimines showed an increasingly granular structure with increased molecular length, uniform coalesced spheres of around 200-250 nm diameter being formed in the presence of PEHA (Figure 6.1). Additional experiments were conducted wherein silica samples precipitated in the presence of PEHA were collected at different times. Inspection of the silica samples collected at different maturation times from PEHA showed that spheres formed at the earliest isolation times (35 min) and remained unchanged in appearance up to 7 days maturation (Figure 6.2).

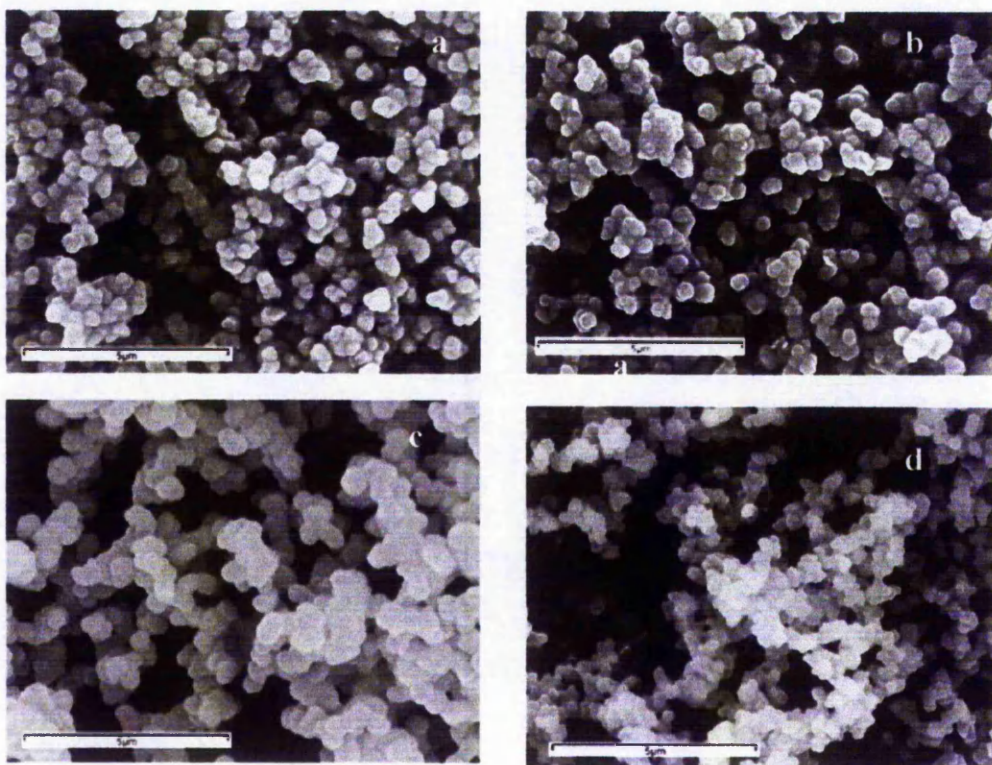


Figure 6.2 Scanning electron micrographs of silica condensed in the presence of PEHA isolated at a) tgel½, b) tgel, c) 1 day, d) 7days. Scale bars all 5μm.

Furthermore, when the ratio of amines from PEHA to Si was varied from 0.1 to 2 (or 10% - 200%) material isolated at fixed time points showed an increased aggregate uniformity and particle size with as initial PEHA content was increased (Figure 6.3). A

switchover in silica morphologies was observed at around $N:Si = 0.5$, where the formation of particulate silica was evident. The particles also appeared sharper suggesting that they were more highly condensed.

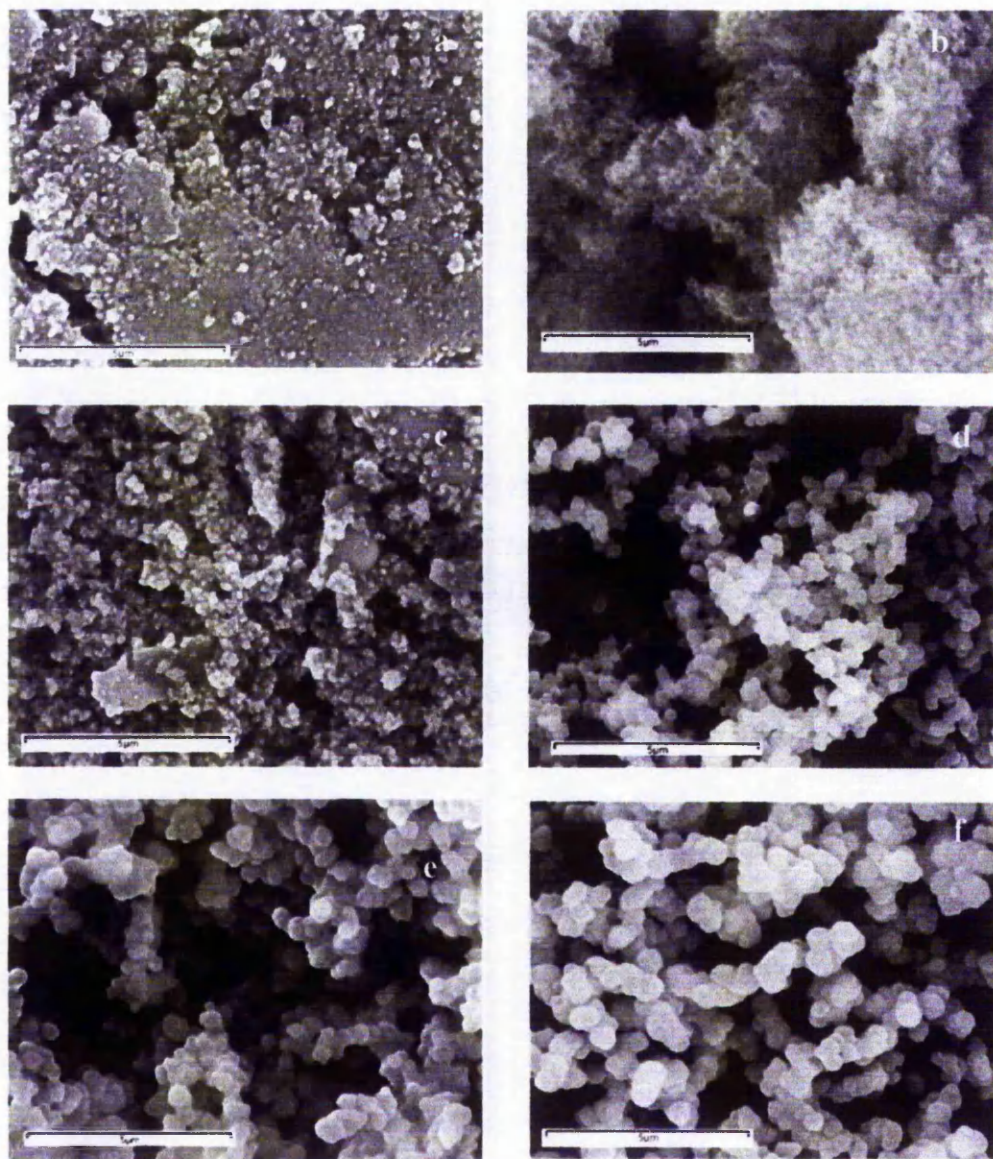


Figure 6.3 Scanning electron micrographs of silica condensed in the presence of PEHA at levels of a) 0% b) 13% c) 25% d) 50% e) 100% f) 200% Scale bars all 5 μ m.

Nitrogen gas adsorption analyses were performed on the isolated silicas. Surface areas determined by multi point BET¹⁷ analysis showed a reduction with increased homologue size and maturation times (Figure 6.4). The reduction in surface area was particularly noticeable in the case of silica condensed in the presence of PEHA where surfaces were reduced to such an extent that measurements could not reliably be made. The natural polyamines showed similar surface area reducing abilities when compared on the basis of chain length but were slightly more effective when compared on the basis of amine moiety per molecule. Pore volumes and radii determined by the BJH method¹⁸ for silica condensed in the presence of the ethyleneimine homologues both showed a general increase with molecular length up to TEPA, but on increasing to PEHA practically no mesopores and only a much reduced micropore population was detected (Figure 6.4). Using the pore volume and radii data estimates of pore numbers were made showing that the transition between porous and an essentially non porous material was observed at an ethyleneimine homologues in excess of 5 amine units per molecule (Figure 6.5).

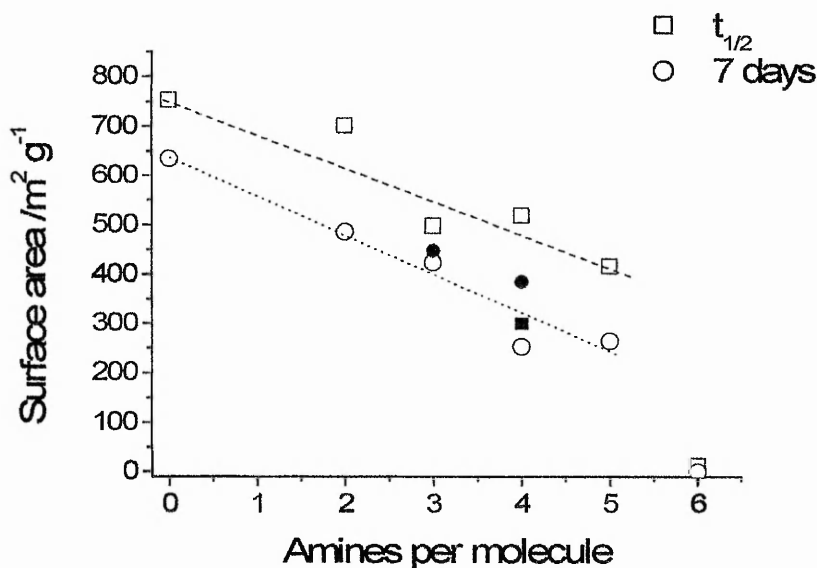


Figure 6.4 Surface area measurements of silica condensed in the presence of ethyleneimines isolated at tgel^{1/2} and 7 days spermidine and spermine are solid data points.

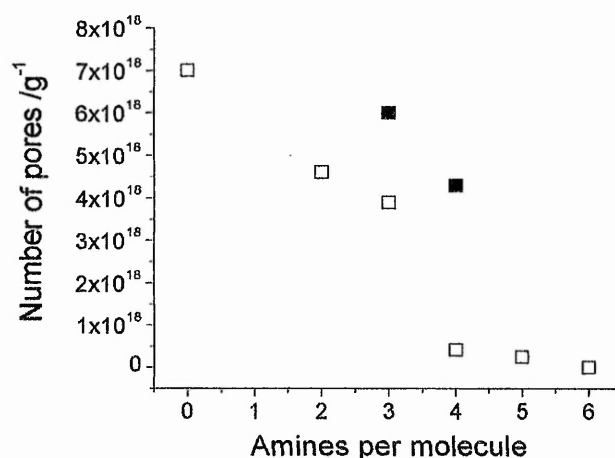


Figure 6.5 Estimated Number of pores/g for silica condensed in the presence of ethyleneimine after 7 days maturation. Spermidine and spermine are solid data points.

The increased pore sizes with increasing chain length and decreasing surface area with maturation time can be regarded as typical behaviour for increasingly rapidly aggregating silica nanoparticles of uniform size. The rapid aggregation causing disperse pore size formation due to time constraints on particle reorientation and compaction and Ostwald ripening probably causing the observed surface area reduction. The behaviour of the naturally occurring polyamines throughout suggest that they influence the condensation and aggregation process largely as a consequence of their chain length and charge separation and as such do not behave in an unexpected or a specific manner *in vitro*.

Due to the unusual ability of PEHA to generate almost “glassy” silica, further analysis was carried out by varying PEHA concentration. Increasing the PEHA concentration between 10% and 200% (3 and 60 mM) with respect to amine:silicon content resulted in a rapid decrease in the observed surface areas (Figure 6.6). Heat treatment of the silica to remove any entrained organic material resulted in a restoration of some of the surface areas but this was almost entirely due to the appearance of micropores. Some mesoporosity could be measured at $t_{\text{gel}}^{1/2}$ ($\sim 12 \text{ m}^2 \text{ g}^{-1}$) for these samples but at longer maturation times even this disappeared. Pore volume/radii measurements made show that the material isolated at $t_{1/2}^{\text{gel}}$ for PEHA contained a range of pores in the micro to meso

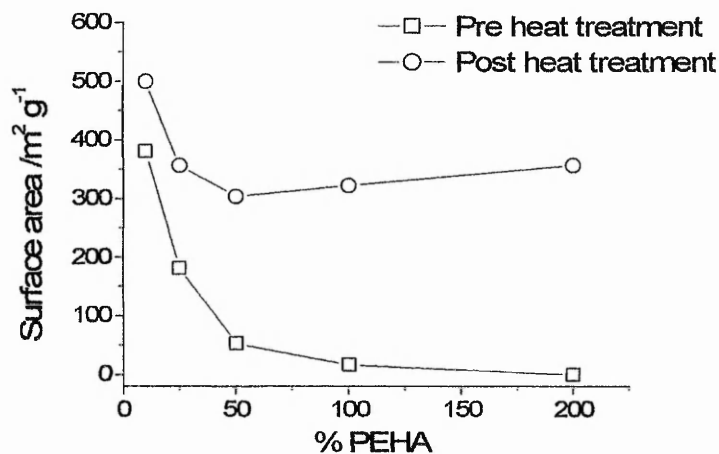


Figure 6.6 Surface area of silica isolated from condensing systems containing 3-60mMdm⁻³ of PEHA before and after heat treatment.

domains but by 60 minutes (which was also the time of onset of precipitation) all but the micropores had disappeared. The solution chemistry of the silicifying systems was studied in order to investigate the earlier stage of silica formation in the presence of ethyleneimines, spermidine and spermine. The effect of these additives on silica formation kinetics was monitored by the molybdosilicate blue method while particle growth and aggregation was studied using photon correlation spectroscopy (PCS). Relative rate constants, when normalised with respect to the blank sample, for the trimerisation reaction were found to vary from 1.9-2.64 from MEDA to PEHA (Figure 6.7). Relative rate constants found for spermidine and spermine were *ca.* 2.3. In the previous chapter we have proposed a mechanism driven by hydrophobic entropic effects where rates were seen to increase with increasing hydrophobic nature up to a limiting length where micellisation became dominant. It is possible that this effect is operating here also as the hydrophobic nature of the polyamines increases with chain length. However we would expect the effect to be more pronounced with the naturally occurring polyamines used as the ratio of hydrophobic to amine domains is greater than for the ethyleneimine homologues, which indicates that this increase in rate could be a combination of this effect and the electrostatic binding of monosilicic acid anions to the charged amine groups producing localised increases of the reactive species.

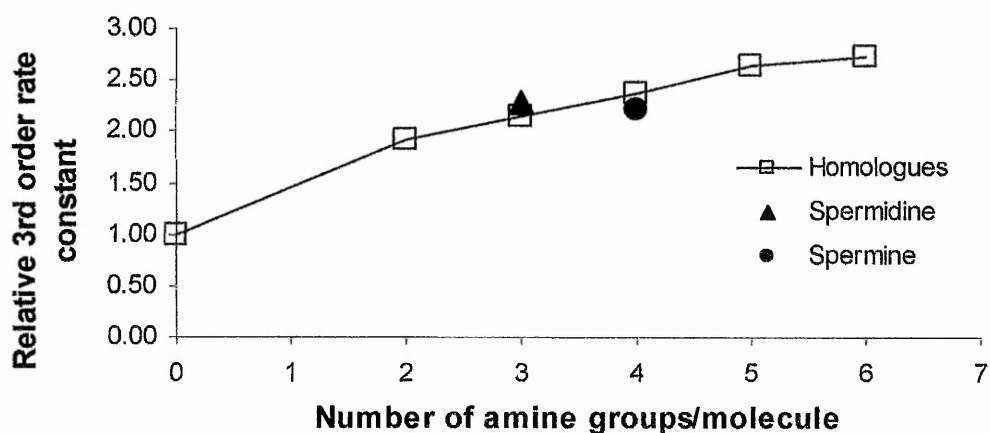


Figure 6.7 Relative 3rd order rate constants for silica condensation

Maximum aggregation rates determined by dynamic light scattering based on the hydrodynamic radii of the forming aggregates increased with increasing homologue length (Figures 6.8 and 6.9). Similarly, spermine caused more rapid aggregation than spermidine. Gelation times decreased correspondingly with homologue length. A step change in both aggregation rate and gelation time was observed between DETA and TETA. Loosely held gels of increasing opacity, which were easily broken by gentle agitation, were formed over the range of homologues from MEDA to TEPA. Silica condensed in the presence of PEHA however, rapidly precipitated from solution after about 70 minutes. Aggregation was not observed for any of the additives until a minimum of 75% of the available orthosilicic acid had condensed to non-molybdenum blue active species with the exception of experiments where PEHA had been added in which case aggregation/growth was observed when as little as 30% condensation had occurred. Data for the natural polyamines used, spermidine and spermine, fell broadly in line with the ethyleneimine homologues in terms of chain length and amine content per molecule with spermidine having a slightly pronounced effect in relation to its amine

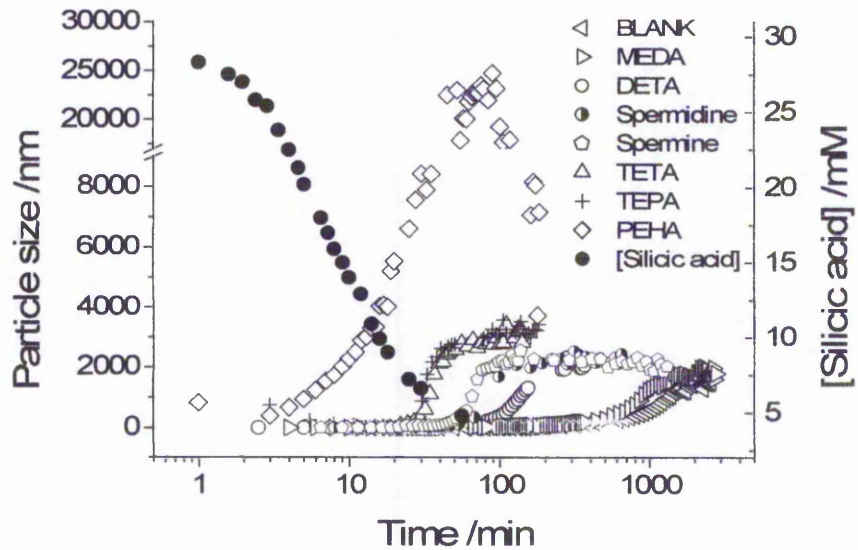


Figure 6.8 Particle growth and aggregation of condensing silica in the presence of polyamines. PCS data showing particle growth

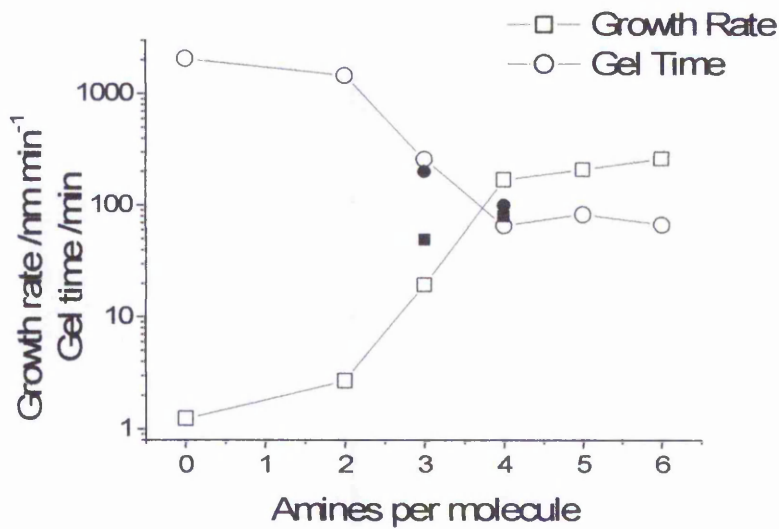


Figure 6.9 Relative growth rates and actual gelation times. Spermine and spermidine are shown as bold data points.

content and spermine a slightly reduced effect. Additional experiments were conducted where the level of PEHA was varied from 10% - 200% (i.e. 3 - 60 mM) with respect to

amine group content. In these experiments, an increased aggregation rate with increasing concentration and a decreasing gelation/precipitation time was observed (Figure 6.10 and 6.11). At levels exceeding 100% PEHA, only small changes in growth rates and gelation/precipitation time was observed, and at levels below 100% PEHA concentration, gelation and not precipitation occurred. Silica isolated from these experiments showed an increasing ease of re-suspension in water with increasing PEHA content even after extensive washing to remove any extraneous polyamine.

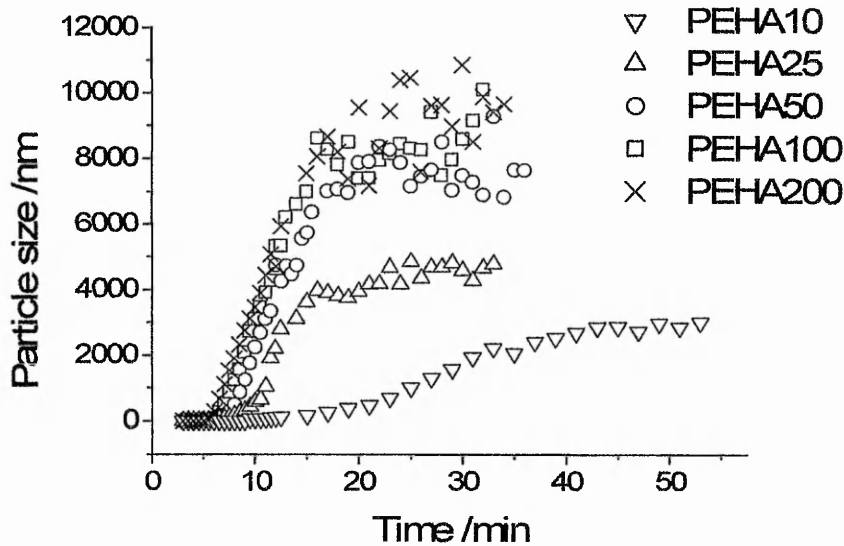


Figure 6.10 Particle growth and aggregation of condensing silica in the presence of PEHA at increasing concentration. PCS data showing particle growth.

6.4 Discussion.

The effects on particle growth/aggregation were considered to be very pronounced when the limited effect of the additive on initial condensation was compared. An obvious cause of increased aggregation is charge neutralisation of the anionically charged silica

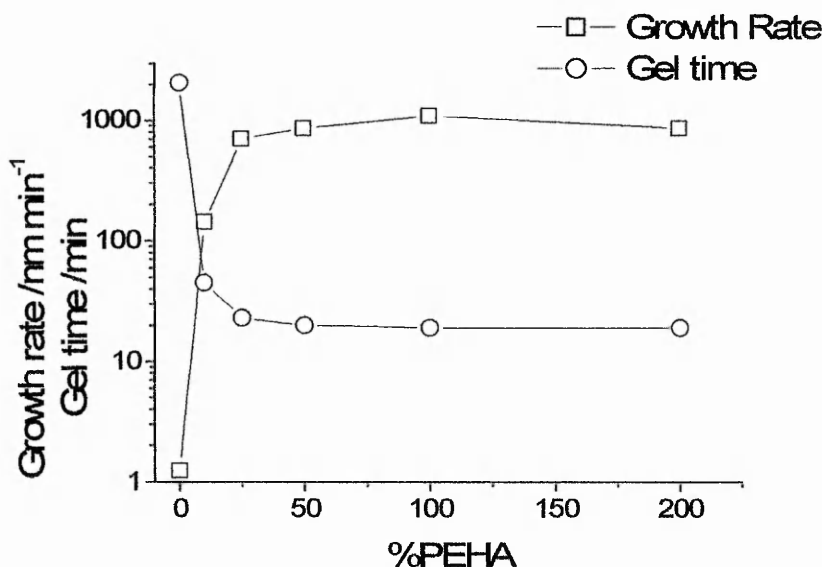
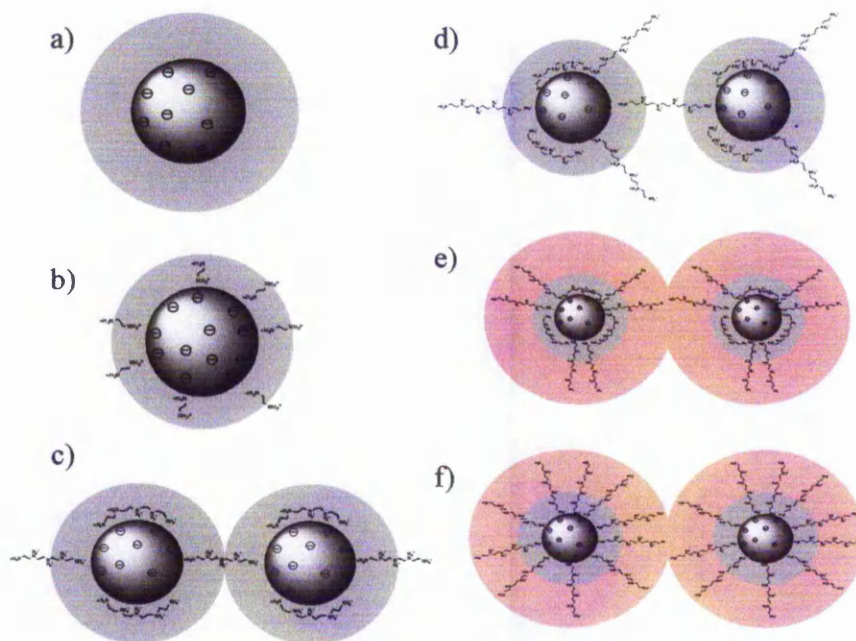


Figure 6.11 Relative growth rates and actual gelation times.

particles by the cationically charged amine species. Assuming a silica particle surface made up of mostly Q3 species and 50% silanol group dissociation, (reasonable assumption at the pH of the experiments),¹⁹ the minimum surface inter anion distance can be estimated to be approximately 5.4 Å, i.e. every other silanol group. The shortest ethyleneimine homologue used in this study was MEDA with an inter amine distance of 3.9 Å (see Table 6.1). Clearly this results in the molecule only being able to attach via one amine group as shown in Scheme 6.1b. All of the other ethyleneimine homologues used have inter-amine distances which allow them to attach along the surface of the particles (Scheme 6.1c). It is known from previous studies that amines, such as the ones studied herein, are able to bind with inorganic polyanions.²⁰ If the polyamines all orient along the particle surface then increased aggregation would be a consequence of the collapse of the electrical double layer and an increased rate with chain length would not be observed. However it is thought that at the concentrations of amines used, surface saturation occurs allowing some of the molecules only to attach at limited number of points. The amine chains are thus forced to extend into, and if long enough, beyond the double layer boundary (Scheme 6.1d,6.1e).

The increase in aggregation rates observed with increasing polyamine length therefore suggests that at least some of the chains extend into the bulk solution and are therefore able to bridge between neighbouring particles. The step change in rates of aggregation and gelling times observed from MEDA to TETA correspond to an increased molecule length from 3.8 to 11.1 Å suggesting that for these particles the surface double layer is of this order. Again in the previous chapter diamines also showed a step change in aggregation rates between the addition of 1,4-butanediamine and 1,6-hexanediamine corresponding to an inter amine distance of 6.3 – 8.7 Å suggesting a shared chain length mechanism, i.e. spanning of the electrical double layer, for the observed step change. The naturally occurring polyamines used in this study, spermidine and spermine, were 11.2 and 16.1 Å in length respectively and accordingly showed the accelerated aggregation effects.



Scheme 6.1 a). Charged silica particle showing double layer boundary barrier to aggregation, b) Reduction of double layer by charge neutralisation, c) Particle bridging by longer polyethylenimine, d) Bridging by PEHA at lower concentrations, e) and f) Partial and complete sol stabilisation at higher PEHA concentrations.

Gels formed showed increasing opacity with polyamine chain length and the longest, PEHA, precipitated silica within minutes. Almost universally with the silica condensing model used here, particle growth is not observed by PCS until in excess of 75% of the available monosilicic acid has condensed to non molybdenum reactive species i.e. after a large population of primary particles has formed. However, monosilicic acid levels at the time of onset of particle formation in the presence of PEHA were around 70% of the initial concentration, suggesting that a smaller number of primary particles were “mopping” up the available monosilicic acid to form the larger low surface area spheres as observed by SEM and nitrogen gas adsorption. These silica spheres of 200-250 nm in diameter had aggregated sufficiently for isolation by centrifugation within 30 minutes of the onset of condensation. Additional experiments conducted with PEHA at amine concentrations varying from 10 – 200% (3mM to 60mM) showed a transition from gelation to precipitation at PEHA amine concentrations in excess of 25% with little change in growth rate and gel times thereafter.

6.4.1 Proposed mechanism for the formation of microporous “glassy spheres”.

Stabilisation of silica sols by polycations is a well known phenomenon and it is likely that at the concentrations of PEHA used here some stabilisation occurs. But due to increasing amine resistance to protonation when neighbouring amine groups are already charged, not all of them will be protonated at pH 7 as might normally be expected.²¹ These amines will be brought into close contact with silanol groups on the surface of the silica particle by electrostatic attraction of positively charged amines on the polyamine chain to deprotonated silanol groups. Modelling of PEHA to ascertain the charge state of the amine groups using the SPARC online calculator showed that uptake of charge on amine groups was resisted by the increasing charge density of charged neighbouring groups. An especially prominent species at pH is the triply charged species below (figure 6.12). Crucially because of the molecules symmetry whether the 3 or 4 amine is charged is irrelevant since the energies are identical. A surface silanol group in the vicinity of the

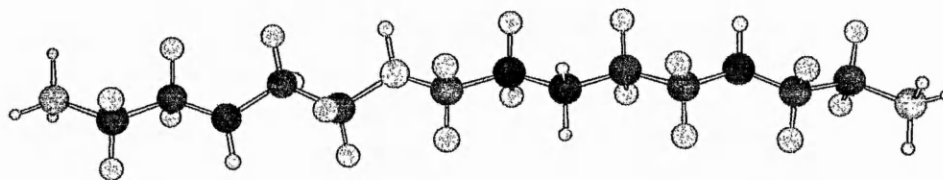
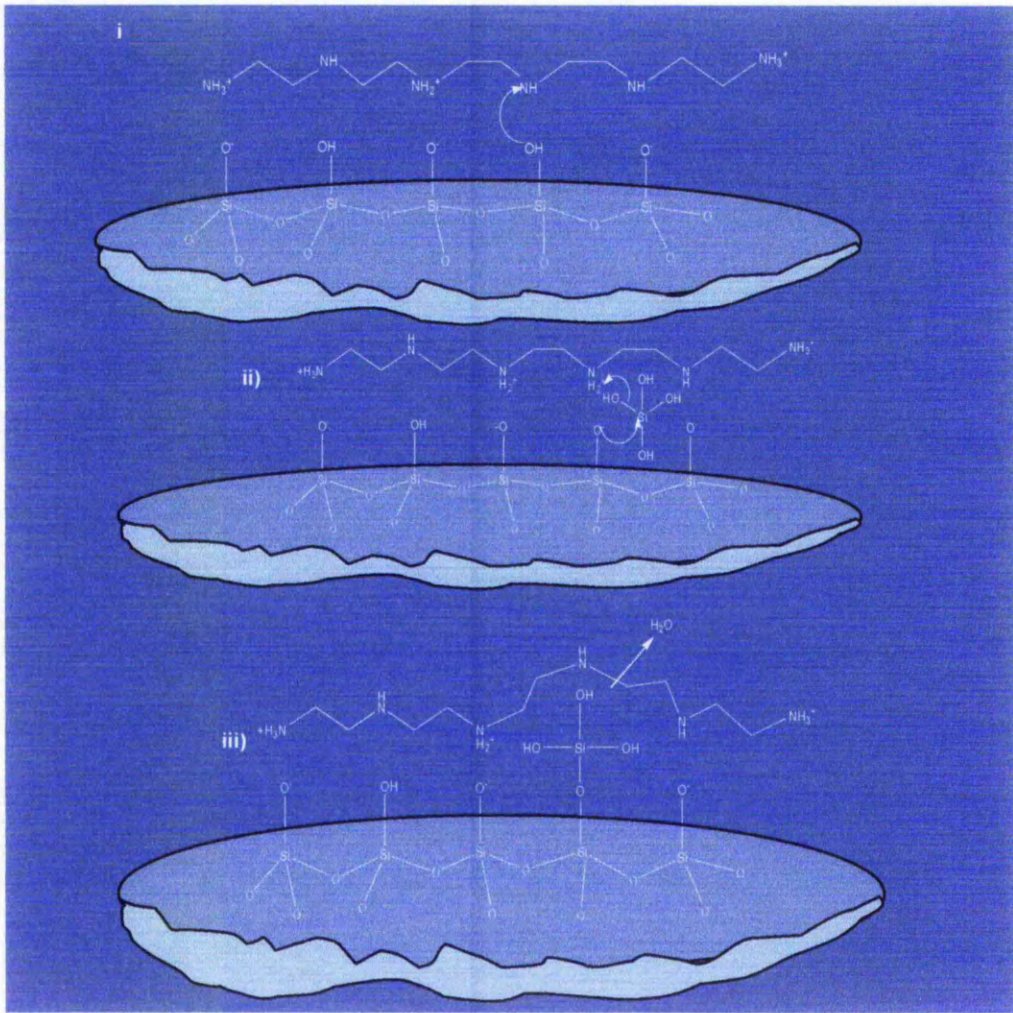


Figure 6.12 Predominant aqueous charged species for PEHA at pH 7. Nitrogen atoms shown as charged (red) and uncharged (blue).

uncharged 3 or 4 amine group could have a proton abstracted from one of its silanol groups and the neighbouring amine would then lose its proton with very little change in energy to the polyamine (scheme 6.2(i)). The siloxy anion is now free to nucleophilically attack any silicon nuclei on nearby monosilicic acid molecules via an S_N2 mechanism (Scheme 6.2(ii)). This is facilitated by the now weakly protonated amine acting as a Brønsted acid (proton donor) back donating the proton, resulting in the production of water as the leaving group (scheme 6.2(iii)). In the absence of the weakly charged amine group direct attack of charged silanols on monosilicic acid results in the formation of a hydroxyl ion, which is a much inferior leaving group, hence the mechanism proposed would be favoured and very little energy change observed by the polyamine during the entire process.

This mechanism would allow particle growth to progress in the absence of aggregation at higher monosilicic acid concentrations and lower primary particle populations resulting in the formation of the larger glassy particles observed. The presence of uncharged amine species is thought to be critical since identical experiments conducted at a pH of 6.0 failed to produce the same effect. Also the experiments conducted at lower amine concentrations resulted in rapid aggregation of primary particles more normally observed. Sedimentable silica levels were also found to decrease with increasing PEHA concentration (Figure 6.13) reinforcing the argument that silica particles may become fully stabilised by the added polyamine. The entrainment of some PEHA in the silica is suggested by both the data collected by ^1H NMR and thermogravimetric analysis conducted on harvested silica after sodium hydroxide digestion (Figures 6.14 and 6.15) and the observed increase in surface area measured by multipoint BET after heat treatment of the silica to $650\text{ }^\circ\text{C}$ (Figure 6.6). The nature of the microporosity found

associated with the surface area increase suggest that its origin is layers of PEHA in the silica spheres rather than molecules trapped in the interstitial voids. In terms of entrainment the naturally occurring polyamines examined showed levels in common with their molecular size rather than number of amine groups.



Scheme 6.2 i) Proton exchange between surface silanol and labile nitrogen.

ii) Nucleophilic attack of siloxy anion on monosilicic acid.

iii) Back donation of proton and elimination of water.

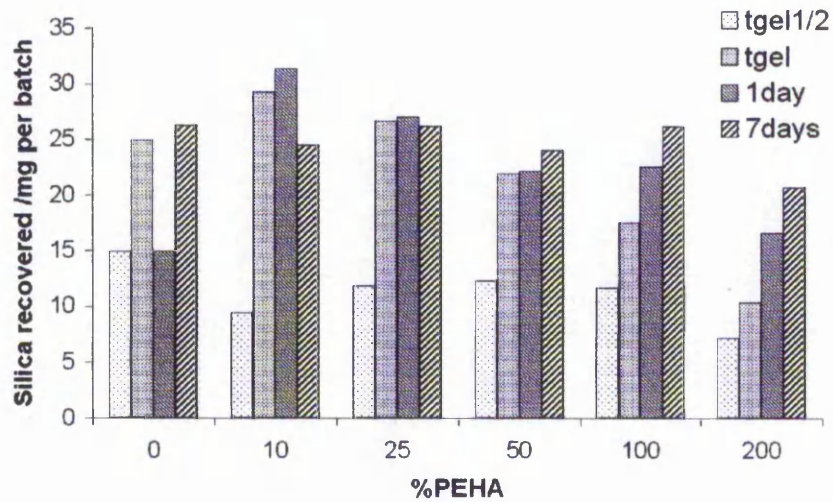


Figure 6.13 Sedimentable silica isolated at different maturation times from condensing systems in the presence of increasing levels of PEHA.

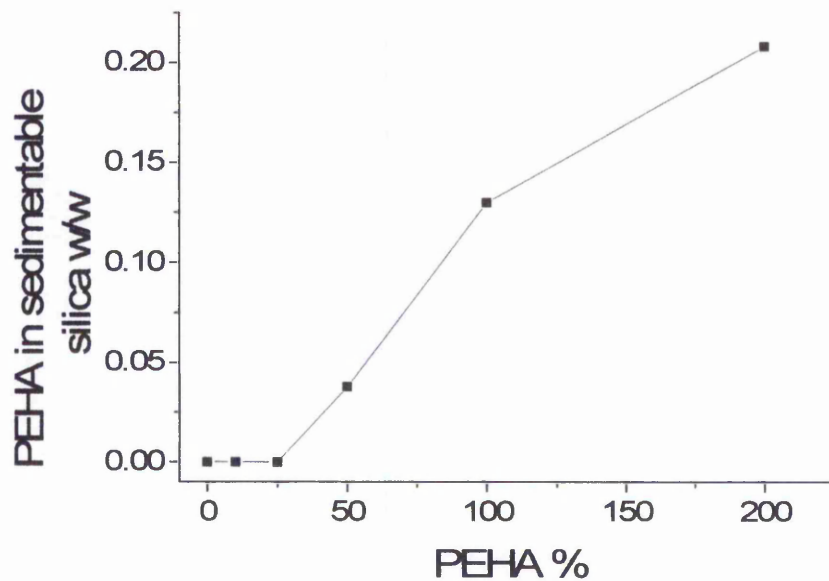


Figure 6.14 Entrained PEHA in 7 day sedimentable silica condensed in the presence of increasing levels of PEHA as determined by ¹HMR.

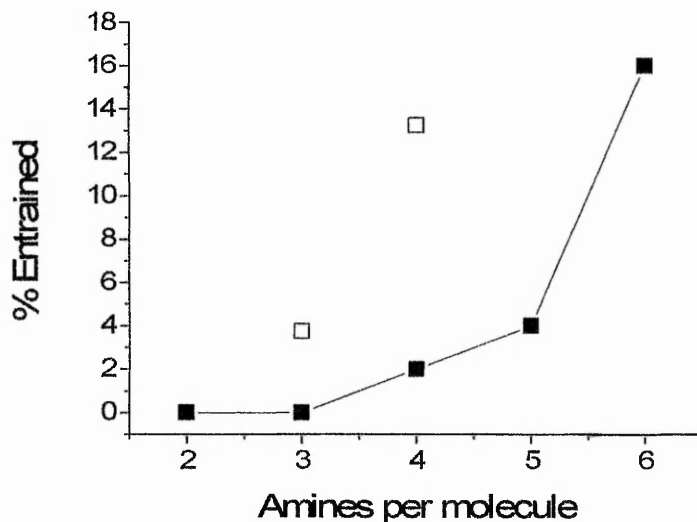


Figure 6.15. Entrained polyamines in 7 day sedimentable silica condensed in their presence determined by thermogravimetric analysis. Spermidine and spermine are shown as unfilled data points.

6.5 Conclusions.

The effects of polyamines of a range of chain lengths, architectures and basicities on the condensation of monosilicic acid and the formation and aggregation of silica particles have been investigated. Slight catalytic activity over condensation correlating to chain length was observed, but not thought to be significant in terms of rates observed during biosilicification, and the naturally occurring amines used showed no special additional effects. Particle growth and aggregation also showed chain length dependent acceleration effects which the naturally occurring amines fell largely in line with. However as the chain was extended to 6 repeat ethyleneimine units, a transition in behaviour and possibly condensation mechanism was observed. That this transition was pH and amine concentration dependent was also shown, allowing the proposal of a mechanism to explain the observations made. The mechanism involves particle stabilisation by reversal in charge and increase in magnitude of the outer double layer. This is followed by uncharged amine facilitating the condensation of monosilicic acid on to the stabilised

spheres via reversible proton exchange, the process driven by water being preferred over a hydroxyl ion as the leaving group. Due to the observed pH sensitivity of the process it should be possible to tailor reactions using the careful choice of amine group basicity and charge separation to enable similar highly condensed silica spheres to be produced over a range of pHs. Also it could be possible that similar mechanisms occur during the biosilicification process, however this is only speculative at this point in time. The undertaking of studies on a similar range of repeat unit propyleneimine homologues could help to clarify this matter and future work is being undertaken in this direction.

6.5 References.

- 1) N. Kröger, , R. Deutzmann, , C. Bergsdorf, and M. Sumper, (2000). *Proc. Natl. Acad. Sci. USA* 97, 14133-14138.
- 2) S. S. Cohen, *A guide to the polyamines*, Oxford University Press, New York, 1998.
- 3) S. V. Patwardhan, S. J. Clarson and C. C. Perry, *Chem. Commun.*, 2005, 9, 1113.
- 4) S. V. Patwardhan, C. Raab, N. Husing and S. J. Clarson, *Silicon Chem.*, 2003, 2, 279.
- 5) D. Belton, G. Paine, S. V. Patwardhan and C. C. Perry, *J. Mater. Chem.*, 2004, 14, 2231; T. Coradin and J. Livage, *Colloids Surf. B*, 2001, 21, 329; T. Coradin, O. Durupthy and J. Livage, *Langmuir*, 2002, 18, 2331; L. Sudheendra and A. R. Raju, *Mater. Res. Bull.*, 2002, 37, 151.
- 6) S. V. Patwardhan and S. J. Clarson, *J. Inorg. Organomet. Polym.*, 2003, 13, 193.
- 7) S. V. Patwardhan, N. Mukherjee and S. J. Clarson, *J. Inorg. Organomet. Polym.*, 2001, 11, 193; S. V. Patwardhan, N. Mukherjee, R. Maheshwari, K. L. Kiick and S. J. Clarson, *Soft Matter*, 2005, in press.
- 8) S. V. Patwardhan, N. Mukherjee, M. Steinitz-Kannan and S. J. Clarson, *Chem. Commun.*, 2003, 10, 1122.
- 9) S. V. Patwardhan, N. Mukherjee and S. J. Clarson, *Silicon Chem.*, 2002, 1, 47.
- 10) M. Sumper, *Angew. Chem. Int. Ed.*, 2004, 43, 2251.
- 11) R.-H. Jin and J.-J. Yuan, *Chem. Chemmun.*, 2005, 1399; R.-H. Jin and J.-J. Yuan, *Adv. Mater.*, 2005, 17, 885.
- 12) R. R. Naik, P. W. Whitlock, F. Rodriguez, L. L. Brott, D. D. Glawe, S. J. Clarson and M. O. Stone, *Chem. Commun.*, 2003, 238.
- 13) T. Mizutani, H. Nagase, N. Fujiwara and H. Ogoshi, *Bull. Chem. Soc. Jpn.*, 1998, 71, 2017.
- 14) F. Noll, M. Sumper and N. Hampp, *Nano Letters*, 2002, 2, 91.
- 15) K. M. Roth, Y. Zhou, W. Yang and D. E. Morse, *J. Am. Chem. Soc.*, 2005, 127, 325.
- 16) D. Belton, S. V. Patwardhan and C. C. Perry, *Chem. Commun.*, 2005, B504310G.
- 17) S. Brunauer, P. H. Emmett and E. Teller, *J. Am. Chem. Soc.*, 1938, 60, 309.
- 18) E. P. Barrett, L. G. Joyner and P. P. Halenda, *J. Am. Chem. Soc.*, 1951, 73, 373.
- 19) C. C. Perry, D. Belton and K. Shafran, *Prog. Mol. Subcell. Biol.*, 2003, 33, 269.
- 20) A. De Robertis, C. Foti, O. Giuffre and S. Sammartano, *J. Chem. Eng. Data*, 2001, 46, 1425.
- 21) C. De Stefano, C. Foti, A. Gianguzza and S. Sammartano, *Analytica Chimica Acta*, 2000, 418, 43.

Conclusions.

Review of the model system.

A study in to the affects of small molecules on the deposition of silica has been conducted. The model silicifying system used herein has been reviewed and uncertainties involved in several aspects of it have been assessed. Firstly the problematic conversion rate was eliminated. This was a feature of the model system due to the high levels of residual complex which used to occur. At high monosilicic acid levels i.e. at the start of the condensation process the level of precursor complex conversion was found to be around 60%, but as the reaction progressed and levels of monosilicic acid fell, the amount of precursor complex conversion rose to up to 95%. The way this problem was managed previously was to construct a conversion rate table by measuring the effect of adding fixed amounts of precursor to an already condensing system and determine the change at the times taken. This in itself is likely to introduce some errors and efforts have been made in the past to offer an alternative solution. One attempt was to change the conditions of the molybdenum blue assay in order to favour the complete dissociation of residual complex by adjusting the pH of the molybdic acid reagent. Sadly it was found that conditions were already optimum for the maximum level of dissociation at the shortest time. Here the problem was solved simply by eliminating the residual complex precursor from the condensing system. Titrimetry showed that the system was to a degree self buffering in the presence of the complex and it was found that it could be reduced to below 5% of the original level before the pH became too difficult to control. The initial concentration of complex was therefore reduced to 30mMdm^{-3} to prevent the condensation becoming too rapid to monitor, and the pH was adjusted with the careful addition of 2Mdm^{-3} hydrochloric acid. The precursor for the model has also been shown under these conditions to fully dissociate as required in the time frame of the reaction for the monitoring of the early stages of the condensation process to give a supersaturated solution of monosilicic acid almost immediately. No species interfering with the early stages of condensation or with the mechanism of the molybdenum blue assay method used for monitoring the condensation process through the loss monosilicic acid were found. The rate of formation of the molybdenum blue intermediate, silicomolybdic acid, varies with the degree of condensation of complexing silicate species. The

monomer should fully complex with molybdic acid in 2 minutes and the dimer within 10 minutes under the conditions used. Complexation times of higher oligomers and polysilicic acids will take increasing lengths of time and should be observable as absorbance build up delays when monitored at 370nm. Partially condensed samples taken after various times of model condensation were used to see if any significant population of species still reactive to molybdic acid survived in the system for a significant level of time after the formation of the supersaturated monosilicic acid solutions. No changes in the condensation profile were observed to suggest that this may be the case. Samples were taken after between 1 minute and 120 minutes of condensation and showed the same initial rapid build up of complex and a stable absorbance after about 6 minutes. The only difference observed was the final intensity of the complex which was reflective of the amount of monomer remaining in the condensing system. Further investigations were carried out by electrospray ionisation mass spectroscopy and ^{29}Si nuclear magnetic resonance spectroscopy first using a tetramethylammonium hydroxide stabilised solutions of silica which are known to be composed of large populations of cyclic and polyhedral forms. Under negative ion mode mass spectroscopy the presence of these species was shown, indicating their stability to the ionisation technique but also to any collisional activation that can occur as the particle transfer from the liquid phase to the gas phase. The majority of species reaching the detector observed were singly charged silicate species without stabilising counter ions ranging from monomeric species up to the cubic octamer which dominated the spectrum. That these were not merely products of the ionisation and phase transfer process was shown by ^{29}Si NMR which indicated the presence of similar condensation levels for the silicate species from Q_0 to Q_3 . By comparison samples taken from the model system showed only the presence of monomeric silicic acid with no indication of oligomeric condensed species, although the 1,2-dihydroxybenzene ligand generated an ion which interfered with the expected mass of the cyclic silicate trimer. Condensation was still clearly active however as was evidenced by the gradual decrease of the monosilicic acid against an increasing ligand background. This data in conjunction with the absorbance data suggests that once the condensation process begins in a monomeric species the following condensations become increasingly facilitated and the oligomer rapidly grows beyond the size at which it can fully depolymerise to form a silicomolybdic acid complex. Evidence for this was gained by a series of model condensation experiments conducted at

temperatures ranging from 0 to 50°C. The 3rd and reversible 1st order rate constants were isolated from the data and Arrhenius plots constructed to ascertain the activation energies at these two kinetically distinct stages. The activation energy for the forward 1st order stage was found to be 55 kJ mol⁻¹ which is in good agreement with published values. The activation energy for the 3rd order domain however was found to be higher at 77 kJ mol⁻¹ the difference between these two values representing the increasing ease at which an increasingly condensed silicate species can be deprotonated. In addition experiments carried out at decreasing pH showed evidence of limitation to the degree at which residual oligomeric and particle surface silanol can be deprotonated. The relationship between the log of the third order rate constant and the hydroxyl ion content remained linear over the pH range 4.7 to 6.8 suggesting no change in the deprotonation mechanism. But for the first order rate domain the rate constant increased at a decreasingly as the hydroxyl ion concentration increased. This indicated a resistance to deprotonation probably as a consequence of increasing charge density on the silicate surface. Finally statistical analysis four repeat data sets showed excellent reproducibility of the model system analysis showing that there was a 95% confidence that the true value fell within $\pm 4\%$ of the recorded value.

The influence of small molecule additives to the model system.

Amino acids were found to make small but significant differences to the kinetics and aggregation in the model system apparently related to their isoelectric points. The ability of more basic amino acids to locally concentrate oppositely charged anionic silicate species was thought to contribute to this effect. Growth rates of aggregates were similarly affected due to the well established consequence of charge neutralisation of the anionic silica particles. Both these effects were shown to increase with the addition of increasingly long lysine oligomers. Surface areas of the precipitated silica was found to decrease with hydrophobicity rating of the amino acid added. Whether this was an entropic effect caused by localised clustering of the more hydrophobic amino acids was not clear. All silicas produced in the presence of amino acids bearing nitrogen containing side chains had a more granular appearance, although why this should apply to amines equally to amides is unclear although hydrogen bonding may be implicated. The addition of diamines at fixed amine to silicon mole ratios again increased the kinetic rates in relation to chain length. The

only difference between the additives in solution was their relative hydrocarbon domains. The kinetic changes could then be explained by the entropy of the hydrophobic effect. When the diamines are taken in to solution the driving force is the solvation of the positively charged amine end groups. Considering their solubility a large amount of hydrophobic material is taken in to the system. The response of the water is to maintain as many hydrogen bonds with other water molecules by arranging themselves around the hydrophobic parts of the diamine molecules in such a way that they maximise hydrogen bonding with themselves and minimise hydrogen bonding with the carbon chain. This limits the degrees of freedom of the surrounding water molecules and this is thought to limit the amount of free water available to solvate ionic species. With reduced solvation anionic species such as silicates become more reactive. But with increasing chain length these entropic effects are limited by the formation of micelles in an attempt to limit the surface in contact with water, and so the kinetic effect is also limited by carbon chain length.

Aggregation rates were observed to increase with chain length as the mildly charged silica particles were bridged by the larger diamines and some structure formation in the matured silicas that may have been tempered by increasing chain flexibility was suggested by gas adsorption analysis and scanning electron microscopy.

The addition of multiply charged cationic molecules in the model as synthetic mimics of the polyamines found in silicifying organisms showed largely the same effects as the diamines, the amine separation appearing to produce no discernable effect with the naturally occurring amines with three and four membered carbon separators showing characteristics which were a combination of the amine number and the overall chain length. The exception was pentehylenhexamine which produced almost glassy microporous silica within minutes. We believe it to be a happy coincidence of amine group separation and pH that results in the material observed. With increasing repeat amine units the ease of protonation decreases due to localised charge density set up by neighbouring charged amines. Also at the pH of the experiments approximately 50 % of the surface silanol groups of any silica particles can be expected to be deprotonated, the inter silanion distance being approximately that of the charged interamine distance. The electrostatic localisation of the amine on to the silica particles then allows the free and protonated amines to act as alternately proton donors and proton acceptors with little energy barrier in either direction. This mechanism has the advantage to the condensation process in that it result in a better

leaving group, (H₂O), than in its absence, (OH). Entrainment of the polyamine then confers microporosity on to the silica after calcination. The fact that only pentaethylenhexamine showed this behaviour shows how important the pKa's of neighbouring amine groups may be in silicifying processes and also the charge separation of the surface silanions. Additionally we believe that aggregation prevention by the formation of a reverse charge stabilisation boundary also plays a role as the effect was observed only at specific pH and a minimum level of polyamine was required to affect the switch from fine particle mesoporous silica to dense microporous material.

Further work.

Projected future work focuses on the way amines may be employed in studying diatom silica biosynthesis, by analysing the effects of synthetic chemical mimics on the model system. Preliminary work (not reported here) using a cationic polysaccharide derivative produced stable silica sols when added to the model system. These sols were shown to remain unchanged for several months and could be used as a model to investigate the behaviour of particulate silica with polyamines in condensing silica systems, enabling us to observe isolated particle growth and deposition/cementation.

The critical nature of the charge state of the amine species in the condensation mechanism suggested as the condensed material changes from porous to non-porous needs to be investigated with respect to charged amine separations and charged surface silanol groups. A comparative study of ethyleneamines with propylamines would be useful in this respect, and the steric influences of amine methylation as observed in diatom polyamines could lead to a further understanding of their role in biosilicification.

The effects of short polyamines of various architectures and concentrations on stable and quasistable silicate solutions requires further investigation into the possibility of solution destabilising and particle stabilising mechanisms proposed in natural systems. Evidence of lowered monosilicic acid solubilities in the presence of short polyamines would allow further insights into the biosilicification process especially with respect to diatoms with the suspected involvement of amine species.

The combined effects of long polyamines which are known to cationically stabilise silica sols at critical polymer/particle ratios in conjunction with the shorter polyamines needs to be addressed in light of the diatom situation where both are found associated with the biosilica. Whether these act in the process together, or sols stabilised by the peptides, are initially produced, followed by destabilisation of the sol under possibly enzymatic hydrolysis of the peptides, and release of the side chain amine modifications which then allows cementation of the preformed silica particles needs to be investigated as a possible paradigm for the biosilicification process. The

use of mixed species additions possibly using the cationic polysaccharide referred to in the 1st paragraph to mimic the cationic peptide in conjunction with shorter chain polyamines may result directly in larger sphere stabilised sols due to prevention of aggregation of the smaller spheres enabling further condensation of silica onto the isolated nuclei. Continued growth of silica particles may be possible by continuous supply of monosilicic acid and polyamine up to a critical silicon/polysaccharide ratio. Destabilisation of the sol could be achieved at any stage by chain hydrolysis of the polysaccharide with a suitable hydroxylase.

Further to the effects of sol stabilisation of variously sized silica particles, the possibility is raised for the formation of core-shell materials currently under investigation for applications such as photonics, and the production of quantum dots by doping and containment within the silica particle. The silica surfaces may then be functionalised to prevent aggregation and also modify the hydrophobicity-hydrophilicity of the particles as required.

The use of long chain amines and polycationic species in the condensation of other oxides such as those based on germanium, vanadium, zinc, titanium, chromium, tantalum etc should also be investigated as the use of these materials in electronic/optical devices is dependant on the control of particle size, shape and ordered depositional control.

Appendix i.

This appendix describes the error analyses performed on data sets collected during this study.

Error analysis.

Standard deviation.

This is a measure of the average deviation of all values determined within a dataset from the mean of the dataset using:-

$$s = \sqrt{\frac{\sum (x - \bar{x})^2}{n}} \text{-----(1)}$$

Where x = The value of an individual measurement

\bar{x} = The mean of the sample dataset

n = The number of samples in the dataset.

The calculation of the standard deviation for smaller datasets is modified to give the population standard deviation:-

$$\hat{\sigma} = \sqrt{\frac{\sum (x - \bar{x})^2}{n - 1}} \text{-----(2)}$$

The use here of $(n-1)$ increases the size of the observed standard deviation to take into account the increasing uncertainty generated by the use of smaller sample sizes.

The normal distribution.

From a population of continuous variables the distribution of values for a large number of results should approach a Gaussian curve and this represents how likely each value of the random variable is.

A normal distribution in a variable, x , with a mean of μ and variance σ^2 :-

$$p(x) = \frac{1}{\sigma\sqrt{2\pi}} e^{-(x-\mu)^2 / (2\sigma^2)} \text{-----(3)}$$

Normal distribution curves are always bell shaped and the area bordered by the curve and the x axis is always the same. The height and spread of the curve varies depending on the two parameters mean and standard deviation. The greater the standard deviation the greater the spread of the curve.

An inherent property of the normal distribution curve is that 68% of the data set will fall within ± 1 standard deviation of the mean, 95% within ± 2 and 99% within ± 3 .

The standard normal distribution is a normal distribution with a mean of 0 and a standard deviation of 1, so applying the formula:-

$$z = \frac{x - \bar{x}}{s} \text{-----(4)}$$

transforms a normal distribution to a standard normal distribution.

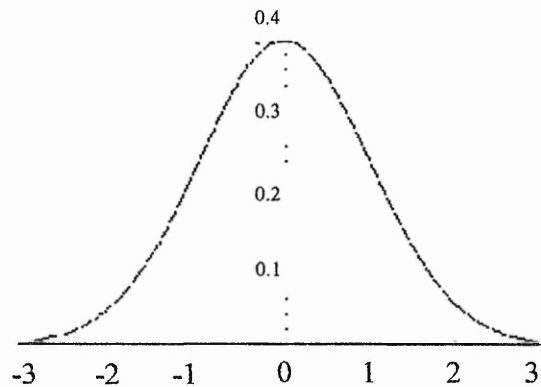


Fig i. Standard normal distribution

Using this z score provides a way of presenting results from a test set evaluated in terms of probability of variance from the mean dependent on the standard deviation of the newly acquired data.

Confidence intervals.

The standard error of the mean:

$$\hat{\sigma}_x = \frac{s}{\sqrt{n}} \text{-----(5)}$$

Where s = the sample standard deviation
and n = the number of samples

If we wish to say at what value the limits are 95% certain that the true mean lies between them then the standard error of the mean is calculated as:

$$\hat{\sigma}_x = \frac{s}{\sqrt{n}} \text{-----(6)}$$

The confidence interval, (C.I) is given by:

$$C.I = \bar{x} \pm z\hat{\sigma}_x \text{-----(7)}$$

However, smaller samples which are normally distributed follow a modified curve known as the t distribution where the population envelope becomes increasingly flat and hence describes distributions that are dependent on the sample size.

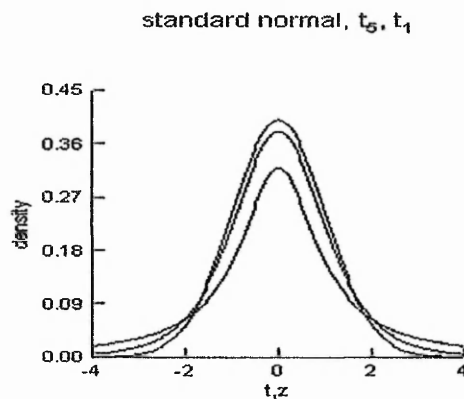


Fig ii. Normal distributions with decreased sample number.

For example the 95% confidence z value of 1.96 is dependent on a large number of determinations (>30). The corresponding t value varies depending on the number of degrees of freedom and the confidence interval becomes:

$$C.I = \bar{x} \pm t_x \hat{\sigma}_x \text{-----}(8)$$

In the case of the data set used in the error analysis of chapter 3 in the review of the model system, 4 repeat determinations were carried out giving a number of degrees of freedom of $n - 1 = 3$. For a 95% confidence with 3 degrees of freedom the t value is 3.182. Using the analogous formula (8), where t is substituted for z gives a confidence interval of $1.16 \times 10^{-6} \pm 8.21 \times 10^{-8} \text{ mM}^{-2} \text{ dm}^6 \text{ s}^{-1}$ for the third order rate constant, meaning that a sample analysed under the conditions used only has a 5% chance of falling outside of these values by chance alone. The implication therefore is that the data acquired for the modified model systems with single additive alterations show that these additives in many cases produced significant kinetic effects.

Treatment of the photon correlation spectroscopy with the t test modified confidence interval allows the mean rate bar to be plotted with upper and lower confidence interval bars:

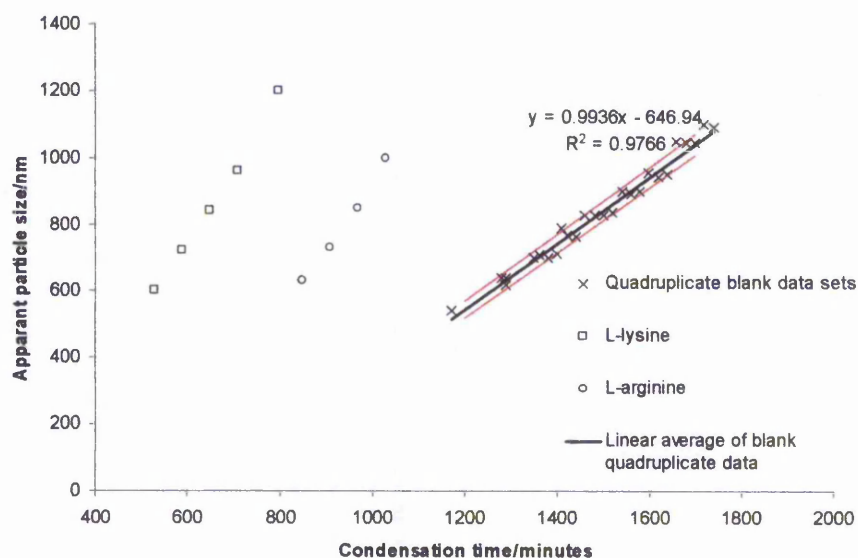


Fig iii. Analytical comparison of the mean maximum aggregation rate of the model condensing system with upper and lower 95% confidence interval lines, (in red), with that of the most significantly affecting added amino acids.

The mean slope of 4 data sets constructed was found to be 0.994nm min^{-1} with a standard deviation of 0.073nm min^{-1} , giving modified t test 95% confidence limits of $\pm 0.116\text{nm min}^{-1}$. Construction of upper and lower confidence limit lines and co-plotting of basic amino acid additive data clearly demonstrates the significance of the additives on aggregation rates.

Treatment of the gas adsorption data from analyses on 4 repeat model condensed silica's gave a mean surface area of $606\text{m}^2\text{g}^{-1}$, with a standard deviation of $20.8\text{m}^2\text{g}^{-1}$ giving a modified t test 95% confidence limit of $\pm 33.1\text{m}^2\text{g}^{-1}$.

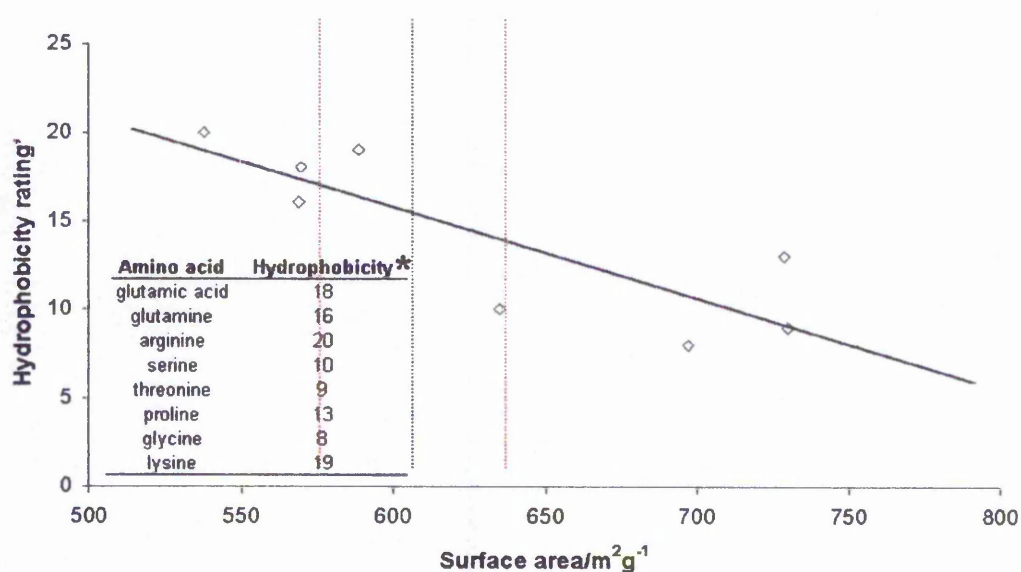


Fig iv. Example of gas adsorption data analysis applied to silica condensed in the presence of amino acids of various side chain functionalities. Black dotted line = mean for 4 repeat blank model silica's, red dotted lines = upper and lower 95% confidence limits.

The data collected shows that provided that experiments were controlled in the ways and to the tolerances described in chapter 4 then we can be confident that significant effects were found on the kinetics, aggregation rates and surface areas determined for silica condensing in the presence of a number of simple additives.

Publications.

C.C. Perry, D. Belton, K. Shafran., *Prog Mol Subcell Biol.* 2003;33:269-99.

Studies of biosilicas; structural aspects, chemical principles, model studies and the future.

D. Belton, G. Paine, S. V. Patwardhan, C. C. Perry., *Journal of Materials Chemistry*, 2004, 14(14), 2231 - 2241

Towards an understanding of (bio)silicification: the role of amino acids and lysine oligomers in silicification

D. Belton, S. V. Patwardhan, C. C. Perry

Chemical Communications, 2005, (27), 3475 - 3477

Putrescine homologues control silica morphogenesis by electrostatic interactions and the hydrophobic effect

D. J. Belton, S. V. Patwardhan, C. C. Perry *Journal of Materials Chemistry.*,

Spermine, spermidine and their analogues generate tailored silicas: Inter-amine spacing is important in generating tailored silicas. In press.